

DOE/NASA/0249-83/1  
NASA-CR-168177

NASA-CR-168177  
19840009005

# **Integral Inverter/Battery Charger for Use in Electric Vehicles**

David Thimmesch  
Gould Inc  
Gould Research Center, Electronics Laboratory

**September 1983**

**LIBRARY COPY**

SEP 15 1984

Prepared for  
National Aeronautics and Space Administration  
Lewis Research Center  
Under Contract DEN3-249

LANGLEY RESEARCH CENTER  
LIBRARY, NASA  
HAMPTON, VIRGINIA



NF02600

for  
**U.S. DEPARTMENT OF ENERGY**  
**Conservation and Renewable Energy**  
**Office of Vehicle and Engine R&D**

## DISCLAIMER

This report was prepared as an account of work sponsored by an agency of the United States Government. Neither the United States Government nor any agency thereof, nor any of their employees, makes any warranty, express or implied, or assumes any legal liability or responsibility for the accuracy, completeness, or usefulness of any information, apparatus, product, or process disclosed, or represents that its use would not infringe privately owned rights. Reference herein to any specific commercial product, process, or service by trade name, trademark, manufacturer, or otherwise, does not necessarily constitute or imply its endorsement, recommendation, or favoring by the United States Government or any agency thereof. The views and opinions of authors expressed herein do not necessarily state or reflect those of the United States Government or any agency thereof.

Printed in the United States of America

Available from

National Technical Information Service  
U S Department of Commerce  
5285 Port Royal Road  
Springfield, VA 22161

NTIS price codes<sup>1</sup>

Printed copy A07  
Microfiche copy A01

<sup>1</sup>Codes are used for pricing all publications. The code is determined by the number of pages in the publication. Information pertaining to the pricing codes can be found in the current issues of the following publications, which are generally available in most libraries: *Energy Research Abstracts (ERA)*, *Government Reports Announcements and Index (GRA and I)*, *Scientific and Technical Abstract Reports (STAR)*, and publication, NTIS-PR-360 available from NTIS at the above address.

# **Integral Inverter/Battery Charger for Use in Electric Vehicles**

David Thimmesch  
Gould Inc.  
Gould Research Center, Electronics Laboratory

September 1983

Prepared for  
National Aeronautics and Space Administration  
Lewis Research Center  
Cleveland, Ohio 44135  
Under Contract DEN3-249

for  
U.S. DEPARTMENT OF ENERGY  
Conservation and Renewable Energy  
Office of Vehicle and Engine R&D  
Washington, D.C. 20585  
Under Interagency Agreement DE-AI01-77CS51044

*N84-17073 #*

## Table of Contents

	<u>Page</u>
1. Summary.....	1-1
2. Introduction.....	2-1
2.1 Background.....	2-1
2.2 Objectives.....	2-1
2.3 Scope.....	2-2
3. Analysis and Design.....	3-1
3.1 Inverter/Charger Requirements.....	3-1
3.1.1 Inverter.....	3-1
3.1.2 Battery Charger.....	3-3
3.2 Inverter.....	3-4
3.2.1 Circuit Operation.....	3-4
3.2.2 Circuit Parameters.....	3-15
3.3 Integral Battery Charger.....	3-29
3.3.1 Charger Power Circuit Operation.....	3-29
3.3.2 Circuit Parameters.....	3-37
3.4 Inverter/Charger Package.....	3-41
3.4.1 Mechanical Description.....	3-41
3.4.2 Package Weight and Volume.....	3-45
4. Test and Evaluation.....	4-1
4.1 Charger Operation.....	4-1
4.1.1 120 VAC Operation.....	4-1
4.1.2 220 VAC Operation.....	4-4
4.2 Inverter Operation.....	4-9
4.2.1 Power Loss/Efficiency Data.....	4-9
4.2.2 Power Loss Breakdown.....	4-15
4.2.3 Component Temperature Rise.....	4-23
4.2.4 Motor Torque/Speed Curve.....	4-29
5. Results and Conclusions.....	5-1
6. Appendicies.....	6-1
A. Charge Control Board Description.....	A-1
B. Set-up Instructions for Inverter/Charger.....	B-1
C. Schematics and Drawings.....	C-1
7. Definitions.....	7-1
8. References.....	8-1

## List of Illustrations

<u>Figure</u>		<u>Page</u>
3.1-1	NASA Driving Cycle Requirement.....	3-2
3.2-1	AC Motor Control Power Circuit.....	3-6
3.2-2	Initial Power Circuit Current Paths.....	3-7
3.2-3	Main Thyristor Voltage During Turn-off.....	3-9
3.2-4	Inverter Six-Step Waveforms.....	3-10
3.2-5	Current Paths at Start of Commutation Cycle.....	3-11
3.2-6	Commutation Thyristor Current Waveform.....	3-12
3.2-7	Energy Recovery Current Paths.....	3-13
3.2-8	Energy Recovery Rectifier Current Waveform.....	3-14
3.2-9	Optimum Commutation Circuit Parameters.....	3-18
3.2-10	Commutation Capacitor Voltage vs. Peak Motor Current.....	3-19
3.2-11	Powdered Molypermalloy BH Characteristic.....	3-21
3.2-12	Main Thyristor Turn-off Time vs. Battery Voltage.....	3-22
3.2-13	DEN3-60 Transformer Power Loss/Quality Factor.....	3-26
3.2-14	Powdered Molypermalloy Transformer Power Loss/Quality Factor.....	3-27
3.3-1	Inverter/Charger Power Circuit Topology.....	3-31
3.3-2	Inverter/Charger Power Circuit - Breaker Open.....	3-32
3.3-3	Charger Current Paths After SCR7 Gated.....	3-34
3.3-4	Capacitor Voltage During Charger Operation.....	3-35
3.3-5	Charger Output Power vs. Resonant Circuit Capacitance.....	3-38
3.3-6	Charger Power Factor vs. Input Line Capacitance.....	3-39
3.4-1	Inverter/Charger Package.....	3-43
3.4-2	Inverter/Charger Package - Cover Removed.....	3-44
4.1-1	Charger Efficiency/Power Factor at 120 Vac.....	4-2
4.1-2	AC Line Current Waveform at 120 Vac, 1.8kW.....	4-3
4.1-3	Charger Efficiency/Power Factor at 220 Vac.....	4-5
4.1-4	AC Line Current Waveform at 228 Vac, 3.7kW.....	4-6
4.1-5	Charge Profile at 228 Vac.....	4-7
4.1-6	Charger Component Temperature Rise at 3.7 kW.....	4-8

## List of Illustrations (continued)

<u>Figure</u>		<u>Page</u>
4.2-1	Inverter Power Loss vs. Motor Current.....	4-10
4.2-2	Inverter/Motor Efficiency at 785 rad/sec (7500 RPM).....	4-11
4.2-3	Inverter/Motor Efficiency at 576 rad/sec (5500 RPM).....	4-12
4.2-4	Inverter/Motor Efficiency at 189 rad/sec (1800 RPM).....	4-13
4.2-5	Motor Current Waveform at 189 rad/sec/10hp.....	4-14
4.2-6	AC Induction Motor - Equivalent Circuit.....	4-17
4.2-7	Reconstructed Motor Current Waveform.....	4-18
4.2-8	Main Thyristor Power Dissipation vs. Motor Current.....	4-19
4.2-9	Commutation Thyristor Power Loss vs. Motor Current.....	4-20
4.2-10	Commutation Transformer Power Loss vs. Motor Current.....	4-21
4.2-11	Component Temperature Rise at 189 rad/sec (1800 RPM).....	4-24
4.2-12	Component Temperature Rise at 524 rad/sec (5000 RPM).....	4-25
4.2-13	Component Temperature Rise at 681 rad/sec (6500 RPM).....	4-26
4.2-14	Component Temperature Rise During Regeneration.....	4-27
4.2-15	Inverter/Charger Package - Bottom View.....	4-28
4.2-16	Motor Maximum Shaft Torque vs. Speed - 132V Battery.....	4-30
A-1	Charge Control Electronics Block Diagram.....	A-2
B-1	Inverter Input Filter Capacitor, Pre-Charge Circuit.....	B-5

## List of Tables

<u>Table</u>	<u>Page</u>
3.2-1 Inverter Capability.....	3-5
3.2-2 Inverter Design Improvement Areas.....	3-16
3.2-3 Commutation Circuit Loss Comparison.....	3-23
3.2-4 Commutation Transformer Comparison.....	3-28
3.3-1 Charger Capability.....	3-30
3.4-1 Inverter Power Stage - Package Comparison.....	3-42
3.4-2 Areas Addressed to Reduce Package Volume.....	3-42
3.4-3 Inverter/Charger Component Weights.....	3-46
3.4-4 Inverter/Charger - Weight Distribution.....	3-47
4.2-1 Inverter Power Loss Breakdown at 576 rad/sec (5500 RPM)....	4-22

## 1. SUMMARY

The objectives of this NASA/DOE sponsored program were to design, fabricate, test and evaluate an experimental integral inverter/battery charger for use in electric passenger vehicle applications. The inverter power circuit was based on the development effort performed by Gould under NASA-Lewis Contract DEN3-60.

This report discusses the design and test results of a thyristor based inverter/charger. A battery charger is included integral to the inverter by using a subset of the inverter power circuit components. The resulting charger provides electrical isolation between the vehicle propulsion battery and ac line and is capable of charging a 25 kWh propulsion battery in 8 hours from a 220 volt ac line. The integral charger employs the inverter commutation components as a resonant ac/dc isolated converter rated at 3.6 kW. Charger efficiency and power factor at an output power of 3.6 kW are 86% and 95% respectively.

The inverter, when operated with a matching polyphase ac induction motor and nominal 132 volt propulsion battery, can provide a peak shaft power of 34 kW (45 hp) during motoring operation and 45 kW (60 hp) during regeneration. Thyristors are employed for the inverter power switching devices and are arranged in an input-commutated topology. This configuration requires only two thyristors to commutate the six main inverter thyristors. Inverter efficiency during motoring operation at motor shaft speeds above 450 rad/sec (4300 rpm) is 92-94% for output power levels above 11 KW (15 hp). The combined ac inverter/charger package weighs 47 kg (103 lbs).



## 2. INTRODUCTION

### 2.1 Background

The Gould Research Center, Electronics Laboratory, completed in August of 1980 the development of a first-generation experimental ac propulsion system, for use in electric passenger vehicles. The ac propulsion system consisted of an inverter, an ac induction motor and the associated control electronics. This experimental development effort was sponsored by the U.S. Department of Energy and managed by the NASA-Lewis Research Center under Contract DEN3-60. In August of 1981, development of a second generation experimental inverter was initiated under NASA-Lewis Contract DEN3-249. The contract objectives were to modify the DEN3-60 inverter power stage topology to include a battery charger, increase the inverter power capability to provide a vehicle with diesel equivalent acceleration performance and reduce the weight and volume of the combined inverter/charger power stage.

Both inverters utilize state-of-the-art thyristor power semiconductors and microprocessor based control circuitry to regulate the speed and torque of a conventional squirrel cage polyphase ac induction motor. The motoring control electronics developed during NASA-Lewis Contract DEN3-60 was used in the development of the DEN3-249 inverter. To realize the increased power capability of the DEN3-249 inverter the motoring control electronics must be tailored to the operating characteristics of the ac induction motor. Performance using the DEN3-60 motoring control electronics only allows inverter operation in non-vehicle driving regimes. Charge control electronics was developed for use with the integral on-board battery charger and added to the system during the second contract.

### 2.2 Objectives

The specific objectives of this contract were:

1. Incorporate an isolated 3 kW on-board battery charger into the existing inverter design.

2. Increase the inverter peak power capability from 26 kW (35 hp) to 34 kW (45 ph).
3. Reduce the volume and weight of the inverter power stage developed under Contract DEN3-60 by 50% and 30%, respectively.

### 2.3 Scope

The contract work scope consisted of the design, fabrication, test, evaluation and delivery of a combined experimental inverter and battery charger power stage for use in electric vehicle applications. The motoring control electronics developed during NASA-Lewis Contract DEN3-60 and a standard ac induction motor were used to test and evaluate the new inverter power stage. Charge control electronics was developed for use with the integral on-board battery charger.

### 3. ANALYSIS AND DESIGN

#### 3.1 Inverter/Charger Requirements

The design of the inverter and integral onboard battery charger was based on the following requirements.

##### 3.1.1 Inverter

The power handling requirements of the inverter power stage were established by five vehicle operating modes;

Repetitive operation per the SAE-J227a, Schedule D driving cycle shown in Figure 3.1-1,

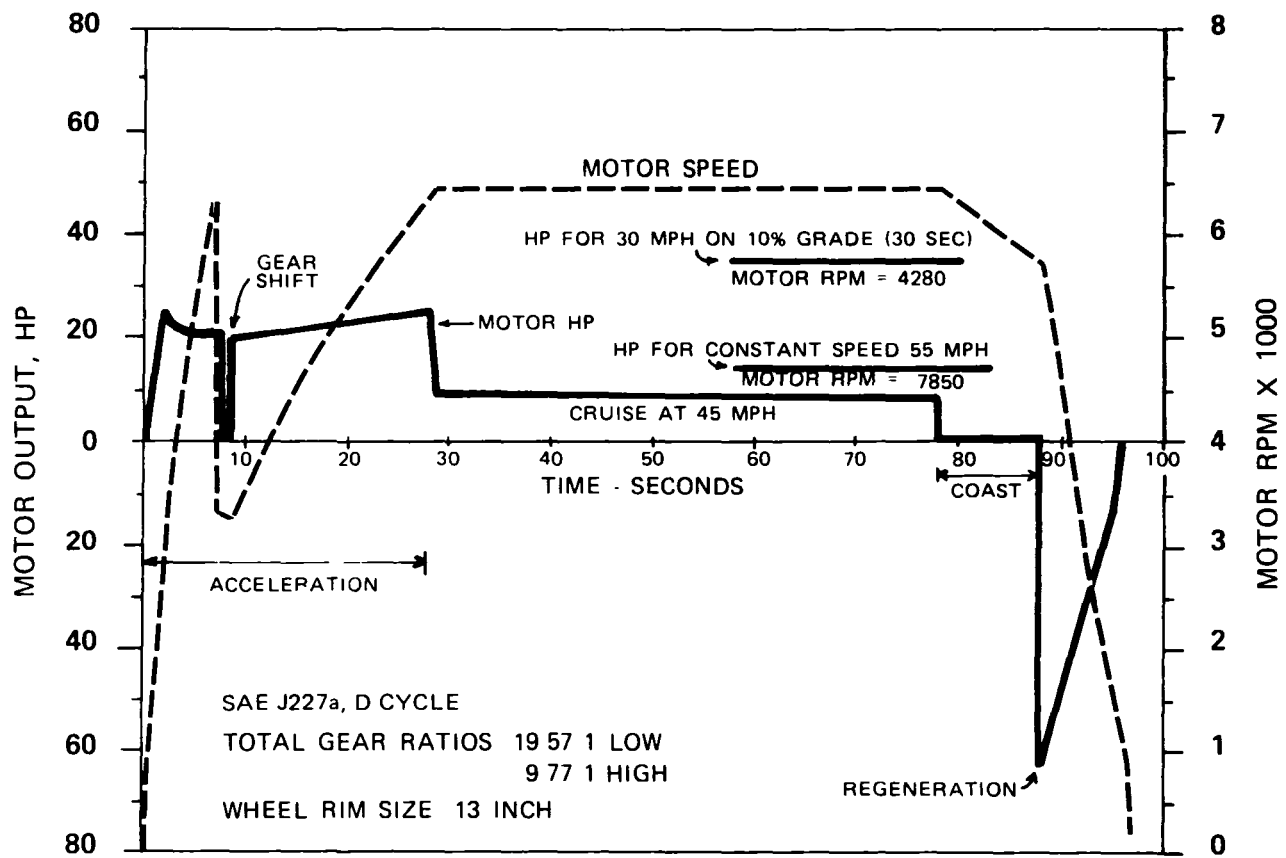
Steady-state operation at a motor shaft power of 11.2 kW (15hp) which corresponds to vehicle operation at a constant 88.5 km/h (55 mph),

Operation at a motor shaft power of 26.1 kW (35 hp) for 30 seconds which corresponds to vehicle operation at 48.3 km/h (30 mph) on a 10% grade,

Operation at an average motor shaft power of 33.6 kW (45 hp) for 16 seconds which corresponds to vehicle acceleration from 40.2 - 88.5 km/h (25-55 mph),

Operation at a motor shaft torque of 60 N-m and an average shaft power of 29.8 kW (40 hp) for a total of 8 seconds which corresponds to a diesel equivalent vehicle acceleration from 0-48.3 km/h (0-30 mph).

The inverter is also to have the capacity to provide regenerative energy to the propulsion battery, be self-protecting, interface with existing and improved lead-acid battery sources and operate over an ambient temperature range of -34°C to 49°C.



(0699)

Figure 3 1-1 SAE - J227a, Schedule D

### 3.1.2 Battery Charger

The design of the battery charger was based on the following requirements;

The charger is to be an integral part of the inverter and utilize the existing power and control circuitry to the greatest extent possible.

The charger is to have the capability of charging a completely discharged lead-acid battery from a nominal 220 volt, 60 Hz, single phase residential power source in less than 8 hours. Charger operation from a nominal 120 volt, 60 Hz ac line is also desired.

The battery is to be isolated from the ac line power source to prevent electric shock hazards to operating personnel.

## 3.2 Inverter

The inverter power circuit topology is presented and its operation described. The design areas addressed to increase the inverter power capability and efficiency are presented. The capability of the new inverter power stage, compared to the DEN3-60 inverter, is presented in Table 3.2-1.

### 3.2.1 Circuit Operation

The input-commutated inverter circuit topology developed during this contract is presented in Figure 3.2-1. The basic goal of minimum materials cost gives the input-commutated topology an important advantage compared to most alternative thyristor inverter configurations as it contains fewer power components. This inverter topology requires only two commutation circuits, one for the positive bus and one for the negative bus, to commutate all six main thyristors in the three-phase bridge.

The power switching stage shown in Figure 3.2-1 allows connection of each of the three motor lines to either the positive or negative battery terminal. The actual conduction paths are provided by the main thyristors (SCR1-6) and the freewheeling rectifiers (D1-6). The remaining semiconductors (SCR7,8, D7,8), transformers (T1,2) and capacitors (C1,2) are involved in the commutation (turn-off) of the main thyristors. This commutation circuitry is necessary to divert the motor current from a conducting main thyristor so that it will regain its voltage blocking capability. Capacitor C3 provides a low impedance path in parallel with the battery for the main inverter and commutation circuit current.

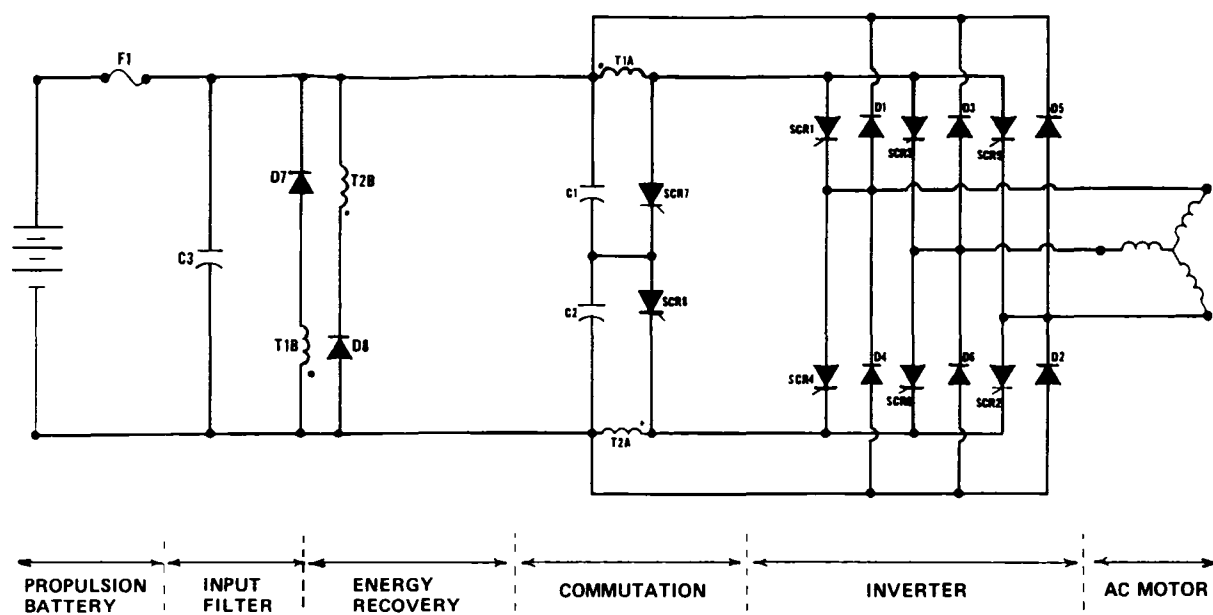
The power circuit initial conditions are presented in Figure 3.2-2 with main thyristors SCR1, 2 and 3 conducting current. It is desired to commutate SCR1 and turn on SCR4. Capacitors C1 and C2 have been charged with voltage polarities as indicated. Commutation thyristor SCR7 is gated on, placing the initial capacitor voltage,  $V_{oc}$ , across transformer winding, T1A. If the voltage across winding T1A is greater than the battery voltage,  $V_B$ , then main

Table 3.2-1

Inverter Power Stage -- Capability

	DEN3-60	DEN3-249
Motor Maximum Line Current:	275 Arms	375 Arms
Nominal Battery Voltage:	120 Vdc	132 Vdc
Motor Peak Shaft Power:	26 kW	33 kW
Efficiency @ 15 kW & 575 rad/sec:	90%	93%
Thermal Capability (PWM):	Limited	Continuous
Weight:	61.3 kg (135 lbs)	46.8 kg (103 lbs)**
Volume:	.087 m <sup>3</sup> (5292 in <sup>3</sup> )	.047 m <sup>3</sup> (2907 in <sup>3</sup> )**

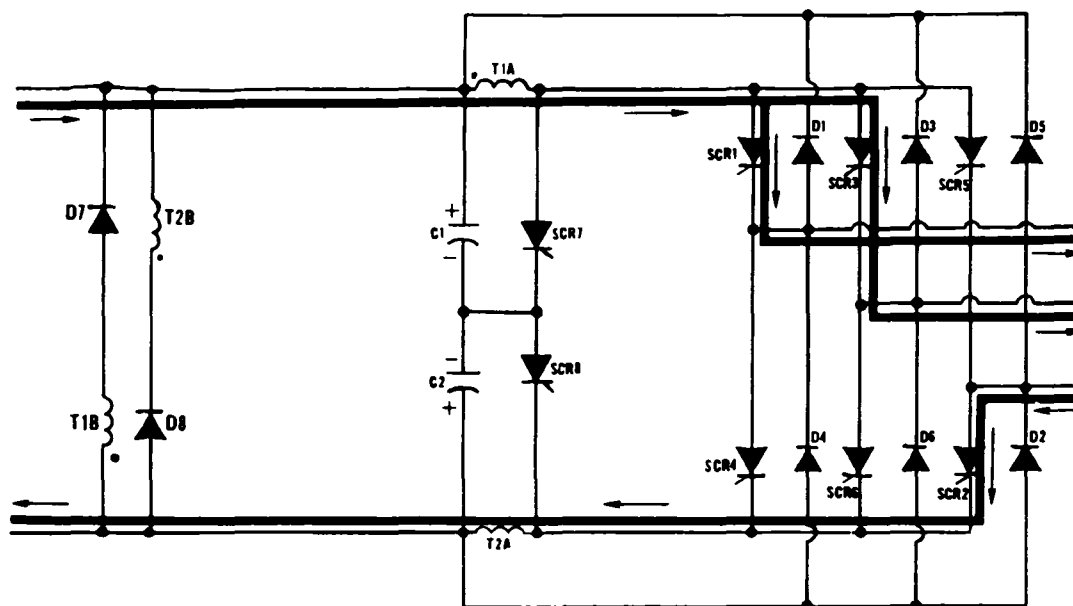
\*\* Includes 3.6 kW Battery Charger



(0691)

Figure 3.2-1 AC Motor Control, Power Circuit



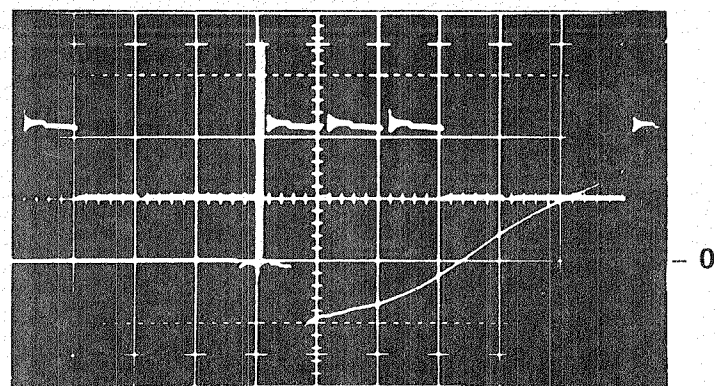


(2603)

**Figure 3.2-2 Initial Power Circuit Current Paths**

thyristors SCR1 and SCR3 will both be reversed biased and turn-off. The circuit paths by which the top main thyristors are reversed biased include winding T1A, the input filter capacitor, C3, and the bottom freewheeling rectifiers (D2, D4, D6). The voltage across thyristor SCR1 during the turn-off interval is shown in Figure 3.2-3. Since thyristors SCR1 and SCR3 are both turned-off their combined current, equal to the peak motor line current ( $I_{pk}$ ) in Figure 3.2-4, is diverted to thyristor SCR7.

Gating commutation thyristor SCR7 will allow C1 to discharge and C2 to charge through the circuit paths indicated in Figure 3.2-5. The current in SCR7 during the commutation interval is shown in Figure 3.2-6. In Figure 3.2-6 the transfer of current from the main thyristors to SCR7 is indicated by the rapid increase in current at the start of the commutation cycle. When the voltage across capacitor C1 has reached a pre-determined value, with polarity as shown in Figure 3.2-5, energy recovery rectifier D7 will be forward biased and current will transfer from thyristor SCR7 to rectifier D7 as indicated by the change in current in Figure 3.2-6 from a half-sinusoidal waveform to a negative sloped ramp. For rectifier D7 to be forward-biased the voltage across winding T1B must be greater than the battery voltage ( $V_B$ ). After rectifier D7 is forward-biased the battery voltage (multiplied by an appropriate turns ratio) will appear across winding T1A and, since capacitor C1 has been charged in the opposite direction, thyristor SCR7 will be reversed-biased and turn-off. The excess energy contained in transformer T1 is returned to the propulsion battery via winding T1B and D7 as shown in Figure 3.2-7. The current in D7 is shown in Figure 3.2-8. Thyristors SCR3 and SCR4 are now gated on and the commutation cycle is completed. The second negative sloped change in current in D7, at the end of the energy recovery interval, is a result of current transferring from winding T1B back to T1A when SCR3 is gated on. The commutation circuitry is now properly charged for a bottom bus commutation which must occur before the top main thyristors can again be commutated.

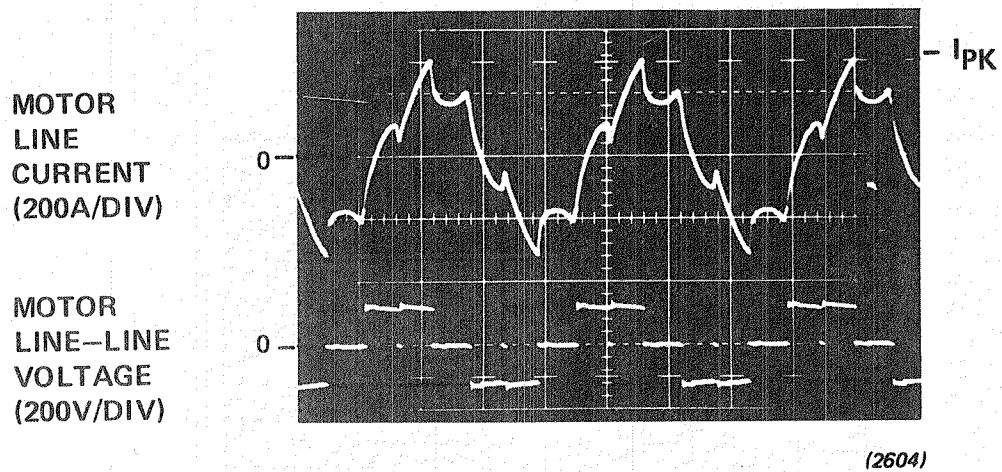


100 V/DIV

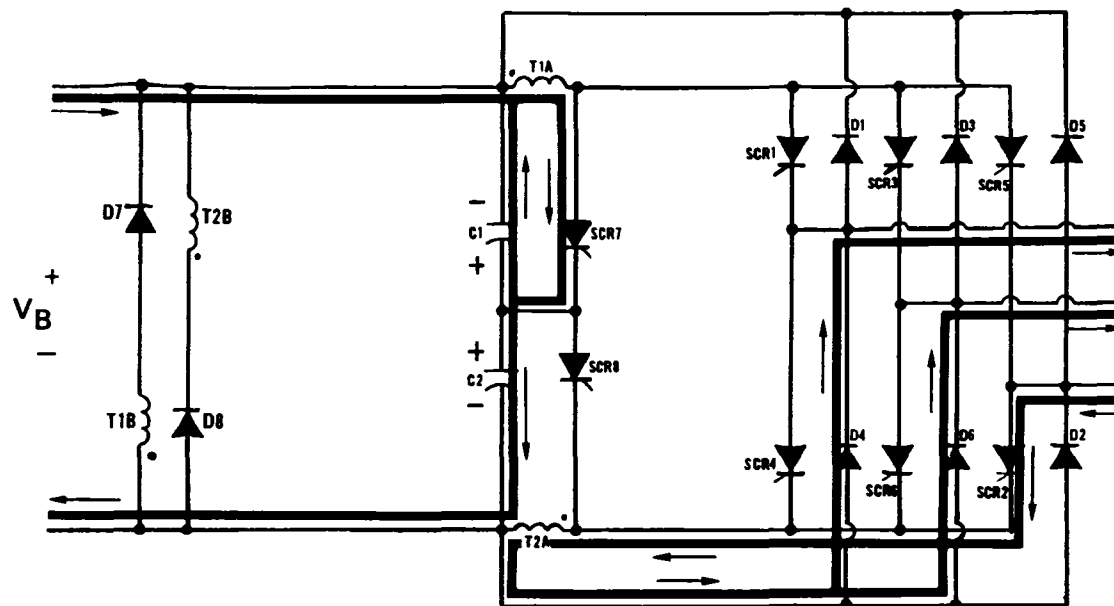
5  $\mu$ SEC/DIV

(2605)

**Figure 3.2-3 Main Thyristor Voltage Waveform during Turn-Off**

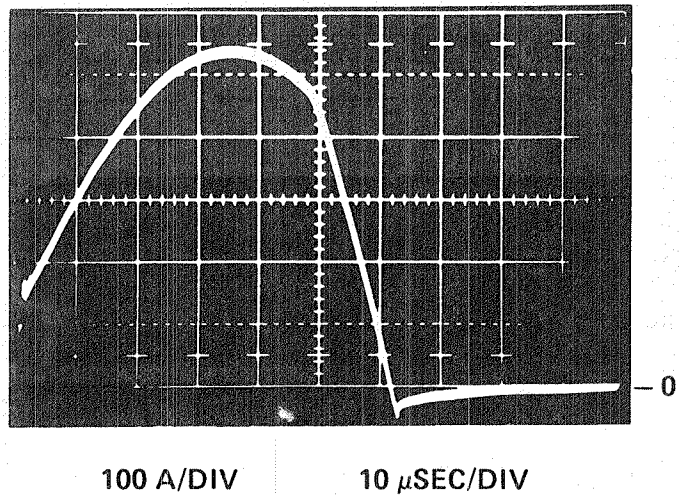


**Figure 3.2-4 Motor Line Current and Line - Line Voltage  
(Six - Step Operation)**



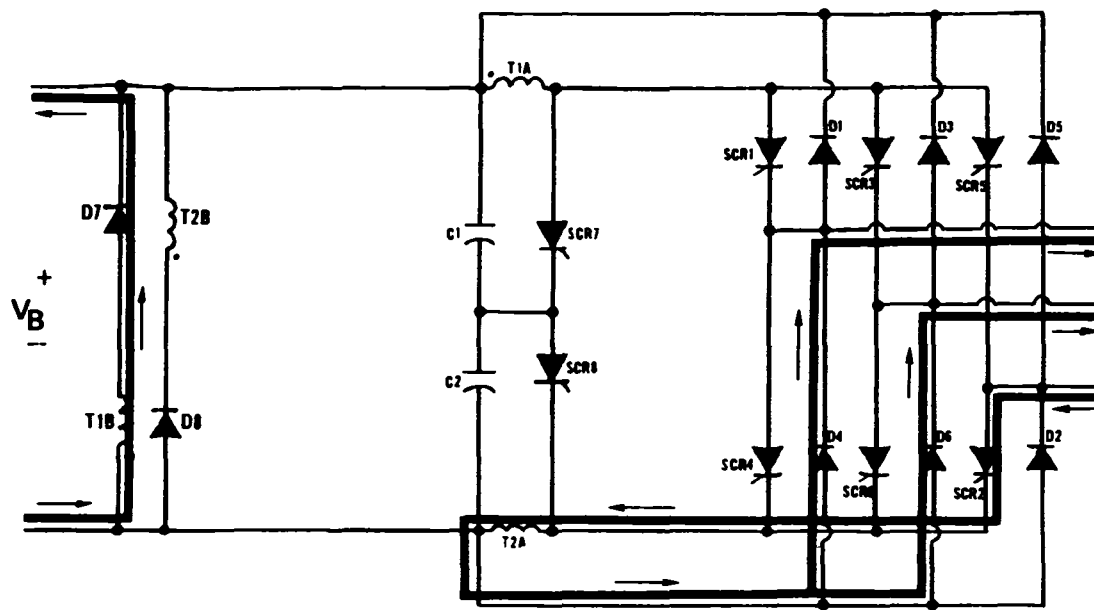
(2602)

Figure 3.2-5 Currents Following the Initiation of a Commutation Cycle



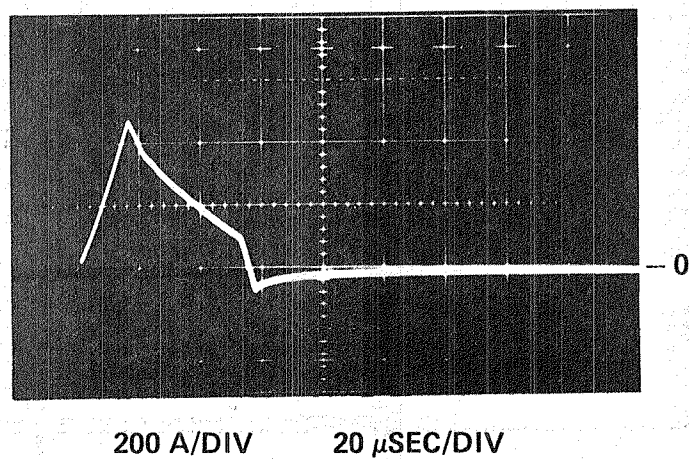
(2606)

**Figure 3.2-6    Commutation Thyristor Current Waveform**



(2601)

Figure 3.2-7 Energy Recovery Current Paths



(2607)

**Figure 3.2-8      Energy Recovery Rectifier Current Waveform**



### 3.2.2 Circuit Parameters

The design issues addressed during this contract to improve the performance of the DEN3-60 inverter power stage are listed in Table 3.2-2. The majority of these improvements were directed at reducing the losses of the commutation circuit by using improved components and by reducing the commutation circuit stored energy. The design relationships used to select the inverter circuit parameters are identified and a discussion of how these circuit parameters were modified to take into account circuit parasitics is presented.

For the input-commutated inverter shown in Figure 3.2-1 the time the main thyristors are reversed-biased, assuming no circuit parasitics, can be expressed as<sup>1</sup>;

$$t_{rev} = \cos^{-1} \left[ \frac{VB/V_{oc}}{1 + \left[ \left( \frac{L}{C} \right) \left( \frac{I_{pk}}{V_{oc}} \right)^2 \right]^{\frac{1}{2}}} \right] - \cos^{-1} \left[ \frac{1}{1 + \left[ \left( \frac{L}{C} \right) \left( \frac{I_{pk}}{V_{oc}} \right)^2 \right]^{\frac{1}{2}}} \right] \frac{\pi [LC]^{\frac{1}{2}}}{180} \quad (1)$$

where;

$t_{rev}$  is the circuit turn-off time,  $VB$  is the propulsion battery voltage,  $V_{oc}$  is the initial voltage on the commutation capacitor,  $I_{pk}$  is the peak motor line current,  $L$  is the magnetizing inductance of winding T1A and  $C$  is the total commutation circuit capacitance ( $C_1 + C_2$ ). For minimum commutation circuit stored energy the capacitance ( $C$ ), inductance ( $L$ ) and initial capacitor voltage are given by <sup>1</sup>;

$$L = \frac{1.8 VB t_{rev}}{I_{pk}} \quad (2)$$

$$C = \frac{1.8 I_{pk} t_{rev}}{VB} \quad (3)$$

$$V_{oc} = 1.8 VB \quad (4)$$

where the commutation circuit stored energy is defined as the total energy

TABLE 3.2-2

Inverter Power Stage -- Design Improvements Areas  
(DEN3-60 vs. DEN3-249)

Commutation Circuit Stored Energy Reduced 50%  
Commutation Magnetics - Quality Factor Increased  
Commutation Capacitors - Quality Factor Increased  
Number of Thyristors Reduced from 10 to 8  
Battery Filter Capacitor Volume Reduced 50%  
Power Stage Volume Reduced 45%  
Power Stage Weight Reduced 25%

stored in L and C and is a function of the peak motor current (which is also the inverter bus current) and initial capacitor voltage as given by;

$$E_s = \frac{1}{2} C V_{oc}^2 + \frac{1}{2} L I_{pk}^2 \quad (5)$$

The commutation circuit component values for minimum stored energy are presented in Figure 3.2-9 as a function of the peak motor line current ( $I_{pk}$ ) for a battery terminal voltage of 120 volts and a main thyristor reverse-bias time of 14 usec. The main thyristors selected were General Electric C384M devices having a maximum specified turn-off time of 10 usec at a junction temperature of 125°C. The nominal battery voltage is 132 volts, however during motoring operation the battery terminal voltage decreases due to the battery internal resistance. The actual component values were selected for minimum stored energy at the peak motor current anticipated during vehicle operation at 15hp (i.e.  $I_{pk} = 200-300$  Amps) as opposed to vehicle operation at 45 hp (i.e., 700 amps). The values selected were a total commutation capacitance (C) of 56 uf and a TIA magnetizing inductance (L) of 11 uh.

Due to the finite leakage inductance existing between the transformer A and B windings and the parasitic inductance present in the commutation circuit, the initial capacitor voltage ( $V_{oc}$ ) increases with increasing motor current as shown in Figure 3.2-10. This second order effect allowed the commutation circuit parameters to be selected for efficient operation at 15 hp while also having the capability to commute the main thyristors at 45 hp. The penalty is increased commutation losses at the higher power levels, however, operation at these power levels (i.e., 45 hp) is only required for 16 seconds. The advantage is more efficient operation at 15 hp.

Under ideal conditions the capacitor voltage will remain constant at 216 volts independent of motor current however, as stated previously the capacitor voltage increases with increasing motor current due to the leakage inductance between the transformer A and B windings. This leakage inductance results in an overshoot in the capacitor voltage that is a function of the energy stored in the commutation circuit. Under ideal conditions the capacitor voltage is given by equation 6;

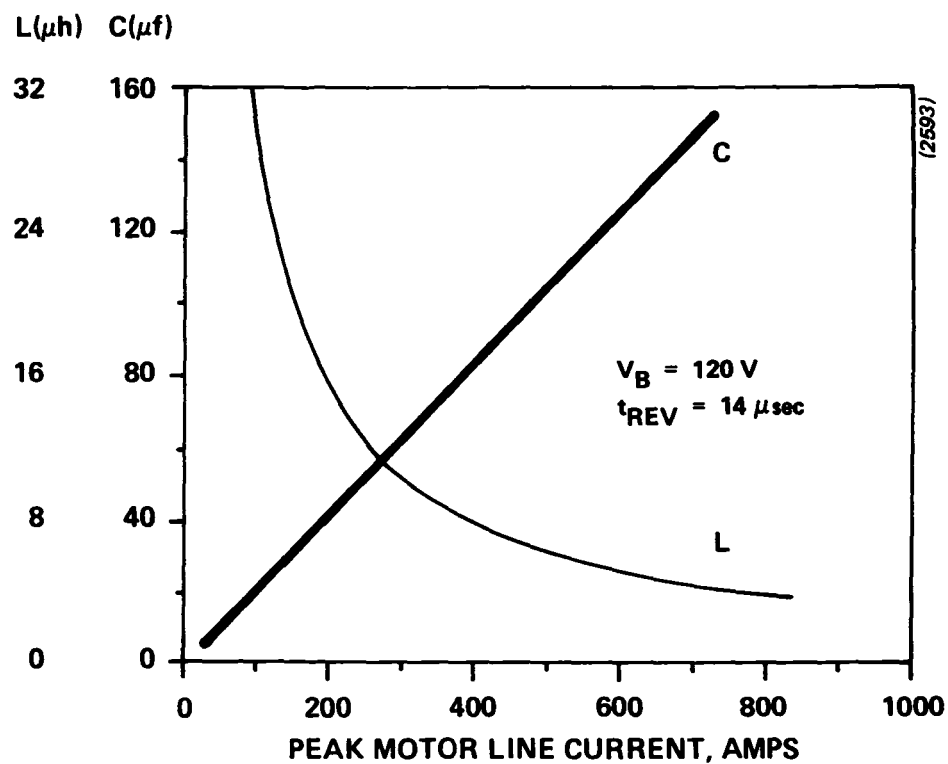


Figure 3.2-9 Optimum Commutation Circuit Parameters Based on Minimum Stored Energy

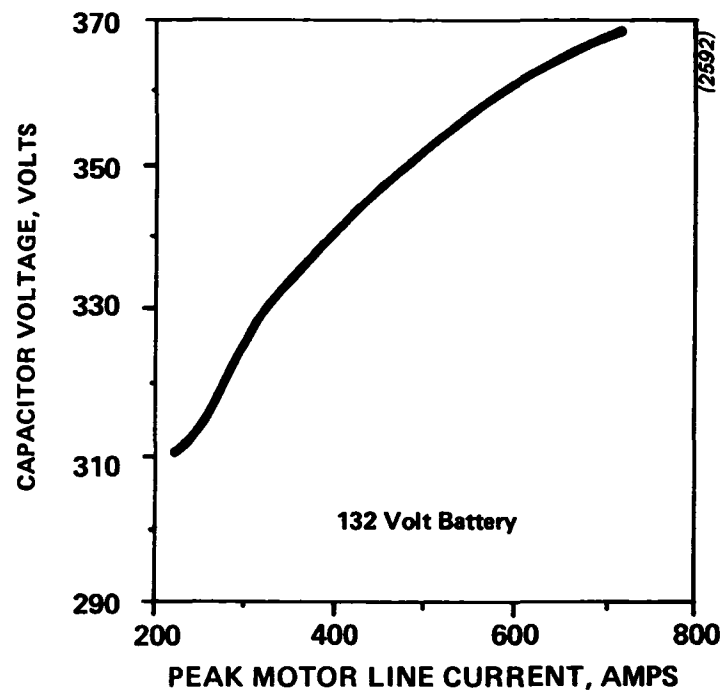


Figure 3.2-10 Commutation Capacitor Voltage ( $V_{OC}$ ) vs. Peak Motor Current (Measured)

$$V_{oc} = V_B (1 + N_A/N_B) \quad (6)$$

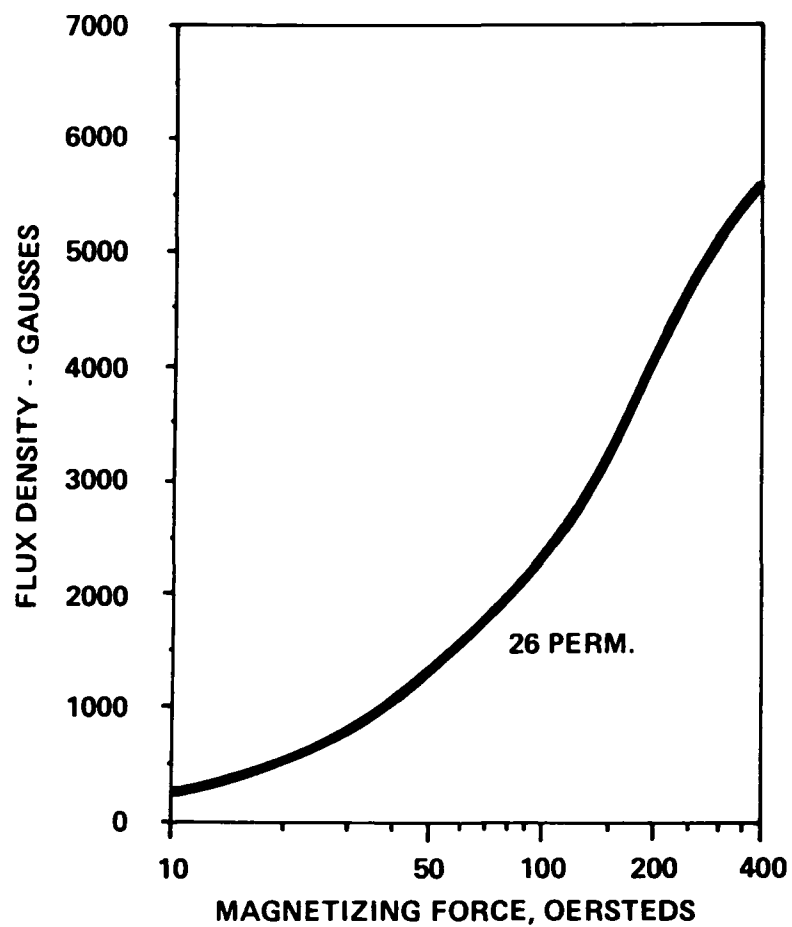
where  $N_A$  is the number of turns on the A winding and  $N_B$  is the number of turns on the B winding. The overshoot in capacitor voltage can be approximated by equation 7 below;

$$\Delta V_{oc} = \left[ \frac{2 E_s}{L} \right]^{\frac{1}{2}} \left[ \frac{N_A}{N_A + N_B} \right] \left[ \frac{L_{stray}}{C} \right]^{\frac{1}{2}} \quad (7)$$

where  $L_{stray}$  is equal to the leakage inductance between the transformer A and B windings (1.8 uh) and the parasitic inductance present in the commutation circuit (1.0 uh). Based on ideal conditions and using equation 6 the turns ratio ( $N_A/N_B$ ) is equal to 0.8. At a peak motor current of 200 amps the calculated overshoot in the commutation capacitor voltage is 66 volts for an initial capacitor voltage of 282 volts ( $V_{oc} + \Delta V_{oc}$ ). As the peak motor current increases above 200 amps the current in the A winding also increases resulting in a further increase in the commutation capacitor overshoot.

A second factor which also increases the sensitivity of the commutation circuit to variations in motor current is the non-linear BH characteristic of the powdered molypermalloy core material used in the commutation transformers. The BH characteristic of this core material is presented in Figure 3.2-11 which indicates that the permeability changes from 26 at 3024 amps/meter (38 oersteds) to 14 at 31832 amps/meter (400 oersteds). This non-linear permeability means that the T1A winding inductance changes from 20 uh at low current levels to approximately 11 uh at high current levels. This permeability change increases the stored energy, at a peak motor current of 200 amps, from 2.45 to 2.7 joules and the initial capacitor voltage from 282 to 286 volts. At higher peak motor currents the increase in capacitor voltage is more significant. For example, at a peak motor current of 700 amps the calculated initial capacitor voltage is 336 volts.

The calculated main thyristor turn-off time for an initial capacitor voltage of 336 volts, a peak motor current of 700 amps and a propulsion battery voltage of 120 volts is 13.9 usec. The measured main thyristor turn-



1 TESLA = 10,000 GAUSS

1 OERSTED = 79.58 AMPS/METER

(2618)

Figure 3.2-11 Powdered Molypermalloy BH Characteristic

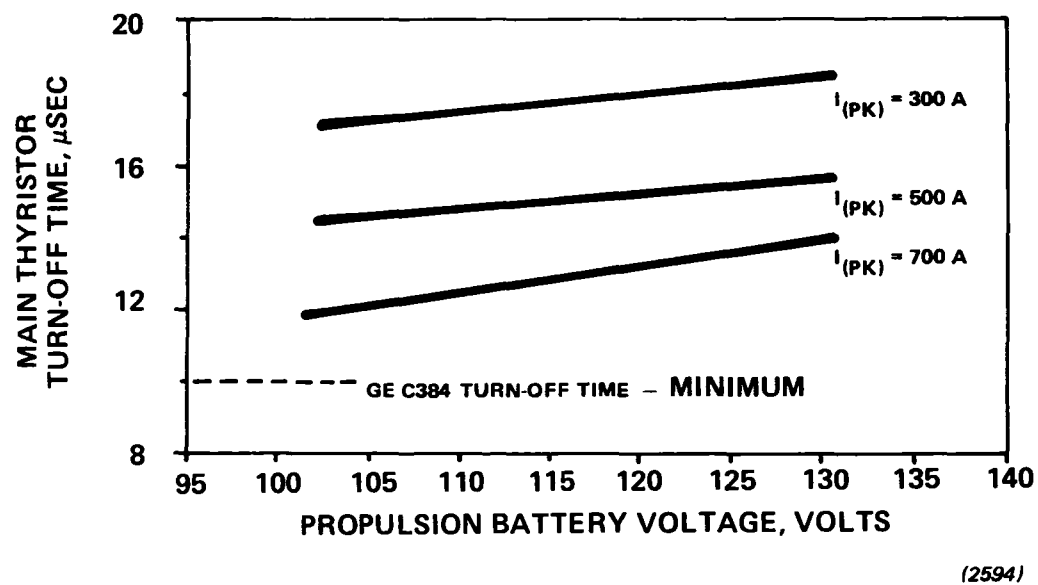


Figure 3.2-12 Main Thyristor Turn-Off Time vs. Battery Voltage (Measured)



off time as a function of peak motor current and propulsion battery voltage is shown in Figure 3.2-12.

The difference in commutation circuit losses between the DEN3-60 inverter and the new inverter is summarized in Table 3.2-3. As indicated previously the energy stored in the commutation circuit of the new inverter at a peak motor current of 200 amps is 2.7 joules. The initial capacitor voltage in the DEN3-60 inverter was held constant at 440 volts (PWM operation) using thyristors as the energy recovery device. The DEN3-60 commutation capacitance was 60 uf and the T1A winding inductance was 5 uh. At a peak motor current of 200 amps the energy stored in the commutation circuit of the DEN3-60 inverter was 5.9 joules.

Each time the commutation thyristor was gated in the DEN3-60 inverter approximately 17% of the commutation circuit stored energy was dissipated as heat. In the new inverter the energy lost per commutation was reduced to 10% of the total stored energy. The reduction in energy lost per commutation was achieved by using powdered molypermalloy core material and litz wire in the construction of the commutation transformers and all-polypropylene commutation capacitors as opposed to paper-polypropylene. As indicated in Table 3.2-3, using lower loss commutation components and minimizing the stored energy reduced the commutation circuit losses by over 70% at a commutation frequency of 1100 Hz. The end result is the new inverter can operate continuously in the PWM mode of operation whereas the DEN3-60 inverter could only operate for a limited period of time due to heating of the commutation capacitors.

TABLE 3.2-3

Commutation Circuit Loss Reduction -- Summary

	DEN3-60	DEN3-249
Stored Energy @ $I_{pk} = 200$ A	5.9 Joules	2.7 Joules
Energy Lost Per Commutation (Kc)	17%	10%
Circuit Power Loss @ Com Freq of 1100 Hz	1100 watts	300 watts

During the development of the DEN3-60 inverter it quickly became evident that the commutation transformers (T1, T2) were responsible for a significant percentage (35%) of the inverter power loss. It was also obvious that to successfully reduce the inverter/charger package volume and provide a battery charger with acceptable efficiency (i.e., 85%) the transformer losses would need to be reduced. To accomplish this a reliable method for measuring transformer loss at high current (i.e., 200 amps) and flux levels (i.e., 3-10 kg) was needed. Based on the hypothesis that the discrete gap present in the tape wound C cores was responsible for a significant percentage of the losses the testing method had to be flexible to allow different core, coil and gap configurations to be tested and compared. This hypothesis was verified and resulted in the use of powdered molypermalloy core material which has a distributed gap.

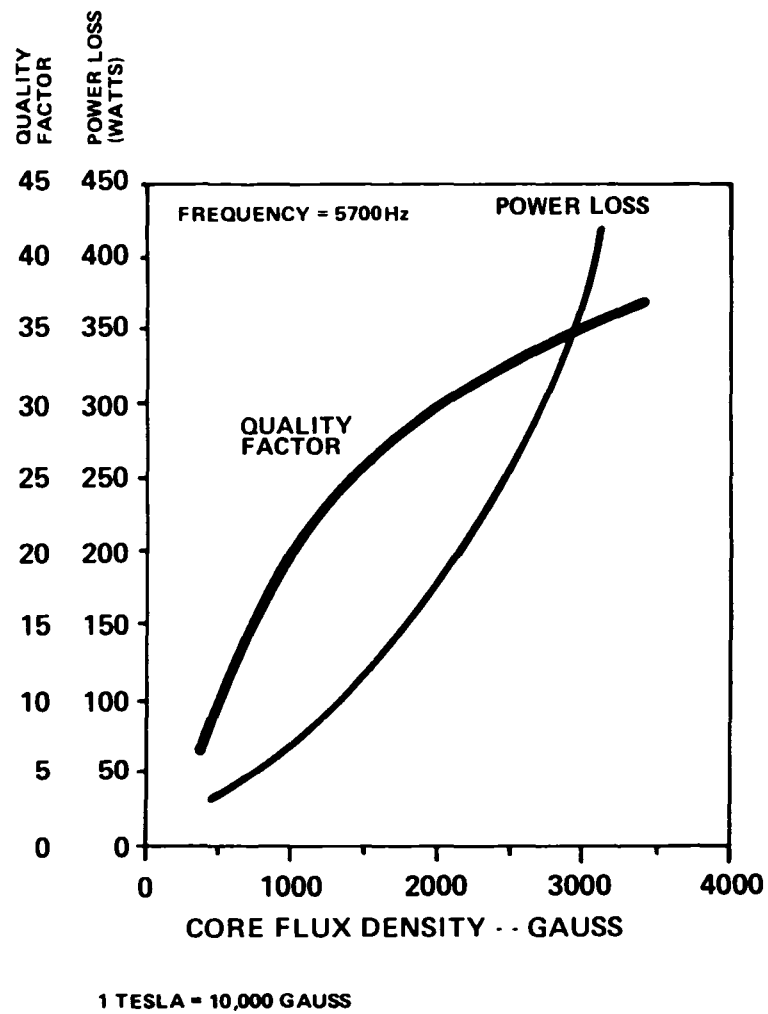
The test method used was to connect one winding (T1A) of the commutation transformer in parallel with a low-loss capacitor and excite the resulting LC network with a high power amplifier. The resonant frequency of this parallel LC network was determined by adjusting the amplifier frequency until the input current to the LC network was at its minimum value. At the resulting resonant frequency point the RMS current in the parallel LC circuit ( $I_L$ ), the RMS value of the fundamental input current and the RMS voltage across the LC circuit were measured. The quality factor (Q) of the LC network was determined using the definition for Q given by equation 8 below;

$$Q = 2\pi \frac{\text{Peak Stored Energy}}{\text{Energy Lost Per Cycle}} \quad [8]$$

To improve the reliability of these measurements the capacitor effective resistance ( $R_{eff}$ ) as a function of frequency and current was determined using the above resonant frequency test procedure and an air coil inductor fabricated from litz wire. The power lost in the capacitor ( $I_L^2 R_{eff}$ ) was subtracted from the total power lost in the LC network to obtain the transformer (T1A winding) power loss and quality factor. Several different types of capacitors were evaluated with a metalized polypropylene capacitor having high current terminations selected for core testing over an all-polypropylene capacitor due to its constant effective resistance with frequency and

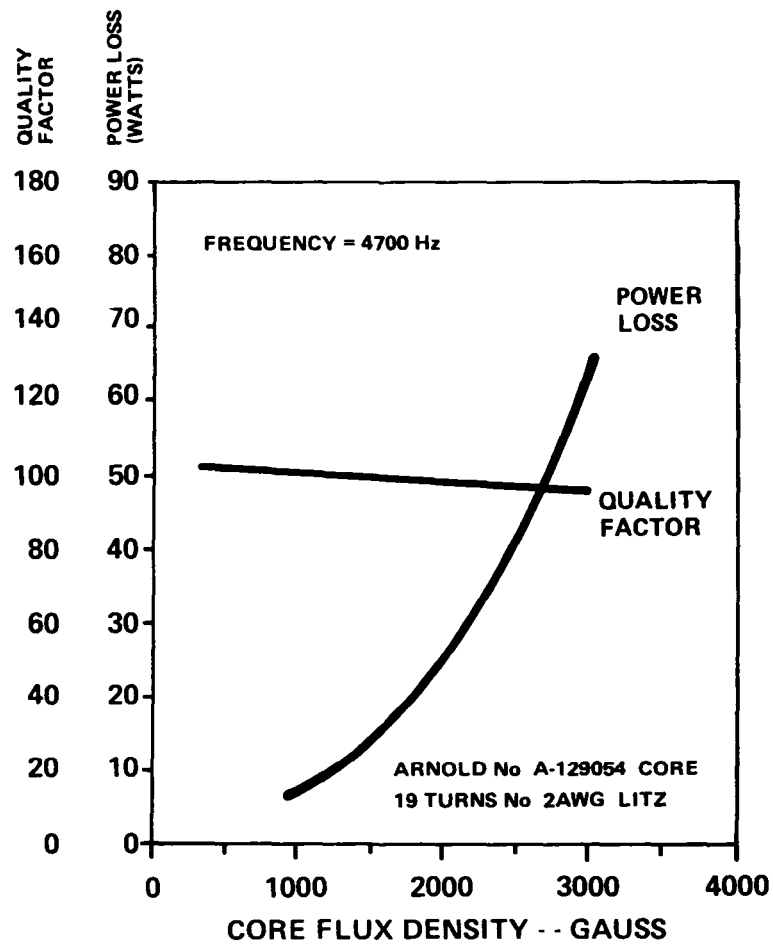
current. The RMS value of the fundamental input current was measured using a Princeton Applied Research lock-in amplifier (Model 5204). The lock-in amplifier was required due to the third harmonic input current produced by the core non-linear BH characteristic, especially with the powdered molypermalloy material.

The measured power loss and quality factor for the commutation transformer (T1A winding) used in the DEN3-60 inverter and a comparable transformer constructed using powdered molypermalloy core material and litz wire is presented in Figures 3.2-13 and 3.2-14 respectively. The significant increase in quality factor obtained using the powdered molypermalloy core material is evident. Based on separate tests performed using the DEN3-60 transformer core material (2 mil silicon-iron), it was determined that approximately 50% of the transformer losses were attributable to core and coil losses resulting from fringing fields at the gap. The results are summarized in Table 3.2-4.



(2619)

**Figure 3.2-13 Commutation Transformer (T1A)  
Power Loss/Q vs. Core Flux Density (DEN3-60)**



1 TESLA = 10,000 GAUSS

(2620)

**Figure 3.2-14 Powdered Molypermalloy Transformer (T1A)  
 Loss/Q vs. Core Flux Density**

TABLE 3.2-4

## Inverter Power Stage -- Magnetics Improvement (T1, T2)

	<u>DEN3-60</u>	<u>DEN3-249</u>
Quality Factor	35	100
Core Material	2-Mil Silicon-Iron	Powdered Molypermalloy
Construction	Tape Wound C-core	Toroidal
Core Loss	20%	60%
Coil Loss	30%	40%
Core Loss Due to Gap	25%	-
Coil Loss Due to Gap	25%	-

### 3.3 Integral Battery Charger

Operation of the integral on-board battery charger is described and the inverter power stage components used to perform the battery charging function are identified. The design criteria used to select the charger circuit parameters is presented.

The charger developed during this program provides the features listed in Table 3.3-1 with the addition of a four-pole circuit breaker to the inverter power stage as illustrated in Figure 3.3-1. Existing semiconductors are used to convert the ac line voltage into a dc voltage suitable for charging the propulsion battery. Existing transformers, used during motoring to commutate the main inverter thyristors, are used in combination with the circuit breaker to isolate the propulsion battery from the ac line.

#### 3.3.1 Charger Power Circuit Operation

Charger operation is described with the aid of Figures 3.3-1 and 3.3-2. Voltage is supplied to all three phases of the inverter with the ac motor inductance being used to limit the in-rush current. The main rectifiers are used in a bridge configuration to convert the ac line voltage to a full-wave rectified dc voltage which appears across the ac line filter capacitor C4. By operating the circuit consisting of T1, T2, C1, C2, SCR7 and SCR8 as a resonant converter, in a manner similar to that used during motoring operation, energy is transferred from the ac line and capacitor C4 to the propulsion battery via transformer secondary windings T1B and T2B and rectifiers D7 and D8.

During charger operation the circuit breaker is open to separate the battery from the ac line. Isolation is provided via transformers T1 and T2. Capacitor C3 is used to filter the high-frequency charging current. During motoring operation capacitors C1A/C1B and C2A/C2B in Figure 3.3-1 are connected in parallel to provide the required commutation capacitance. During charger operation the circuit breaker separates these capacitors to provide the ac line filter capacitance, C4 (C1A and C2A in series) and the capacitance required for charger resonant circuit operation (C1B and C2B).

Table 3.3-1

INTEGRAL BATTERY CHARGER -- CAPABILITY

Input Voltage Range:	84 - 264 Vac, single phase
Output Voltage Range:	80 - 180 Vdc
Output Power Rating at 220 Vac/20 Amps:	3.6 kW
Output Power Rating at 120 Vac/20 Amps:	1.8 kW
Efficiency at Rated Power:	80 - 86 %
Power Factor at Rated Power:	95%
Charge Profile:	Dual-Level Constant Current





3 - 31

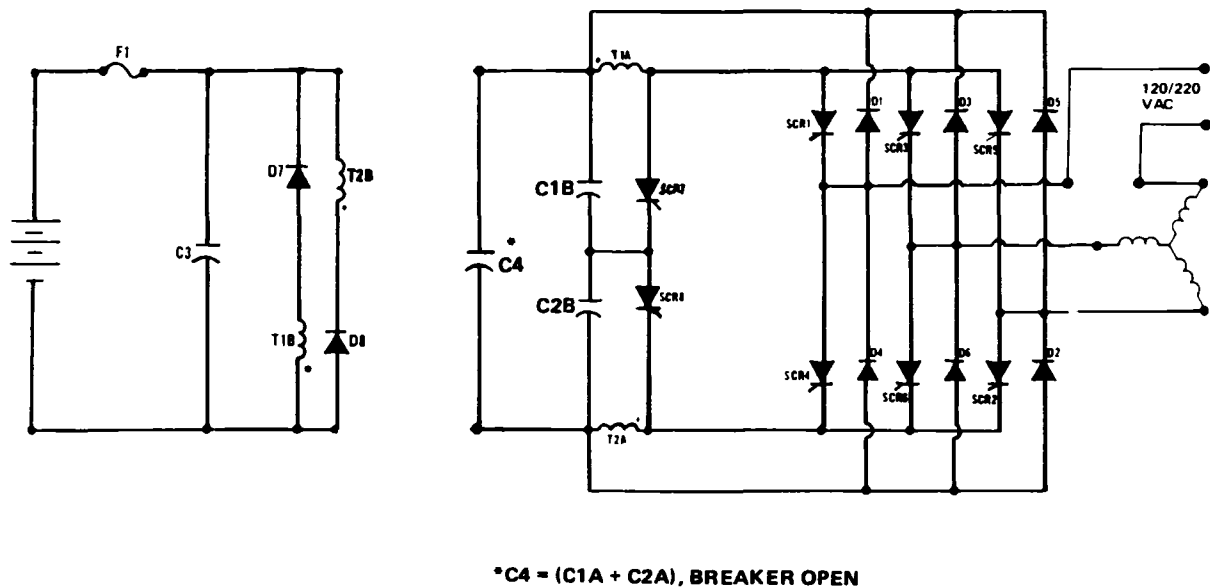


Figure 3.3-2 Controller/Charger Power Circuit – Breaker Open

The power transferred from the ac line to the propulsion battery is a function of the ac line voltage, the capacitance of C1B, C2B and C4, the frequency at which SCR7 and SCR8 are gated ( $f_g$ ) and the efficiency of the resonant LC circuit. Since circuit operation is the same when either SCR7 or SCR8 is gated, the power transferred to the propulsion battery is derived assuming SCR7 is conducting.

Each time SCR7 is gated, energy stored in capacitors C1B and C2B is transferred to the magnetizing inductance (L) of transformer winding T1A. Since the circuit formed by C1B, C2B, T1A and SCR7 is a resonant circuit the current in winding T1A will increase in a sinusoidal manner with the maximum current ( $I_m$ ) being a function of L,  $C_T$  and the initial voltage ( $V_{oc}$ ) on C1B as given by;

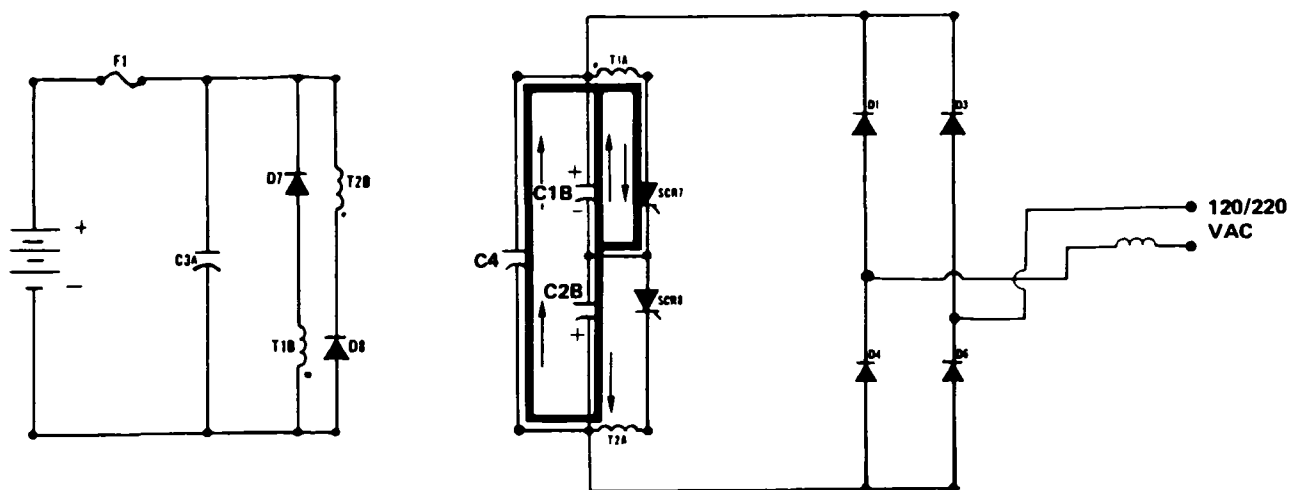
$$I_m = [C_T/L]^{1/2} V_{oc} \quad (1)$$

where  $C_T$  is the total resonant circuit capacitance and is equal to the sum of C1B plus C2B in parallel with C4. When the current in winding T1A is at its maximum value the voltage across capacitor C1B will be zero. As the current decreases from its maximum value capacitors C1B and C2B will charge up with polarities opposite those shown in Figure 3.3-3. When the voltage across capacitor C1B has charged to a value higher than the propulsion battery voltage as determined by the A and B winding turn ratio, rectifier D7 will be forward biased and current will transfer to winding T1B, D7 and the propulsion battery. When this occurs the voltage across capacitor C1B will be higher than the reflected voltage across winding T1A and SCR7 will be reversed biased and turn-off.

The point at which rectifier D7 is forward-biased, shown as  $\theta_T$  in Figure 3.3-4, is given by;

$$\theta_T = 90^\circ + \sin^{-1} (1 - VC4/V_{oc}) \quad (2)$$

where VC4 is the voltage on capacitor C4 and  $V_{oc}$  is the initial voltage on capacitor C1B. The current in the magnetizing inductance, L, of winding T1A



(2598)

**Figure 3.3-3**      **Charger Current Paths after SCR7 Gated**

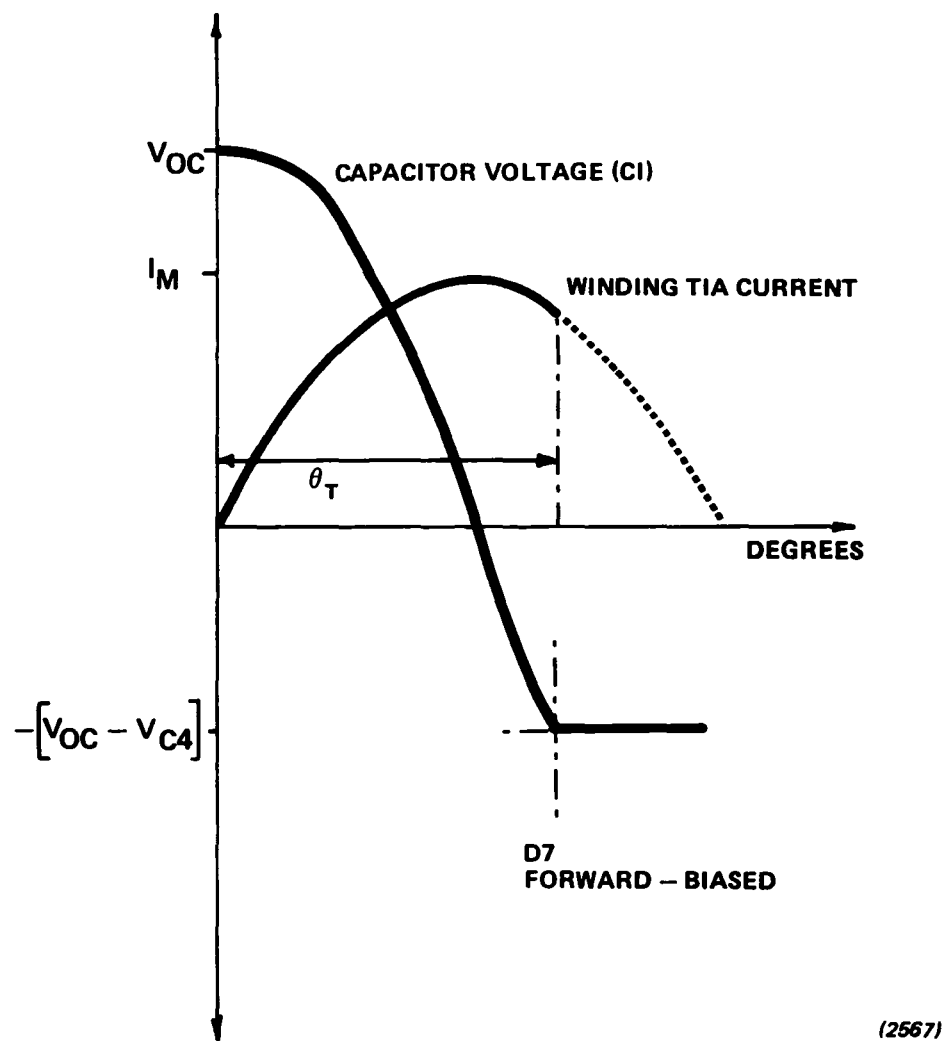


Figure 3.3-4 Capacitor Voltage and Winding Current (TIA) after SCR7 is Gated

when rectifier D7 is forward biased is given by;

$$I_T = I_m \sin \theta_T \quad (3)$$

The power available for charging the propulsion battery is determined by the combined frequency at which SCR7 and SCR8 are gated and the angle ( $\theta_T$ ) at which rectifier D7 becomes forward biased as given by;

$$P_T = \frac{1}{2} L I_T^2 f g \quad (4)$$

Combining equations 1, 3 and 4 the expression for the total power available for transfer to the propulsion battery becomes,

$$P_T = \frac{1}{2} C_T f g V_{oc}^2 \sin^2 \theta_T \quad (5)$$

Each time the resonant circuit is cycled (SCR7 or SCR8 gated) a fixed percentage ( $K_c$ ) of the initial energy stored in the total resonant circuit capacitance,  $C_T$ , is dissipated. The power lost can be expressed as,

$$P_{Loss} = \frac{1}{2} C_T f g V_{oc}^2 K_c \quad (6)$$

Subtracting the total power lost (eq. 6) from the total power available (eq. 5) we obtain the following expression for the charger output power.

$$P_{out} = \frac{1}{2} C_T f g V_{oc}^2 [\sin^2 \theta_T - K_c] \quad (7)$$

The expression for charger efficiency is defined as;

$$\eta = P_{out} / P_T \times 100\% \quad (8)$$

Substituting equations [5] and [7] into equation [8] we obtain;

$$\eta = [1 - K_c / \sin^2 \theta_T] \times 100\% \quad (9)$$

As is evident from equation [9] charger efficiency is primarily dependent on the resonant circuit loss factor ( $K_c$ ) and the angle ( $\theta_T$ ) at which rectifier D7 becomes forward-biased.

### 3.3.2 Circuit Parameters

The charger circuit parameters established by the inverter motoring requirements are; the magnetizing inductance of transformer winding T1A (L), the total inverter commutation capacitance ( $C1+C2$ ) the battery filter capacitance, C3, the transformer turns ratio (NB/NA) and the current ratings of thyristors SCR7-8 and rectifiers D7-D8.

Flexibility in tailoring the performance of the charger was made possible using circuit breaker pole CB1D shown in Figure 3.3-1. This breaker pole allowed the charger resonant circuit capacitance to be decreased and the thyristor (SCR7/8) gating frequency to be increased in order to maximize the charger input ac line power factor. The charger resonant circuit capacitance was selected based on the output power required and the maximum frequency at which thyristors SCR7/8 can be gated.

The maximum gating frequency of thyristors SCR7/8 is approximately 13kHz and is a function of the transformer T1A winding inductance, the charger circuit capacitance, the time required to transfer current from thyristor SCR7 to rectifier D7, the thyristor reverse recovery time and the margin needed to allow SCR7 to regain its blocking capability before thyristor SCR8 is gated on. Charger output power at 13 kHz is shown in Figure 3.3-5 as a function of charger circuit capacitance,  $C_T$ , for 120 Vac operation at low line conditions. For a charger output power capability of 2000-2500 watts at 108 Vac the required charger circuit capacitance is in the range of 10-13 uf. The capacitance values selected were 8 uf for C1B and C2B and 10 uf for C4 for a total circuit capacitance of 12.4 uf.

To provide a charger output power of 3 kW at 220 Vac with a 20 amp ac line circuit breaker the input capacitance, C4, must be small to minimize the ac line reactive current. The relationship between power factor and input capacitance, C4, is shown in Figure 3.3-6. To achieve an input power factor

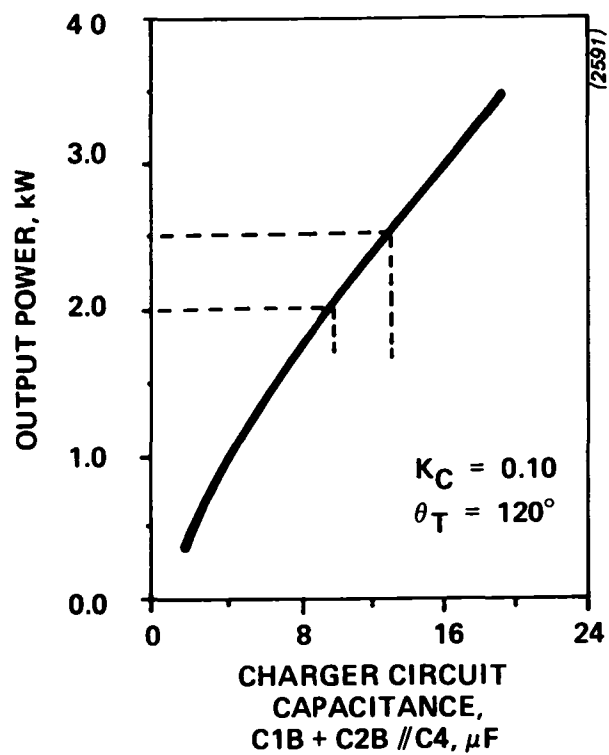


**Figure 3.3-5** Charger Output Power at Maximum Gating Frequency - - - 108 VAC



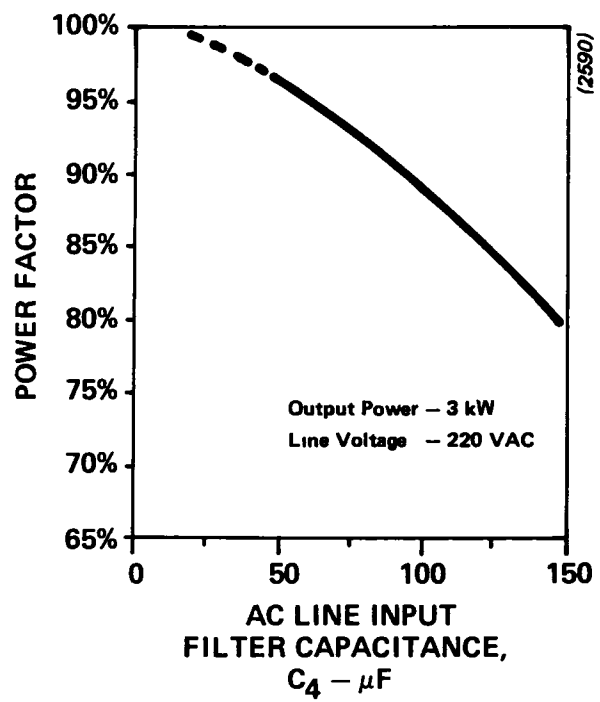


Figure 3.3-6 Charger Power Factor vs. Input Capacitance —  $C_4$

greater than 90% at 220 Vac and 3 kW the input capacitance must be less than 100 uf. The input line capacitor must also have a high rms current rating, since it filters the current pulses generated by the resonant LC circuit, and a voltage rating consistent with 220 Vac operation (i.e. 400 volts). To satisfy all three requirements the inverter commutation capacitors were used as input capacitors during charger operation. The capacitance of C1A and C2A in series 10 uf. The RMS current and peak voltage rating of C1A is 200 amps and 500 volts.

### 3.4 Inverter/Charger Package

The major areas addressed to significantly reduce the package weight and volume are listed in Table 3.4-1. Minimizing the commutation circuit losses described previously was obviously important to achieving the desired reduction in package weight and volume. The use of all-polypropylene commutation capacitors and powdered molypermalloy transformer core material resulted in significant reductions in the dissipation of these components with the result that the inverter has the capability to operate continuously in both six-step and PWM modes of operation. The use of forced air cooling, double-side cooled semiconductors (to reduce the semiconductor junction to ambient-air thermal resistance) and heatsinks sized specifically for each semiconductor were all contributing factors in reducing the package weight and volume.

#### 3.4.1 Mechanical Description

The integral inverter/charger power stage package is shown in Figure 3.4-1. The volume and weight of the power stage is  $.048\text{m}^3$  (2907)  $\text{in}^3$  and 47 kg (103 lbs). A comparison of package dimensions, volume and weight with previously developed electric vehicle inverter power stages is presented in Table 3.4-2. The significant reduction in weight and volume, especially considering that an isolated 3.6 kw battery charger is included in the same package, can be expected to dispel the misconception that thyristor inverters must by nature be large and heavy. As indicated in Table 3.4-1 the ac inverter/charger package is smaller than the dc controller developed for the ETV-1 electric vehicle.

A factor in reducing the package volume was mounting the power components on both sides of a central panel. The end result is shown in Figure 3.4-2 with the semiconductor devices located on the bottom and the commutation components, filter capacitors and circuit breaker located on the top of this central panel. This approach provided two advantages; 1) it allowed the air-flow through the semiconductor heatsinks to be maximized by baffling the air flow through the top half of the package and 2) it minimized the package parasitic inductances.

TABLE 3.4-1

Areas Addressed to Reduce Package Volume

Component Losses Reduced  
 Double-side Cooled Semiconductors Used  
 Forced Air-cooling  
 Heatsinks Sized Specifically for Each Device  
 Two-level Package Design

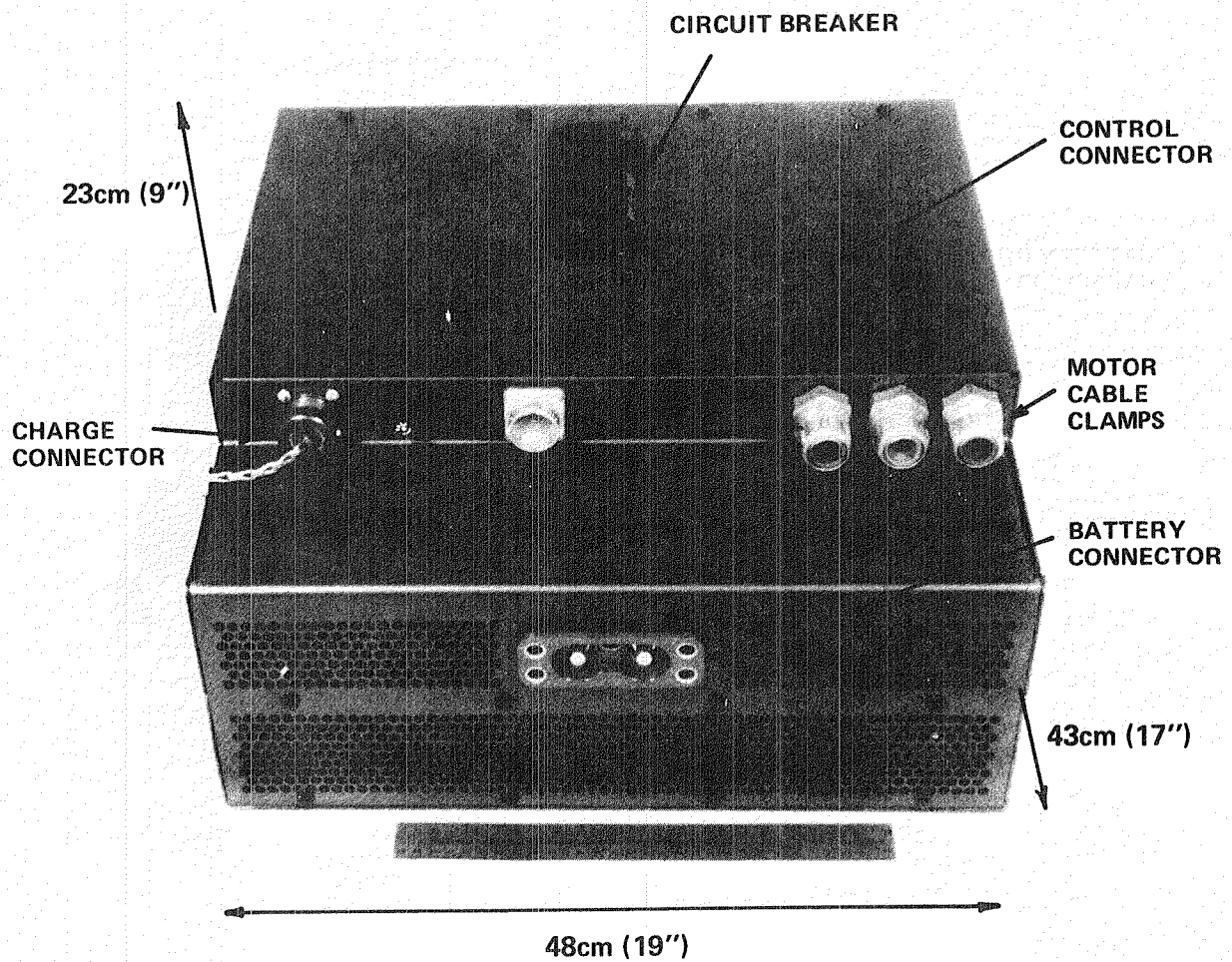
Table 3.4-2

Inverter Power Stage -- Package Comparison

	<u>Vol m<sup>2</sup> (in<sup>3</sup>)</u>	<u>Weight kg (lbs)</u>	<u>Dimensions cm (in)</u>
Gould (DEN3-60)	.087 (5292)	61 (135)	71x53x23 (28x21x9)
GE (DEN3-59)	.130 (7904)	59 (130)	96x66x20 (38x26x8)
Eaton (DEN3-125)	.083 (5040)	60 (131)	71x51x23 (28x20x9)
GE (ETV-1, dc) †	.052 (3168)	43 (95)	56x41x23 (22x16x9)
Gould (DEN3-249)*	.048 (2907)	47 (103)	48x43x23 (19x17x9)

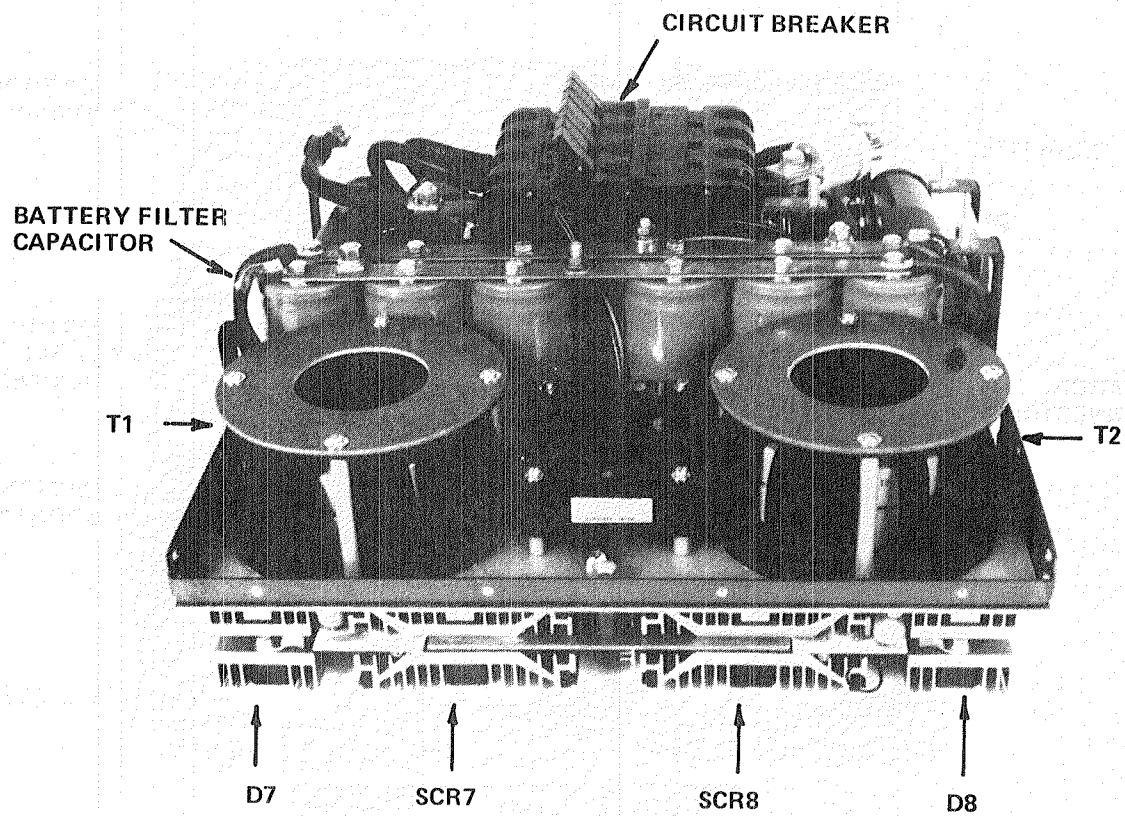
† Includes non-isolated 2.5 kW battery charger

\* Includes Isolated 3.6 kW Battery Charger



(2996)

**Figure 3.4-1** Integral AC Inverter / Charger Power Stage Package



(2997)

Figure 3.4-2 Inverter / Charger Package — Cover Removed

### 3.4.2 Package Weight and Volume

The weight of the individual components and assemblies used in the inverter/charger power stage are listed in Table 3.4-3. Included with the inverter/charger package is a removable fan assembly, which has been sized specifically for dynamometer testing. Utilizing vehicle ram air would significantly reduce the weight and volume of the fan assembly.

The main thyristors (SCR1-6) require the largest heatsinks as a result of the inverter peak and steady-state power requirements. The main rectifier heatsink assembly is 40% smaller as their average dissipation is lower and their maximum junction temperature is higher than the main thyristors (175°C versus 125°C). In a similar fashion the dissipation of the commutation thyristors (SCR7-8) is greater than the energy recovery rectifiers. The weight distribution of the power stage components by function is shown in Figure 3.4-4. As expected the commutation components account for the largest percentage (37%) of the power stage weight.

TABLE 3.4-3

## Inverter/Charger Component Weights

	<u>gm</u>	<u>lbs</u>
Main Thyristor Assy (SCR1-6)	5876	(13)
Main Rectifier Assy (D1-6)	3516	(8)
Com Thyristor Assy (SCR7-8)	1906	(4)
Clamp Rectifier Assy (D7-8)	1146	(3)
Commutation Transformers (T1-2)	9734	(22)
Commutation Capacitors (C1-2)	4568	(10)
Circuit Breaker	2937	(6)
Battery Filter Capacitors (C3)	2826	(6)
Enclosure Aluminum Panels	4911	(11)
Component Mounting Panel	2703	(6)
Bus Bars	2198	(5)
Cable	667	(1)
Current Transducer	1024	(2)
Gate Drive & Snubber PCB's	612	(1)
Battery Shunt/Fuses	575	(1)
Misc (Control Cable, Connectors, Hardware, Etc.)	<u>1569</u>	<u>(4)</u>
Total (Inverter/Charger)	46762	(103 lbs)
Fans	2024	(4)
Fan dc/dc Converter	817	(2)
Mounting Panel	<u>575</u>	<u>(1)</u>
Total (Fan Assembly)	3416	(7.5 lbs)



TABLE 3.4-4

## Inverter/Charger -- Weight Distribution

Commutation Circuit Components	37.1%
Transformers (20.8%)	
Capacitors (9.8%)	
Semiconductors/Heatsinks (6.5%)	
Main Semiconductors/Heatsinks	20.1%
Thyristors (12.6%)	
Rectifiers (7.5%)	
Enclosure and Structural Components	16.3%
Circuit Breaker	6.3%
Bus Bars and Cable	6.1%
Battery Filter Capacitors	6.0%
Misc. (Fuses, Control Cable, Connectors, Etc.)	5.6%
Current Transducers/Shunts	2.5%

## 4. TEST AND EVALUATION

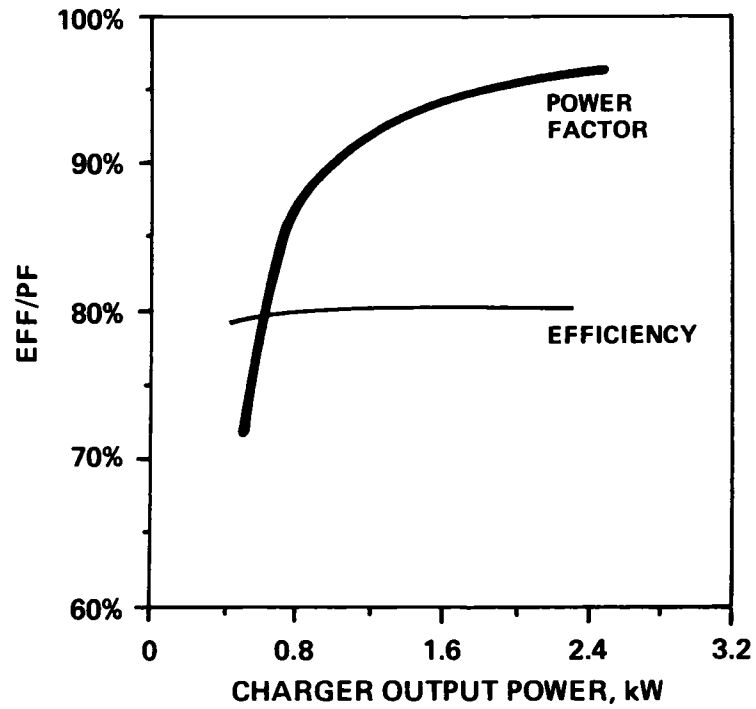
### 4.1 Charger Operation

Operation of the integral on-board battery charger is described with efficiency, power factor and charge profile test results presented.

Operation of the on-board charger requires connecting the charge cable from the ac line interface unit to the power stage and placing the keyswitch in the charge position. The charge control electronics will automatically move the power stage circuit breaker to the charge position, close the ac line contactor located in the interface unit and after a 10 second time delay activate the charger. The initial battery charge current will be selected automatically depending on the ac line voltage applied to the charger. For example, the initial charge current will be 10 amps at 120 vac and 20 amps at 220 vac.

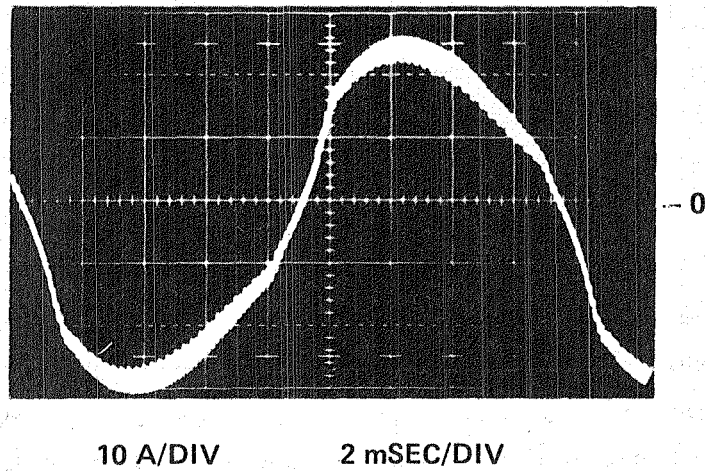
#### 4.1.1 120 Vac Operation

Measured charger efficiency and power factor as a function of charger output power is presented in Figure 4.1-1 for 120 Vac operation. As shown, charger efficiency is constant at approximately 80% over a wide output power range. Charger power factor at 120 Vac and rated output power(1.8kW) is in the range of 95%. The input ac line current waveform at 120 Vac and an output power of 1.8 kW is shown in Figure 4.1-2. The total harmonic distortion of the current waveform shown in Figure 4.1-2 is 12%.



(2586)

**Figure 4.1-1** Charger Efficiency/Power Factor vs. Output Power  
@ 120 VAC



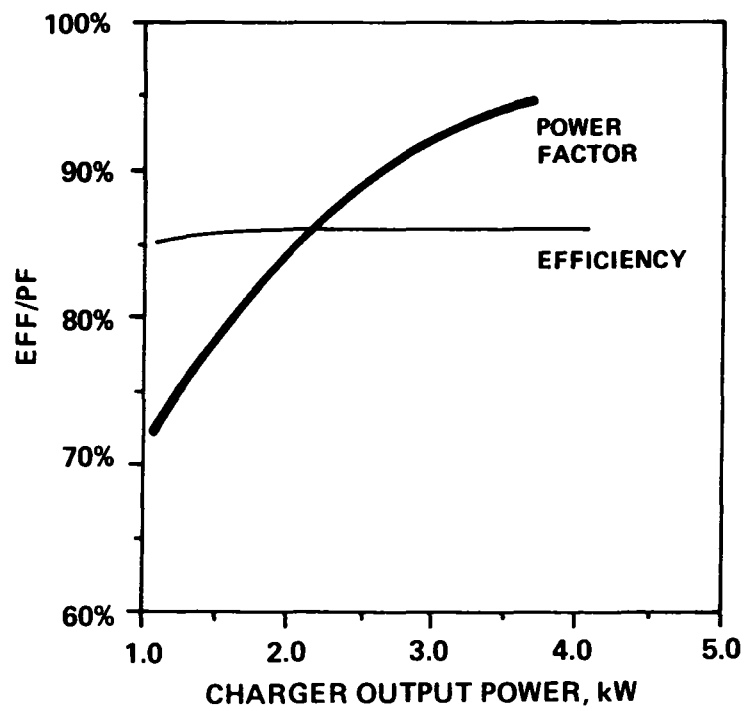
(2608)

**Figure 4.1-2 AC Line Current Waveform at 1.8 kW --- 120 VAC**

#### 4.1.2 220 Vac Operation

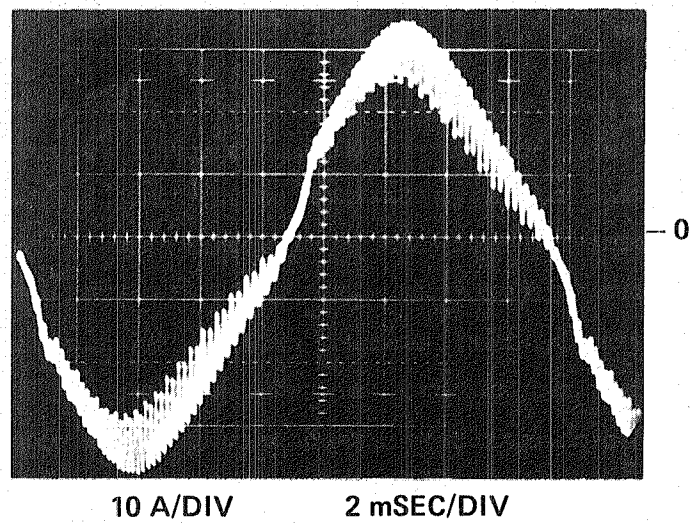
Measured charger efficiency and power factor as a function of output power is presented in Figure 4.1-3 for 220 Vac operation. At this ac line voltage charger efficiency is constant at approximately 86% over a wide output power range. Charger power factor at 220 Vac and rated output power (3.6 kW) is in the range of 95%. The input ac line current waveform at 220 Vac and an output power of 3.7 kW is shown in Figure 4.1-4. The current pulses presented to the ac line by the resonant charger power stage are evident in Figure 4.1-4.

The charge profile obtained at 220 Vac is presented in Figure 4.1-5. The charger control circuit implements a dual-level constant current profile selected primarily for its adaptability to different types of propulsion batteries. Due to this flexibility the particular charge profile used is not optimized for a specific battery. The charge profile has three distinct operating regions. These three regions are; 1) the constant initial charge current region, 2) the constant voltage region and 3) the constant finish current region. The measured battery voltage and current as a function of time are both presented in Figure 4.1-5. The measured temperature rise of selected power components during charger operation at 3.7 kW is shown in Figure 4.1-6. The location of these components within the power stage enclosure is shown in Figure 4.2-15.



(2587)

**Figure 4.1-3**      **Charger Efficiency/Power Factor vs. Output Power @ 220 VAC**



(2609)

Figure 4.1-4 AC Line Current Waveform at 3.7kW - - - 220 VAC

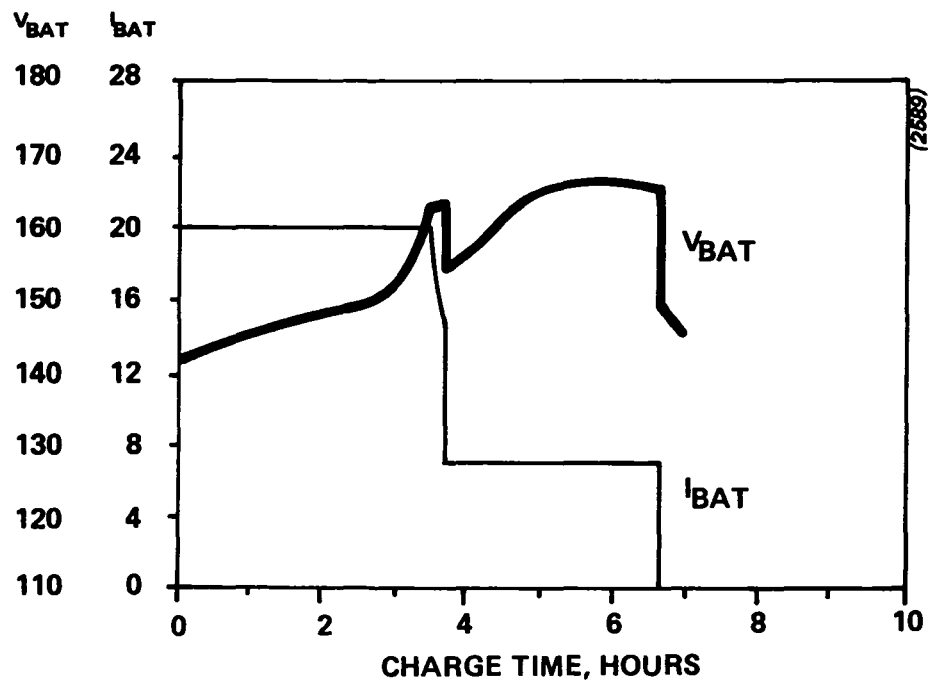
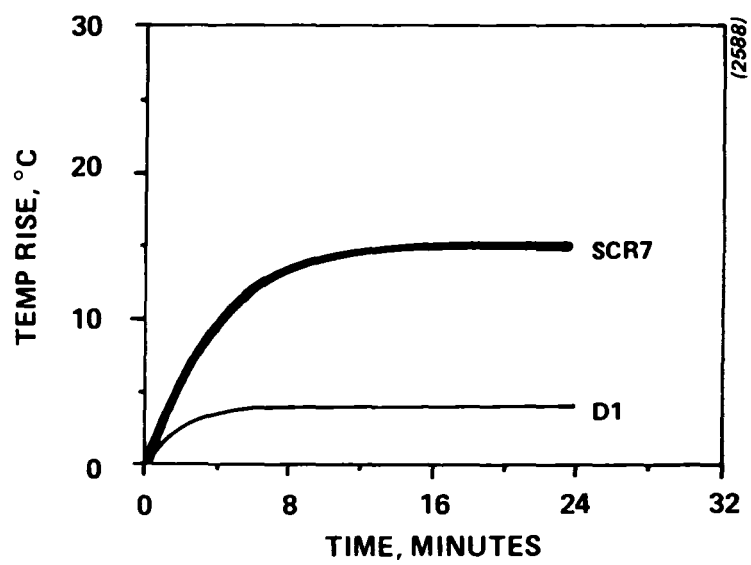


Figure 4.1-5 Charge Profile at 220 VAC - - - Nominal 132 Volt Battery (80% DOD)





**Figure 4.1-6** Charger Component Temperature Rise (Sink – Amb)  
@ 3.7 kW - - 220 VAC

## 4.2 Inverter Operation

Inverter operation requires that the keyswitch be moved to the off position, the charge cable be disconnected from the power stage, the power stage circuit breaker be moved manually to the motoring position and the keyswitch be moved to the motor position.

After the key switch is moved to the motor position the commutation circuit will cycle to charge the commutation capacitors to the required voltage level and the motoring status lights on the control electronics enclosure will light momentarily. Moving the direction selector to either the forward (FWD) or reverse (REV) position and rotating the accelerator control knob will activate the main thyristors and initiate motoring operation.

### 4.2.1 Power Loss/Efficiency Data

Measured inverter power loss during six-step motoring operation is presented in Figure 4.2-1 as a function of motor RMS line current. The measured inverter and motor efficiency (20 hp ac induction motor) at motor shaft speeds of 785 rad/sec (7500 RPM), 576 rad/sec (5500 RPM) and 189 rad/sec (1800 RPM) is presented in Figures 4.2-2, 3 and 4 respectively. Motoring operation at 189 rad/sec (1800 RPM) corresponds to operation in the pulse-width-modulation (PWM) region which occurs at motor speeds below approximately 471-524 rad/sec (4500-5000 RPM) depending on load. PWM operation is characterized by an increase in commutation frequency to decrease the time the main thyristors are on and the applied motor voltage. The motor line current during PWM operation at 189 rad/sec (1800 RPM) and 10 hp is shown in Figure 4.2-5.

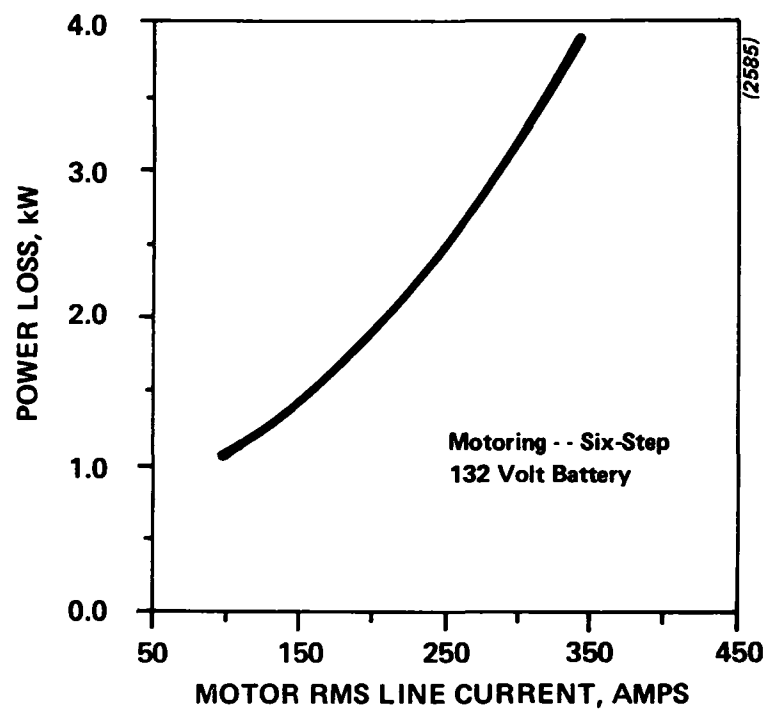
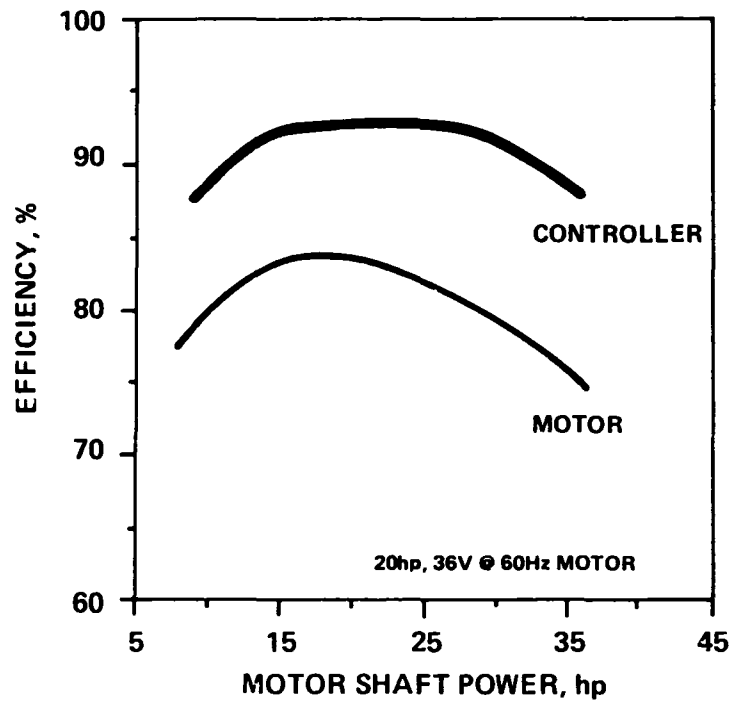
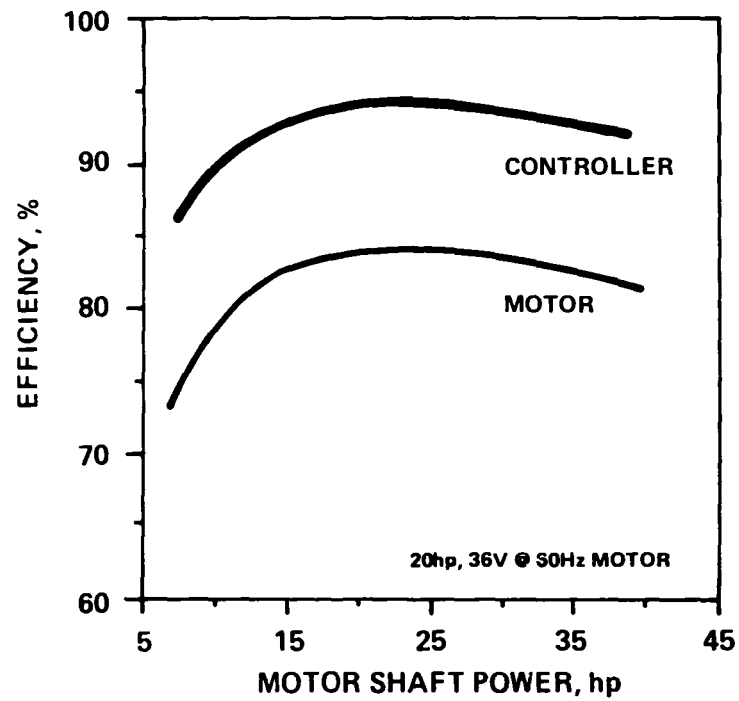


**Figure 4.2-1      AC Controller Power Loss vs. Motor Line Current**



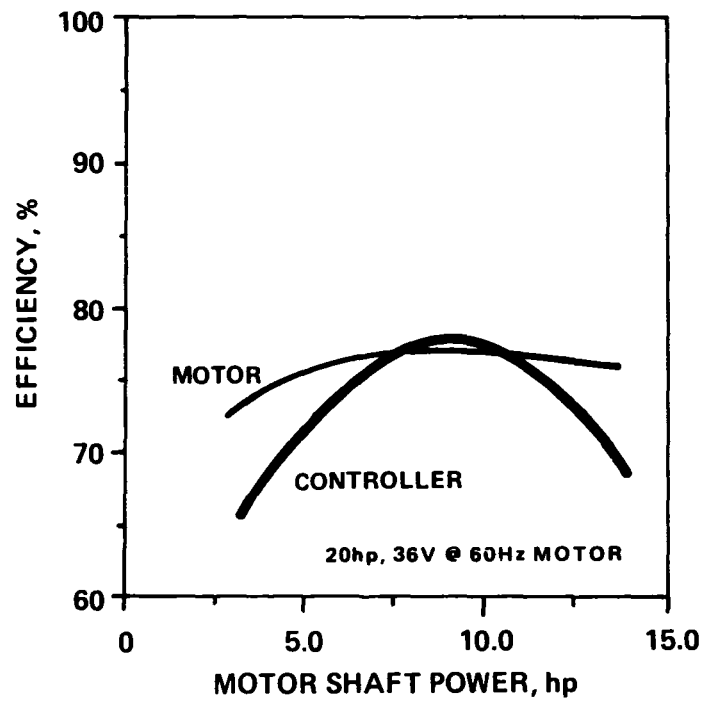
(2621)

**Figure 4.2-2 AC Controller/Motor Efficiency vs. Motor Shaft Power at 785 RAD/SEC (7500 RPM, Six-Step)**



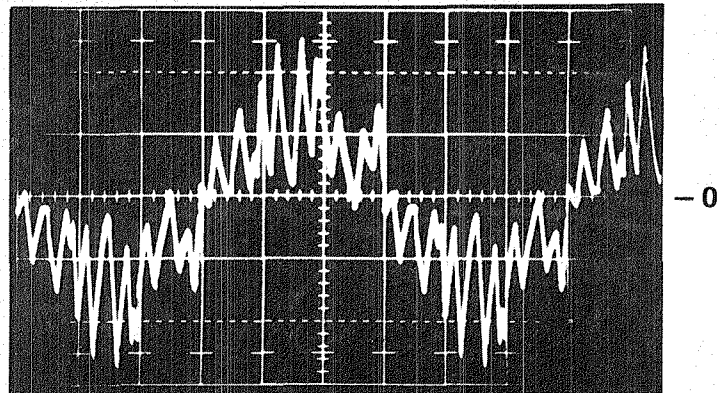
(2622)

**Figure 4.2-3 AC Controller/Motor Efficiency vs. Motor Shaft Power at 576 RAD/SEC (5500 RPM, Six -Step)**



(2623)

**Figure 4.2-4** AC Controller/Motor Efficiency vs. Motor Shaft Power at 189 RAD/SEC (1800 RPM, PWM)



200A/DIV

(2610)

**Figure 4.2-5     Motor Current Waveform at 189 RAD/SEC  
(1800 RPM) 10hp**

#### 4.2.2 Power Loss Breakdown

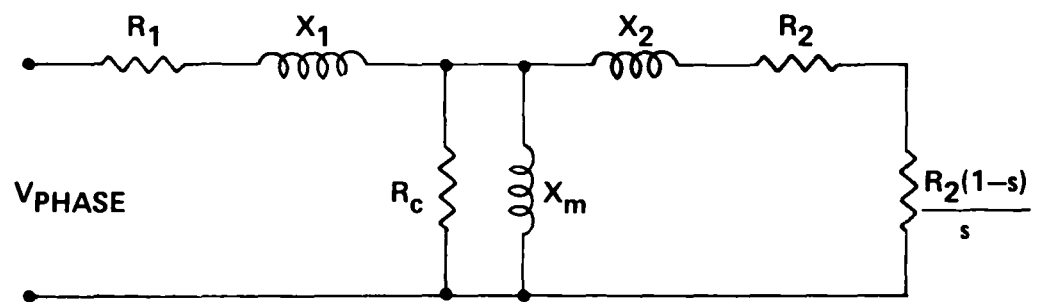
An important step in reducing the inverter power stage weight and volume was obtaining a reliable estimate of the inverter losses. This was accomplished using a computer model of the inverter, motor and propulsion battery that allowed inverter losses to be determined under different steady-state operating conditions. The model utilized the ac induction motor equivalent circuit shown in Figure 4.2-6. The motor parameters shown in Figure 4.2-6 are the stator ( $R_1$ ) and rotor ( $R_2$ ) resistance, the stator ( $X_1$ ) and rotor ( $X_2$ ) leakage reactance, the magnetizing reactance ( $X_m$ ) and the iron and stray load losses ( $R_c$ ). Information on how the above motor parameters vary as a function of motor operating conditions was obtained from Gould's Electric Motor Division. This information included magnetizing inductance as a function of motor voltage, stator and rotor leakage reactance as a function of current and frequency, iron losses as a function of voltage and frequency and stray load losses as a function of voltage, frequency and rotor current.

Inverter losses were calculated by performing a fourier analysis of the inverter output voltage waveform to determine the fundamental and harmonic voltages applied to the motor. The motor equivalent circuit was determined at the fundamental and harmonic frequencies and used in combination with the inverter harmonic voltages to produce a representation of the motor line current. The reconstructed and actual motor line current are presented in Figure 4.2-7 for comparison. The main thyristor losses were calculated using the reconstructed motor line current waveform by numerically integrating the product of the motor line current and instantaneous thyristor voltage drop between 0 and 180 electrical degrees. The calculated main thyristor (SCR1-6) power dissipation as a function of motor RMS line current is presented in Figure 4.2-8 for motoring operation at 576 rad/sec (5500 RPM).

The commutation thyristor power dissipation was calculated using the peak motor line current obtained from the reconstructed motor line current waveform. The calculated thyristor losses include both turn-on and conduction losses. The power dissipation of the commutation thyristors (SCR7-8) is shown in Figure 4.2-9 as a function of motor RMS line current and frequency.

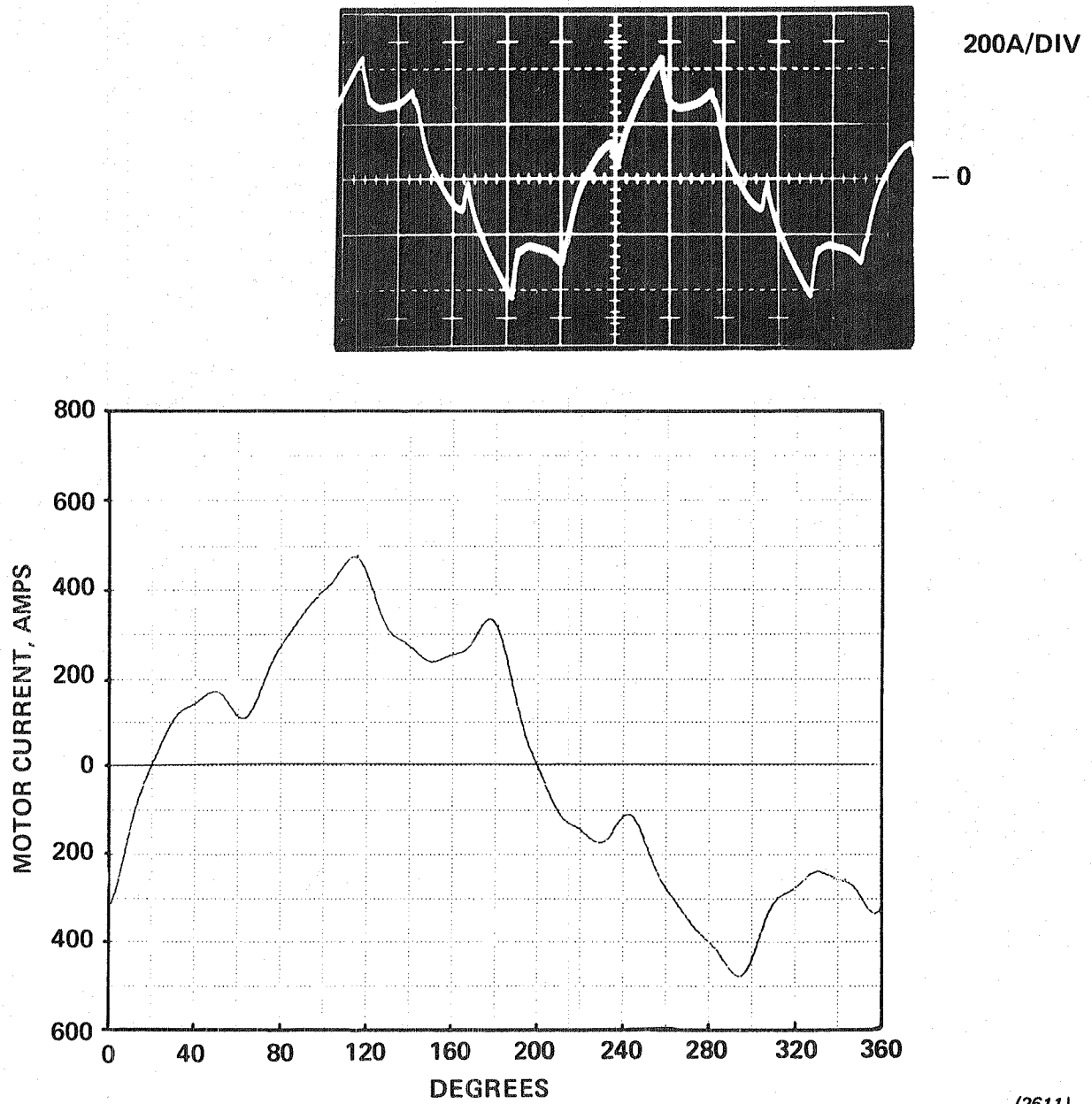


The losses of the commutation transformers were calculated based on the core loss data obtained using the resonant frequency test procedure. The total transformer losses are presented in Figure 4.2-10 and were based on the calculated RMS current in the T1A and T1B windings, the measured resistance of these windings and the core loss data. The significant increase in transformer losses at higher current levels is a result of the T1A winding being in series with the load. A breakdown of inverter losses at 576 rad/sec (5500 RPM) for motor shaft power levels of 15 and 45 hp is presented in Table 4.2-1.



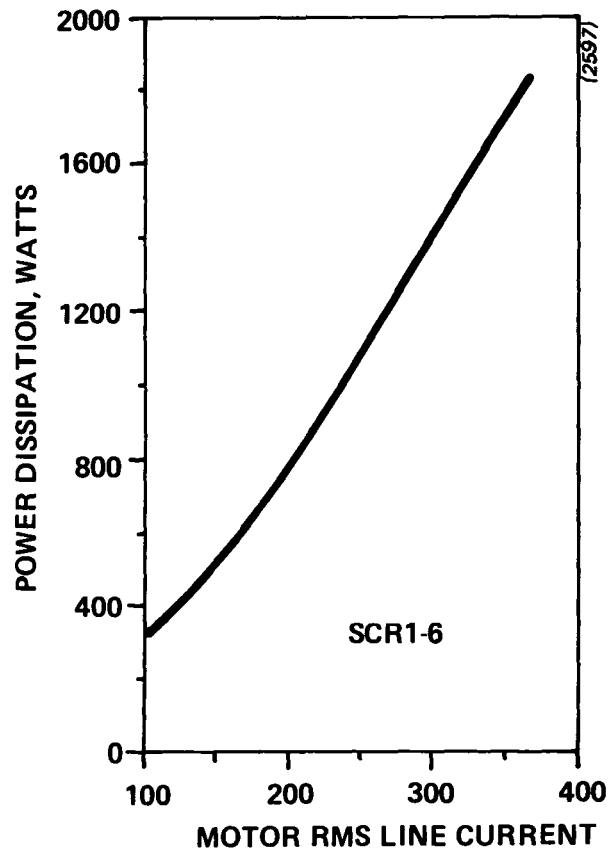
(0481)

Figure 4.2-6 AC Induction Motor – Simplified Equivalent Circuit

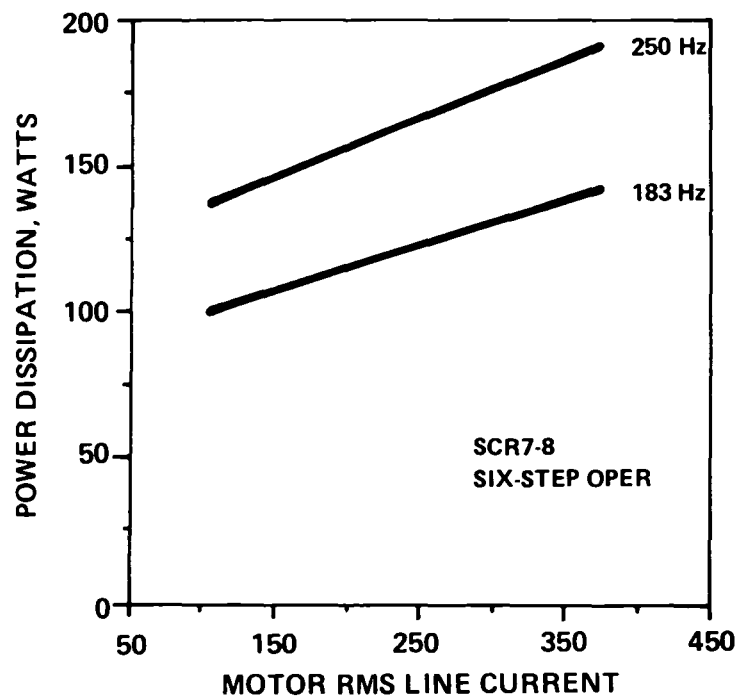


(2611)

Figure 4.2—7 Reconstructed Motor Current Waveform at 30hp/419 RAD/SEC (4000 RPM)



**Figure 4.2-8 Main Thyristor Power Dissipation vs. Motor Line Current (Calculated)**



(2596)

**Figure 4.2-9 Total Commutation Thyristor Power Loss vs. Motor Line Current (Calculated)**

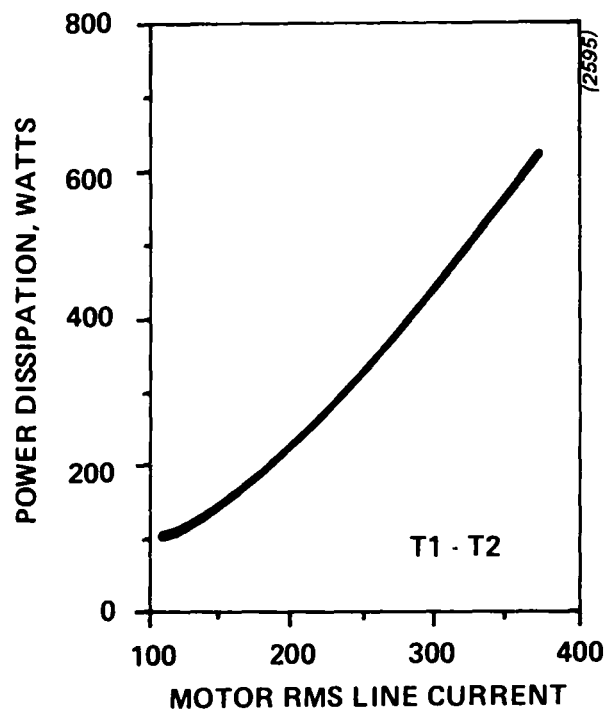


**Figure 4.2-10** Total Commutation Transformer Power Loss vs. Motor Current (Calculated)

TABLE 4.2-1

Inverter Power Loss Breakdown at 576 rad/sec (5500 RPM) (Calculated)

Motor Shaft Power	<u>15hp</u>	<u>45hp</u>
Main Thyristors (SCR1-6)	41%	47%
Main Rectifiers (D1-6)	8	4
Commutation Thyristors (SCR7-8)	11	4
Energy Recovery Rectifiers (D7-8)	6	3
Commutation Transformers (T1-2)	12	16
Commutation Capacitors (C1-C2)	2	1
Snubbers's	2	1
Control Power Supply	8	2
Inverter Resistance	5	12
Motor Cables	<u>5</u>	<u>10</u>
Total	100%	100%

#### 4.2.3 Component Temperature Rise

The measured temperature rise of selected power stage components is presented in Figures 4.2-11, 12 and 13 for motoring operation at shaft speeds of 189 rad/sec (1800), 524 rad/sec (5000) and 681 rad/sec (6500 RPM). Component temperature rise during regeneration at 681 rad/sec (6500 RPM) is presented in Figure 4.2-14. The specific components monitored were main thyristor SCR5, main rectifier D1 and commutation thyristor SCR7. The location of these components within the power stage enclosure is shown in Figure 4.2-15. Air flow direction through the package is indicated in Figure 4.2-15. Since thyristor SCR7 is located at the outlet it will operate at a higher ambient temperature than main thyristor SCR5. As is evident the main rectifier heatsinks are significantly smaller than the main thyristor heatsinks to take advantage of their lower dissipation during motoring operation and their higher junction temperature rating.

The inverter steady-state power rating is 11.2 kW (15hp). As indicated in Figure 4.2-13 the temperature rise of thyristor SCR5 is only 9°C at this power level. During an acceleration from 40-88.5 km/h (25-55 mph) at 33.6 kW (45hp), however, the main thyristor dissipation is approximately 300 watts and the junction temperature must remain below 125°C at this operating point. For a junction to heatsink thermal resistance of 0.13 °C/W (GE C384), a 10°C rise in air temperature above ambient (SCR1) and an ambient temperature of 49°C the initial junction temperature of thyristor SCR1 at 45hp will be 107°C. The 18°C difference between the initial and maximum junction temperature is available for transient operation (i.e., 16 seconds at 45hp).

During PWM operation at 524 rad/sec (5000 RPM) the commutation circuit is operating at its maximum motoring frequency (i.e., approximately 1500 commutations per thyristor) and the dissipation of thyristor SCR7 is at its maximum value. For this operating condition the heatsink to ambient temperature rise of thyristor SCR7 is approximately 40°C as shown in Figure 4.2-12. At an ambient temperature of 49°C the junction temperature is approximately 115°C and is below the maximum junction temperature of 125°C. At the above PWM operating point (i.e., 7.5 kW (10hp) @ 524 rad/sec (5000 RPM)) the temperature rise of the commutation transformer winding was 46°C and the temperature rise of the commutation capacitor case (C1) was only 5°C.



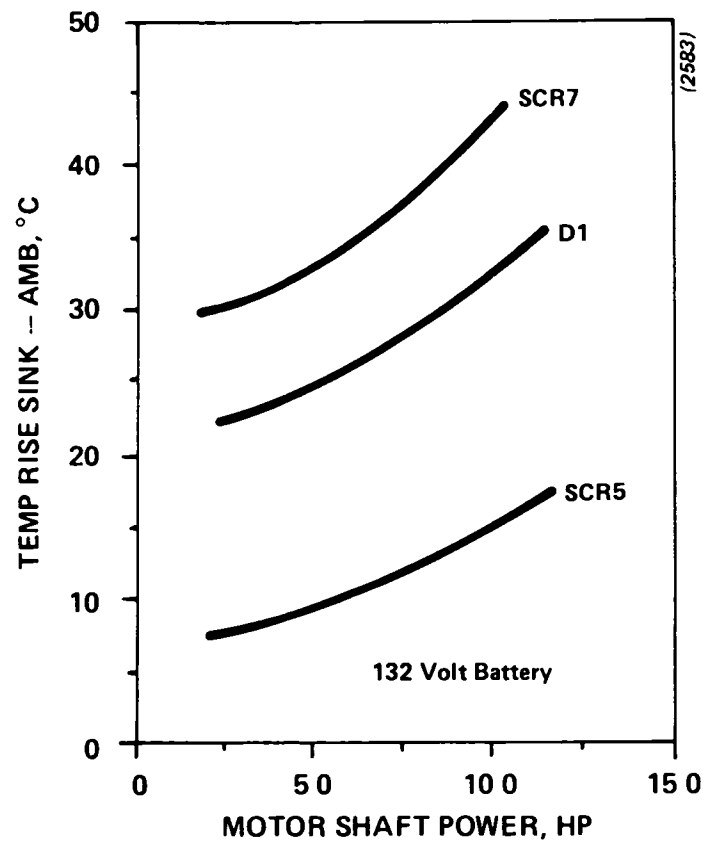
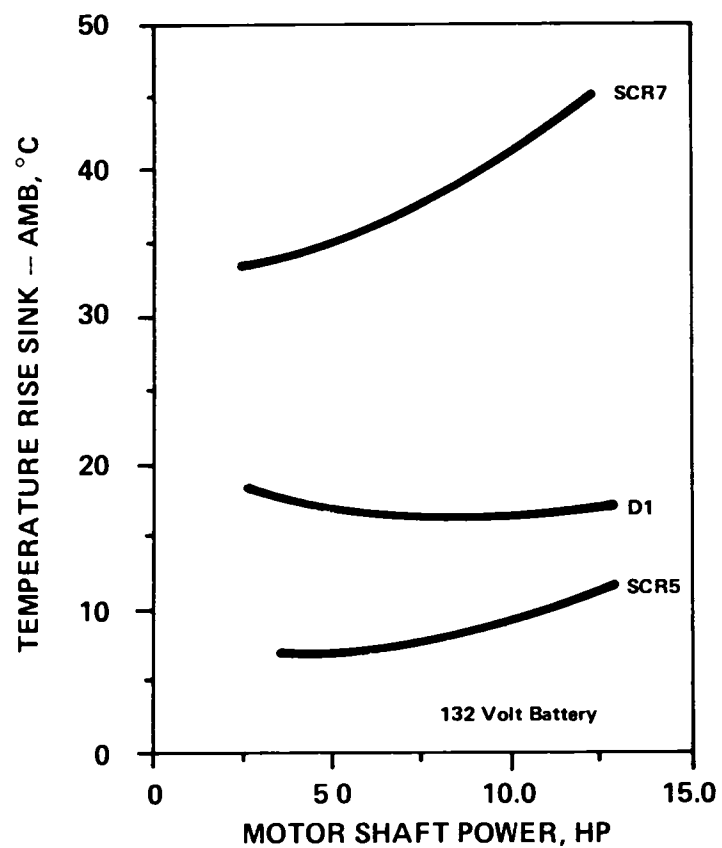


Figure 4.2-11 Measured Component Temperature Rise vs. Motor Shaft Power (Motoring - - -189 RAD/SEC (1800RPM) PWM)



(2581)

**Figure 4.2-12 Measured Component Temperature Rise vs. Motor Shaft Power (Motoring - - - 524 RAD/SEC (5000RPM) PWM)**

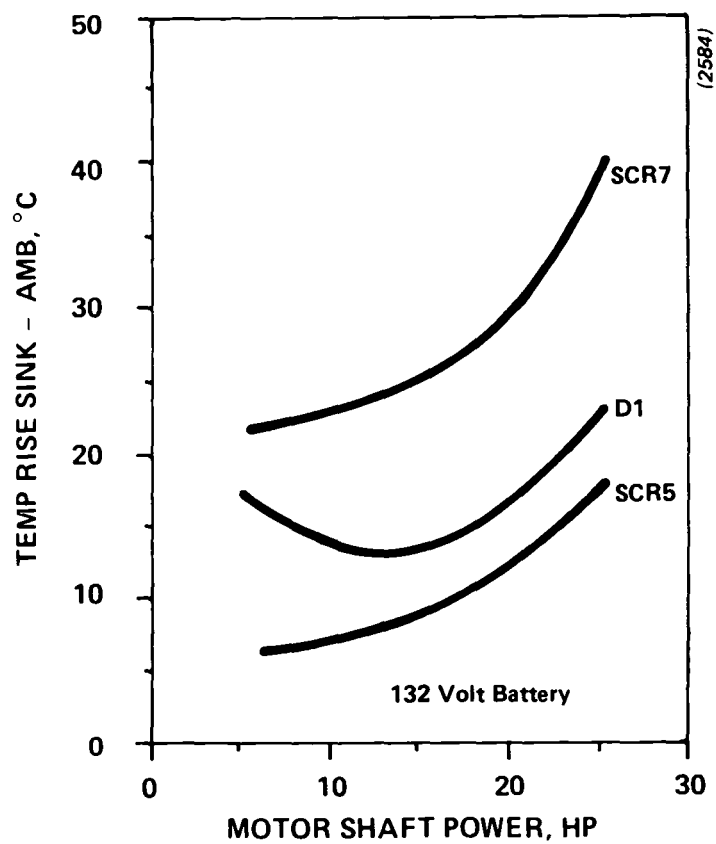


Figure 4 2-13 Measured Component Temperature Rise vs. Motor Shaft Power (Motoring - - - 681 RAD/SEC (6500 RPM) Six - Step)

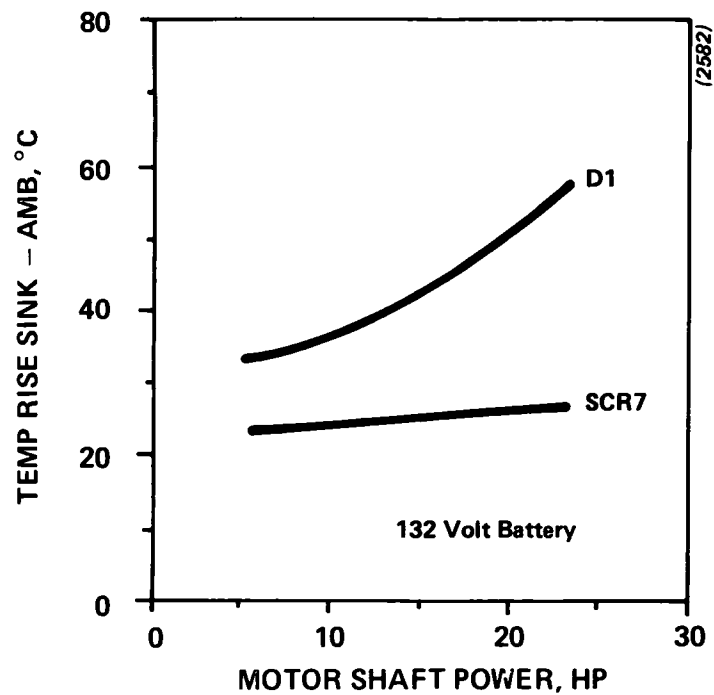
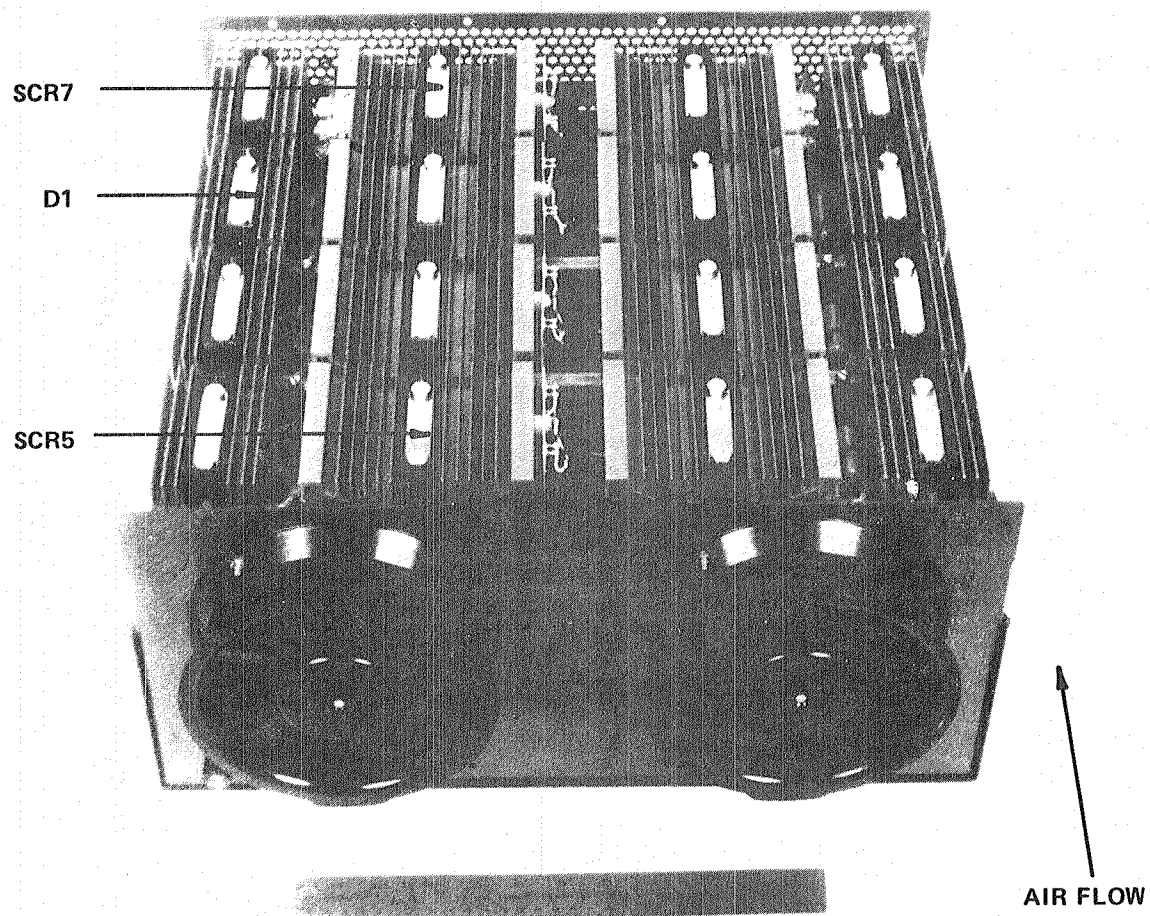


Figure 4.2-14 Measured Component Temperature Rise vs.  
Motor Shaft Power (Regeneration - - - 681 RAD/SEC  
(6500 RPM) Six - Step)



(2998)

**Figure 4.2-15 Inverter / Charger Package -- Bottom View**

#### 4.2.4 Motor Torque/Speed Curve

The maximum measured motor shaft torque versus motor speed is shown in Figure 4.2-16. Below approximately 419 rad/sec (4000 RPM) the inverter is in the PWM operating region and above 419 rad/sec it is in the six-step operating region. The test results presented were obtained using a 20 hp ac induction motor having a voltage rating of 36 volts at 60 Hz, along with a 132 volt (at 2.0 V/cell) battery. The peak shaft power obtained varied from 35 kW (47 hp) at 471 rad/sec (4500 RPM) to 30 kW (40 hp) at 744 rad/sec (7100 RPM). During these conditions, the battery terminal voltage varied between 123 and 129 volts. The peak motor shaft torque obtained at 209 rad/sec (2000 RPM) was 60 N-m. Optimizing the design of both the control electronics and ac induction motor together as a system would result in increased motor torque during PWM operation.

The shape of the torque curve in Figure 4.2-16 for frequencies below 419 rad/sec (4000 RPM) requires some discussion. The non-monotonic nature of this curve is due to the particular set of control electronics and motor used to exercise the power stage. Since the work in this contract did not include the development of a matched set of control electronics and motor, a set of electronics developed for a different power stage (Contract DEN3-60) and an available motor were used to obtain data to generate this curve. As a result, adverse interactions between the controller, power stage, and motor occurred during certain conditions such as exists when the motor shaft speed is approximately 350 rad/sec. The dip in torque at this speed occurs from a certain choice of motor slip frequency combined with a particular PWM pattern and its corresponding harmonic generation. Such harmonic currents in this particular motor causes the power stage to go into cyclical shut-down due to over-current conditions. As stated above, an overall system design based on this power stage along with a custom motor and custom set of control electronics could eliminate such problems and produce a much smoother torque-speed curve for the system.

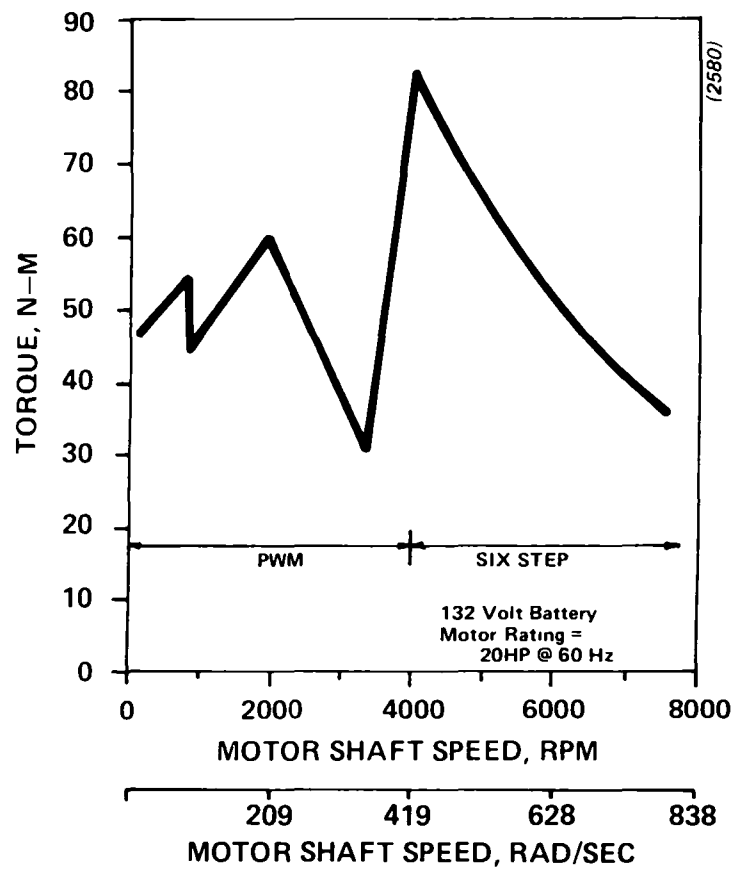


Figure 4 2-16 Motor Maximum Shaft Torque vs Motor Speed

## 5. RESULTS AND CONCLUSIONS

The feasibility of incorporating an on-board battery charger into the inverter, previously developed by Gould under NASA-Lewis Contract DEN3-60, was successfully demonstrated. The resulting isolated battery charger has a rated output power of 3.6 kW at 220 VAC with an efficiency of 86% and power factor of 95% at rated power. Charger operation at power levels up to 1.8 kW at 120 VAC is also possible.

The design objective of significantly reducing the weight and volume of the combined inverter/charger package was successfully achieved. The resulting power stage package weighs 46.8 kg (103 lbs) and measures 49x44x24 cm (19x17x9 in). This is a relatively small package considering that a 50 kVA three-phase inverter and a 3.6 kW isolated battery charger are both provided within the same package.

The third objective of increasing the inverter efficiency and peak power capability was also successfully achieved. The inverter peak power capability as measured at the motor shaft was increased from 26.1 kW (35 hp) to 33.6 kW (45 hp). Inverter efficiency was increased from 90 to 93% at a motor shaft power of 15 kW.

The major conclusions resulting from the design and laboratory test of the integral inverter/battery charger are;

- 1) Use of the inverter commutation circuitry as a battery charger converted the disadvantage normally associated with this circuitry into a significant advantage.
- 2) The input-commutated thyristor inverter has the potential to be a rugged and reliable inverter for use in electric vehicle applications.
- 3) Further development work is needed to significantly reduce the cost and complexity of the control electronics.



- 4) Development of an ac induction motor specifically for use with the input-commutated inverter is needed.
- 5) Development of a PWM switching strategy designed specifically for the input-commutated inverter is recommended (DEN3-60 recommendation)<sup>1</sup>.

## 6. APPENDICES

Appendix A Charge Control Board Description

Appendix B Set-up Instructions for Inverter/Charger

Appendix C Schematics and Drawings

Several protection and interlock features are incorporated into the charger control electronics. These protection features are;

- 1) The motoring function is disabled while the charge cable is connected.
- 2) Should the battery voltage, during charger operation, exceeds 2.75 volts/cell the charger will shutdown. For example, if the propulsion battery is accidentally disconnected during charger operation.
- 3) A 20 amp circuit breaker is included in a separate ac line interface unit. This unit would be located at a permanent charging facility.
- 4) Power is not available on the battery charge cable, which connects to the power stage, until the charge cable is connected to the power stage and the keyswitch is turned to the charge position. This safety feature is provided by the ac line interface unit.

Note:     Use of the ac line interface unit is not required for charger operation however, it is recommended that it be used for safety reasons.

- 5) Should the charger not transfer to the finish current region after a pre-determined period of time (T1 in Figure A-1) the charger will shutdown and the charger fault indicator on the control enclosure will light. This is an indication of a possible defective battery.

## Appendix B

### Set-up Instructions for Inverter/Charger

Presented in this section is the information required to initially apply power to the inverter and battery charger. The major system components are;

- 1) Inverter/Charger Power Stage (Unit 1)
- 2) Control Electronics (Unit 2)
- 3) Accelerator/Brake Assembly (Unit 3)
- 4) AC Induction Motor/Tachometer (Unit 4A/4B)
- 5) AC Line Interface (Unit 5)

The additional components supplied with this system are

- 6) Battery Connector (P5)
- 7) AC Line Cable to Interface Unit Connector (P3)
- 8) Motor Cables (M1, M2, M3)

Prior to applying power examine the system control drawing (SK-142082) to establish the location of each major component (Units 1-5) and how they are interconnected.

#### Motor/Power Stage Connection

- 1) Remove the power stage top cover and locate the three (3) motor bus-bar connections labeled M1, M2 and M3.
- 2) Connect the motor cables labeled M1, M2 and M3 to the power stage bus-bars having the same labels. These cables must be routed through the cable clamps and these clamps tightened.
- 3) Connect the motor cables to the motor leads labeled M1, M2 and M3.
- 4) Replace the power stage top cover.

### Inverter/Charger Power Check

- 5) Connect a 150V, 10 amp variable voltage supply to the battery connector provided. This is a polarized connector and is marked (+) for the positive supply lead and (-) for the negative supply lead.
- 6) With the supply off connect the supply to the power stage.
- 7) Slowly increase the supply voltage from 0 to 150 volts. Move the circuit breaker handle towards the motor cable clamps. The supply current should be less than 0.2 amps. Move the breaker handle towards the charge connector on the power stage. The supply current should be less than 0.2 amps.
- 8) Turn-off the supply.

### Control Electronics Power Check

- 9) Connect the tachometer polarized connector to the control electronics.
- 10) Connect the accelerator/brake polarized connector to the control electronics.
- 11) Place the accel/brake direction selector in the off position (neutral) and rotate the accel and brake control knobs in a counterclockwise direction until they stop.
- 12) Manually move the circuit breaker to the charge position - breaker handle pointing towards charge connector on power stage.
- 13) Turn the keyswitch located on the control electronics front panel to the off position.

- 14) Connect the control electronics to the power stage via the polarized connector on the control cable.
- 15) Increase the power supply voltage to 120 volts.
- 16) Turn the key switch to the charge position. The fans located on the power stage should operate and the current drawn from the supply should be approximately 0.6 amps. The overcurrent indicator light located on the control electronics front panel will light momentarily. The remaining indicator lights will not light.
- 17) Turn the key switch to the off position.
- 18) Move the circuit breaker to the motor position - breaker handle towards motor cable clamps on power stage.
- 19) Turn the key switch to the motor position. The inverter power stage will "beep" and the motoring indicator lights on the control front panel will light momentarily. The fans will also operate. The supply current should be approximately 0.6 amps.
- 20) Turn the key switch to the off position.
- 21) Turn the power supply off and remove the battery connector.

#### Battery Connection

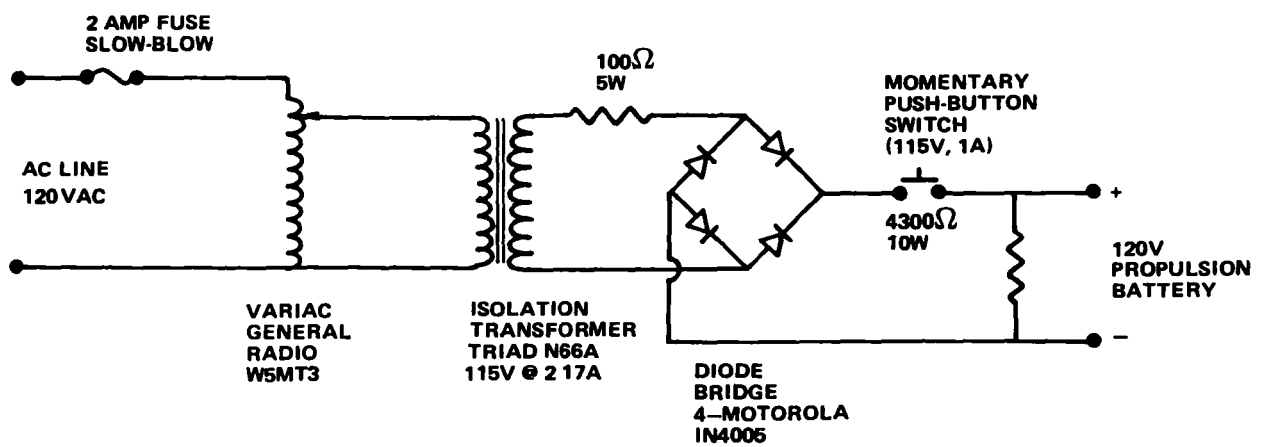
- 22) Connect a nominal 132 volt propulsion battery to the battery connector observing the polarity marked on the connector.
- 23) Connect a separate contactor in series with the propulsion battery to act as an emergency disconnect. This contactor also allows the power stage input filter capacitor bank to be precharged before battery voltage is applied to the inverter

### Input filter capacitor precharge

The input filter capacitor bank, located in the ac inverter power stage, must be pre-charged to 120 volts prior to connecting the propulsion battery to the power stage. If this is not done the capacitor in-rush current when full battery voltage is applied will open the 200 amp input fuse (F1) located in the power stage (reference the system diagram, SR-142082). During actual vehicle operation pre-charging the input capacitor bank could be performed using either the main propulsion battery or a 12 volt accessory battery. Since neither battery source is supplied with this system a separate input capacitor charging circuit is required.

The pre-charge circuit used during our testing is shown in Figure B-1 and allows the input filter capacitor bank to be charged to 120 volts prior to connecting the propulsion battery. Use of this circuit is described below;

- 24) Connect the pre-charge circuit output leads permanently to the battery power leads. This connection can be made either at the battery connector or the battery contactor.
- 25) Adjust the isolation transformer secondary voltage for 90 volts RMS.
- 26) With the battery contactor open connect the propulsion battery to the power stage.
- 27) Charge the input filter capacitor to 120 volts by closing the normally open push-button switch. Measure the voltage at the output of the pre-charge circuit and as soon as the input capacitor is charged to 120 VDC close the battery contactor. The pre-charge circuit is rated for transient operation only.



(2625)

Figure B-1 AC Controller Input Filter Capacitor, Pre-Charge Circuit



### Charger Operation

- 28) Wire the ac line cable to the interface unit connector for 120 or 220 Vac operation as shown in the system diagram (SK-143082).
- 29) Pre-charge the input filter capacitor and connect the propulsion battery to the power stage.
- 30) Connect the interface unit charge cable to the power stage via the polarized connector permanently attached to the interface unit.
- 31) Connect ac line voltage to the interface unit via the cable wired in step 28.
- 32) Turn the key switch to the charge position. The circuit breaker will automatically move to the charge position, assuming it is initially in the motor position, and after a 10 second time delay the charger will operate. The initial charge current will be 10 amps at 120 Vac and 20 amps at 220 Vac.

### Motoring Operation

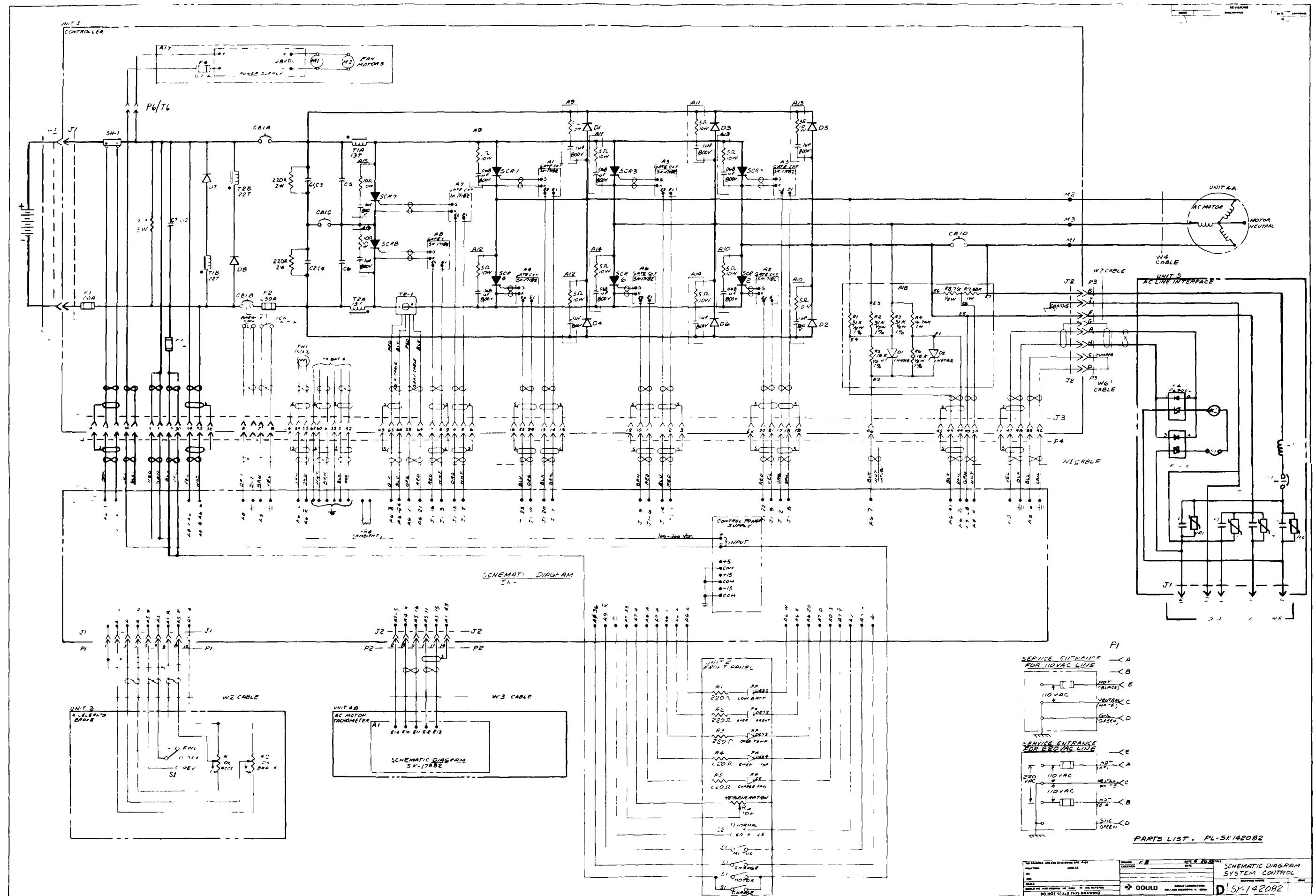
- 33) Turn the keyswitch to the off position.
- 34) Disconnect the charge cable from the power stage.
- 35) Manually move the circuit breaker to the motor position - handle pointing towards the motor cable clamps.
- 36) Pre-charge the input filter capacitor and connect the propulsion battery to the power stage.
- 37) Turn the keyswitch to the motor position. After the keyswitch is moved to the motor position the inverter will "beep" and the motoring status lights on the control electronics enclosure will light momentarily.

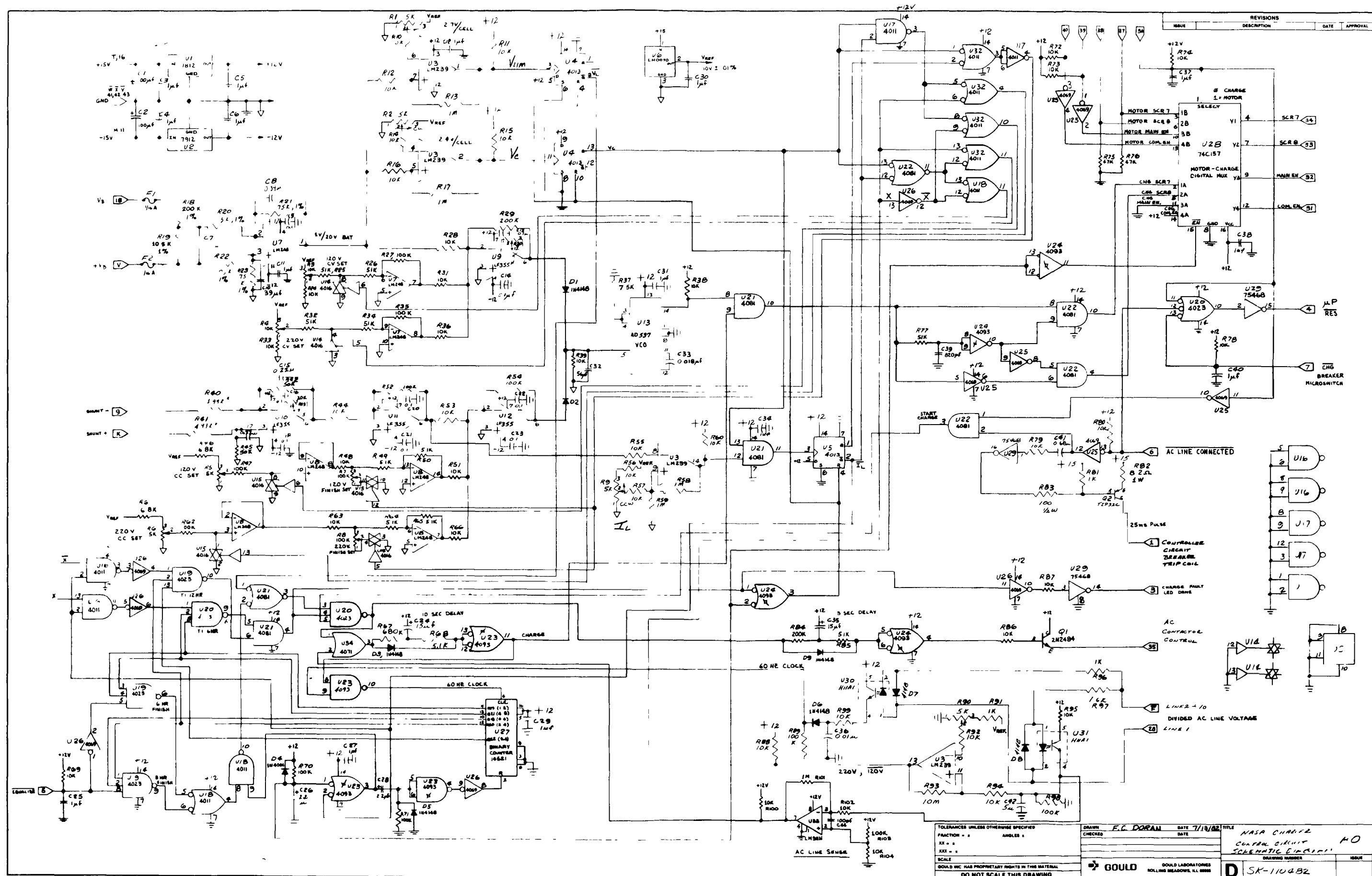
- 38) Move the direction selector to forward (FWD) or reverse (REV) and rotate the acceleration control knob to activate the inverter and motor.
- 39) To stop, turn the accelerator knob to its minimum (MIN) position and turn the regeneration knob to its maximum (MAX) position.
- 40) Turn the key switch to off.
- 41) Disconnect the propulsion battery.

Appendix C  
Schematics and Drawings

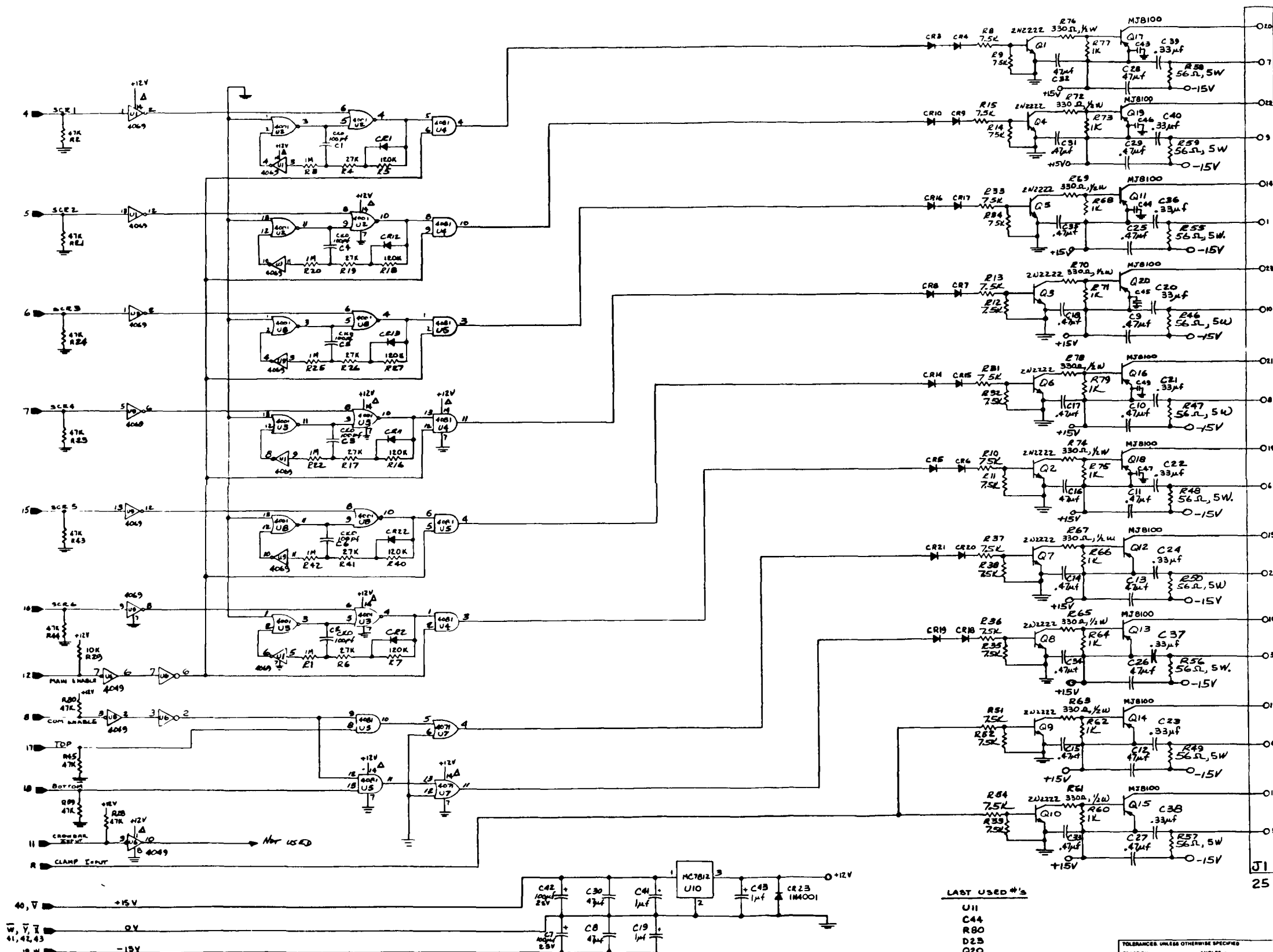
This appendix contains the following drawings for the ac inverter/charger power stage and control electronics. It must be emphasized that these are being provided solely as an aid in interpreting the test results presented in Section 4. The control system based on the circuits in this appendix has not been matched to the inverter/charger developed during this contract (DEN3-249) but rather have been adapted to provide a convenient means of exercising the inverter/charger power conversion electronics in order to carry out the required testing and evaluation for this contract. For optimum overall system performance, it is recommended that the entire control system be redesigned specifically for the inverter/charger power conversion electronics described herein.

<u>Figure</u>	<u>Page</u>
SK - 142082    System Control Diagram	C-2
SK - 110482    Charger Control Circuit (A0)	C-3
SK - 1102182   Gate Drive Amplifiers (A1)	C-4
SK - 1102282   Commutation Thyristor Control (A2)	C-5
SK - 1102382   Main Thyristor Gating (A3)	C-6
SK - 1102482   Sine-Triangle Generator (A4)	C-7
SK - 1102582   Frequency Control (A5)	C-8
SK - 1102682   Signal Interface (A6)	C-9
SK - 1102782   I/O Board (A7)	C-10
SK - 1102882   Microprocessor Board (A8)	C-11
SK - 17882     Tachometer Circuit (Unit 4B)	C-12
SK - 17182     Gate Drive and Snubber Circuits	C-13
SK - 410482    Charger PCB Layout (A0)	C-14
SK - 4102182   Gate Drive PCB Layout (A1)	C-15
SK - 4102282   Commutation Control PCB Layout (A2)	C-16
SK - 4102382   Main Thyristor PCB Layout (A3)	C-17
SK - 4102482   Sine-Triangle PCB Layout (A4)	C-18
SK - 4102582   Frequency Control PCB Layout (A5)	C-19
SK - 4102682   Signal Interface PCB Layout (A6)	C-20
SK - 4102882   Microprocess Board PCB Layout (A8)	C-21



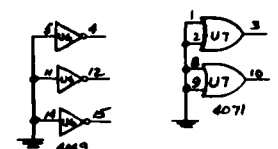


SK - 110482 Charger Control Circuit (AO)



OUTPUTS  
ADJACENT TO EACH OTHER  
AS OPPOSITE SIDES

ALL DIODES - 1N4148 UNLESS NOTED  
ALL RESISTORS - 1/4W, 5% UNLESS NOTED  
NOTE THIS BOARD MADE FROM ATT-WSK  
FIRST USED ON SCHEMATIC SK-211080 REV



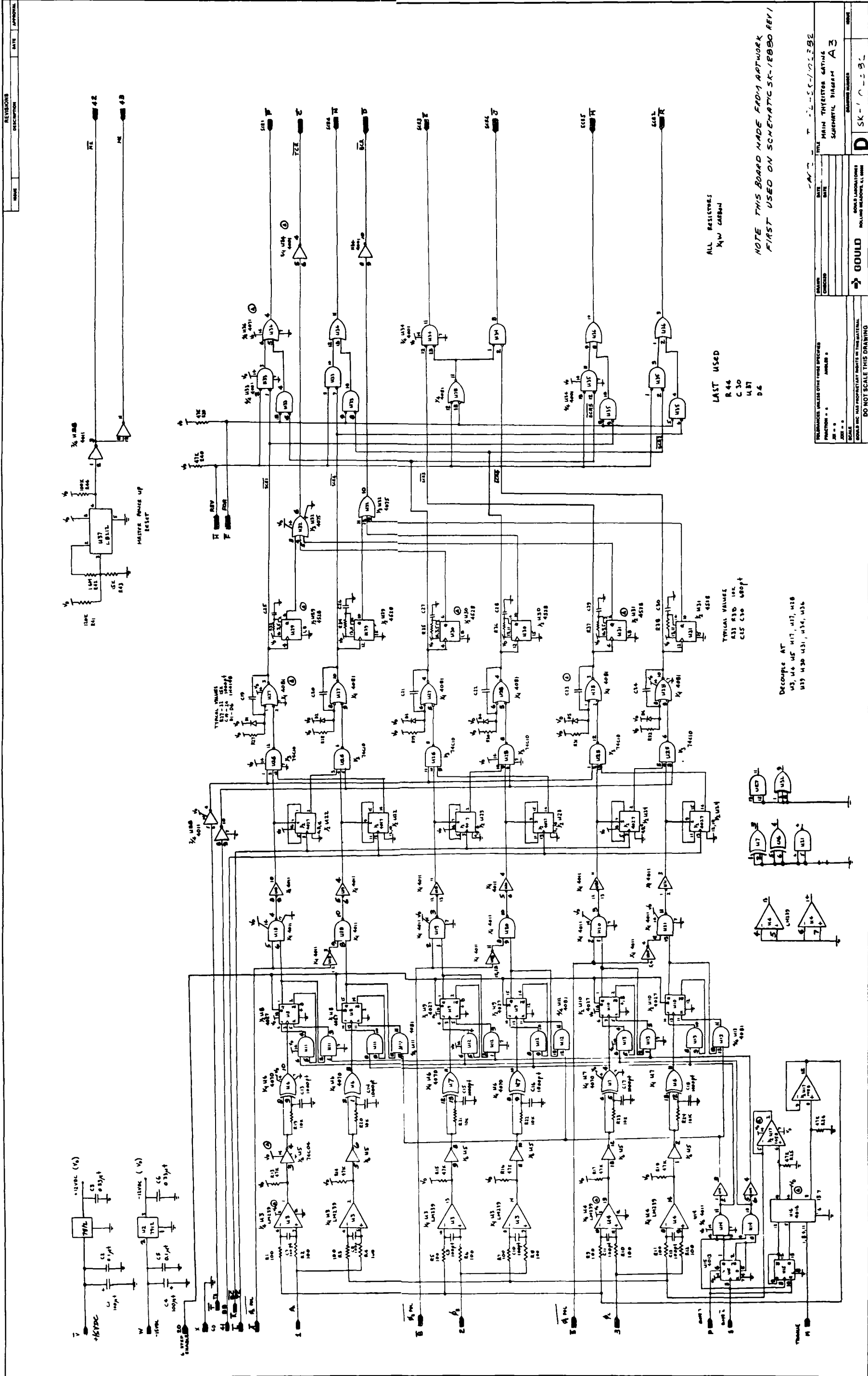
25 PIN CONNECTOR

LAST USED #1's  
U11  
C44  
R80  
D23  
Q20

PARTS LIST, PL-SK-112-31

TOLERANCES UNLESS OTHERWISE SPECIFIED		DRAWN: <i>KA</i>		DATE: <i>10-18-82</i>		TITLE: <b>GATE DRIVE AMPLIFIERS</b>	
FRACTION - 1/100	ANGLES -	CHECKED:		DATE:		SCHEMATIC DIAGRAM <i>A1</i>	
SCALE:		GOULD		GOULD LABORATORIES		DRAWING NUMBER: <b>SK-1102182</b>	
GOULD INC. HAS PROPRIETARY RIGHTS IN THIS MATERIAL		DO NOT SCALE THIS DRAWING		ROLLING MEADOWS, ILL. 60068		ISSUE:	

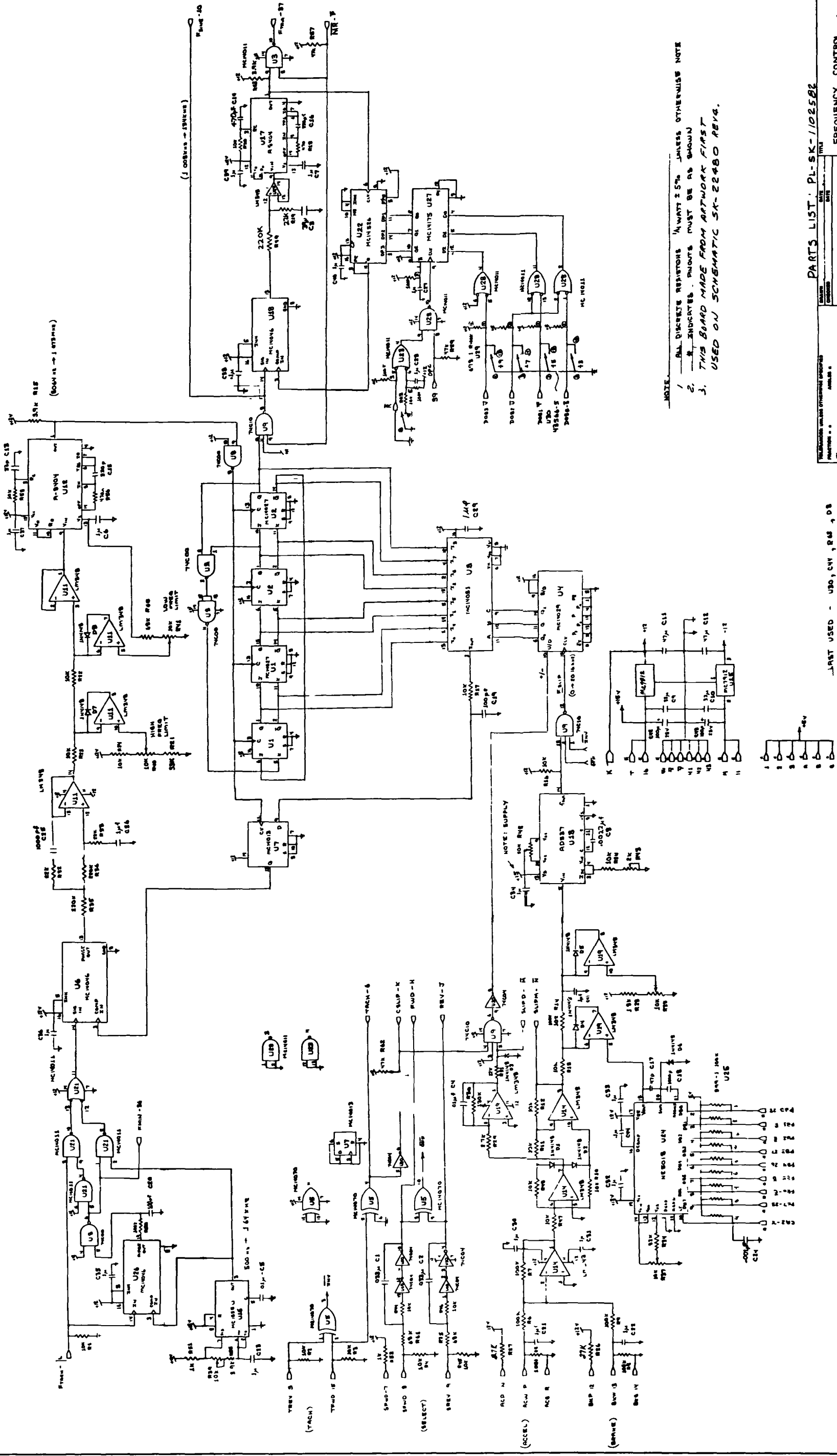




SK - 1102382 Main Thyristor Gating (A3)



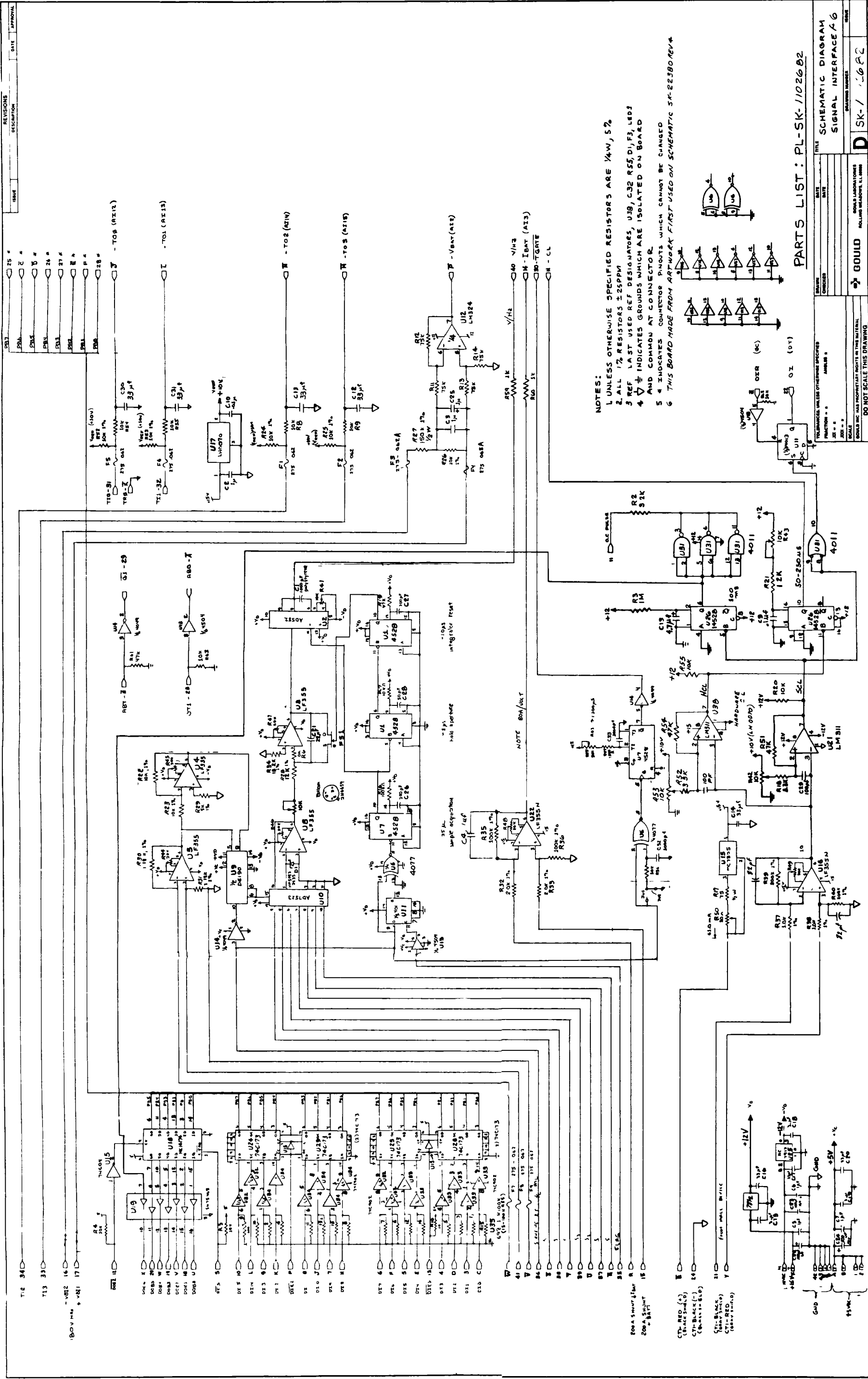


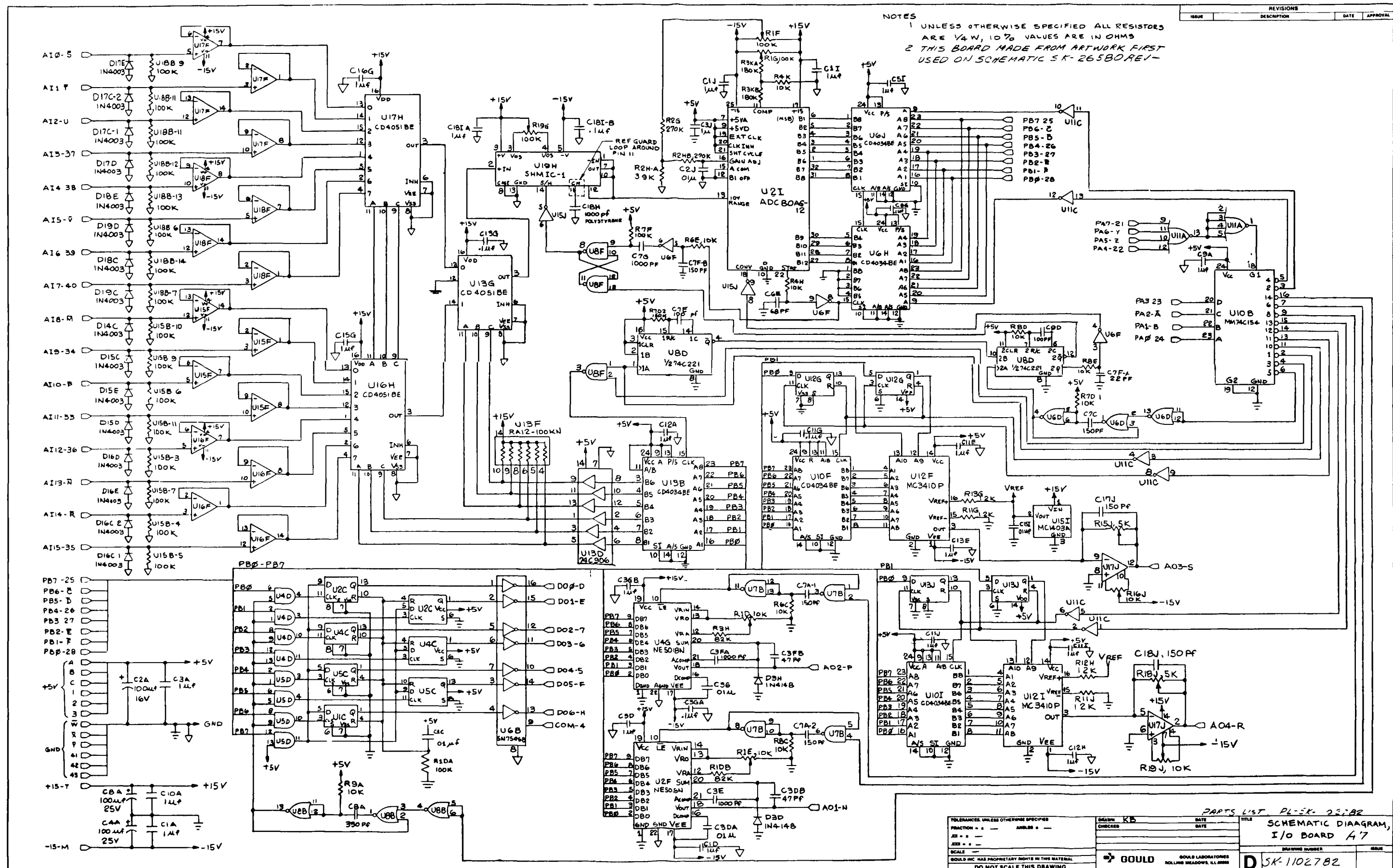


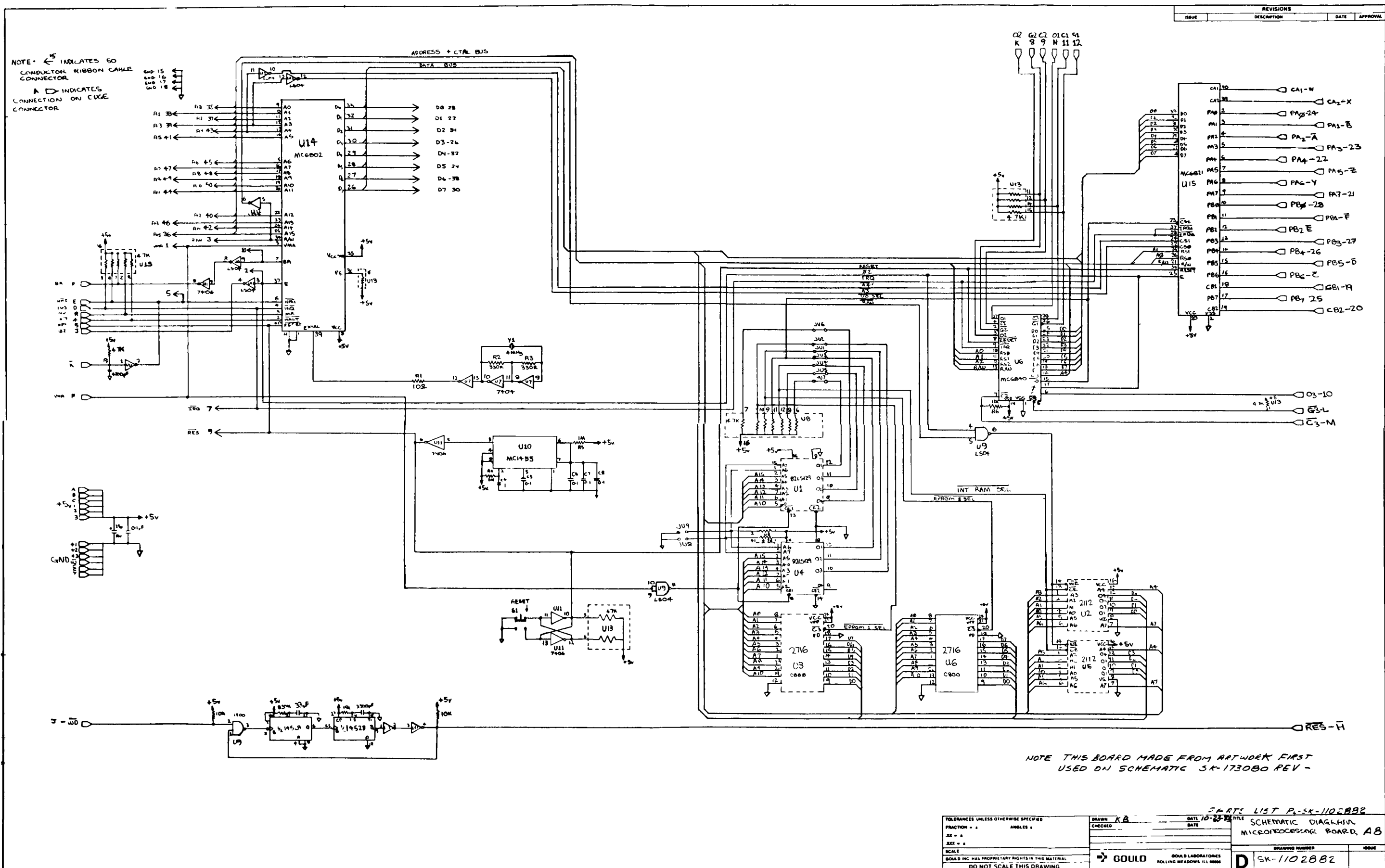
PARTS LIST: PL-SK-1102582

REVISIONS	DATE	APPROVAL
1		
2		
3		
4		
5		
6		
7		
8		
9		
10		
11		
12		
13		
14		
15		
16		
17		
18		
19		
20		
21		
22		
23		
24		
25		
26		
27		
28		
29		
30		
31		
32		
33		
34		
35		
36		
37		
38		
39		
40		
41		
42		
43		
44		
45		
46		
47		
48		
49		
50		
51		
52		
53		
54		
55		
56		
57		
58		
59		
60		
61		
62		
63		
64		
65		
66		
67		
68		
69		
70		
71		
72		
73		
74		
75		
76		
77		
78		
79		
80		
81		
82		
83		
84		
85		
86		
87		
88		
89		
90		
91		
92		
93		
94		
95		
96		
97		
98		
99		
100		

LAST USED - U80, C41, R48, D8

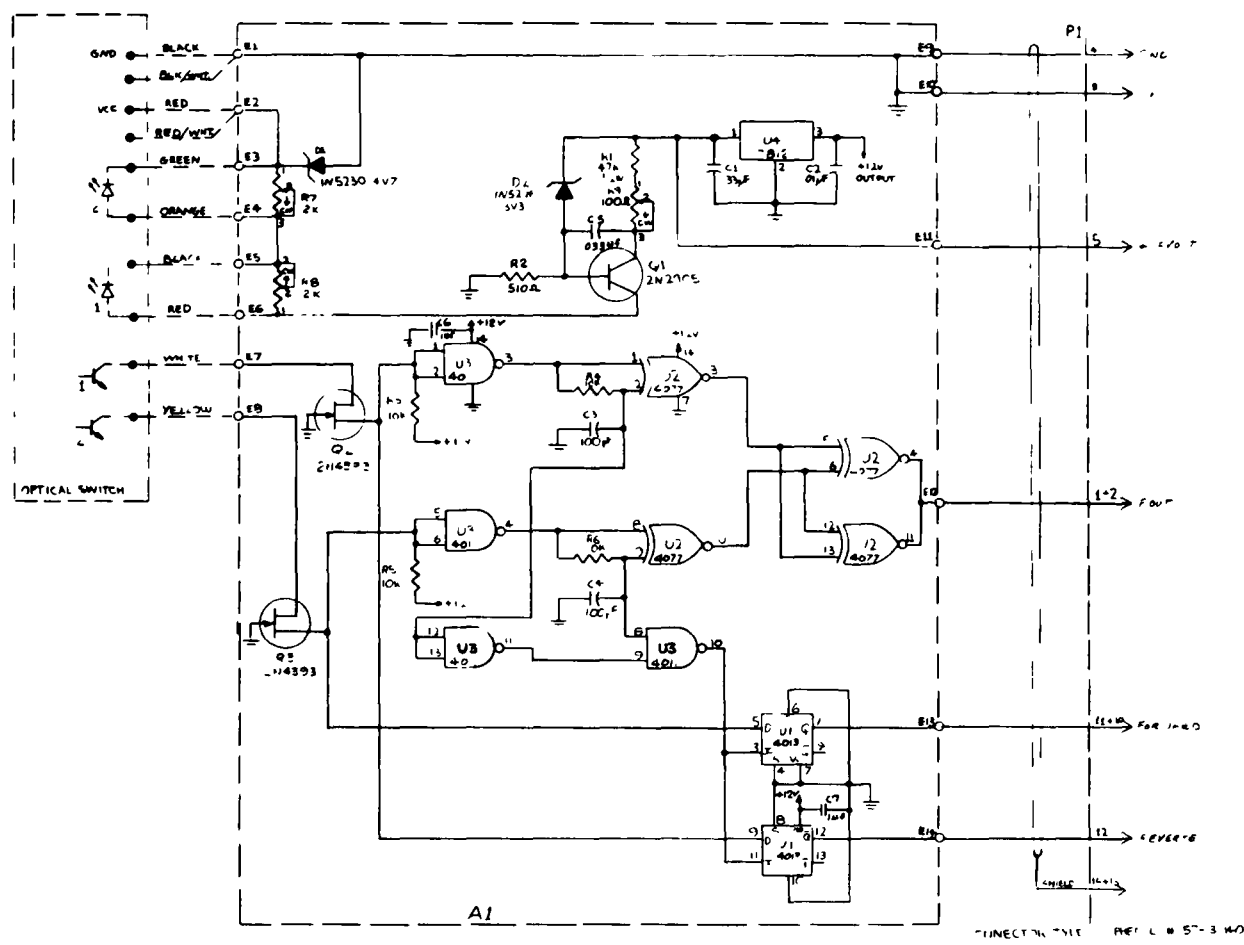






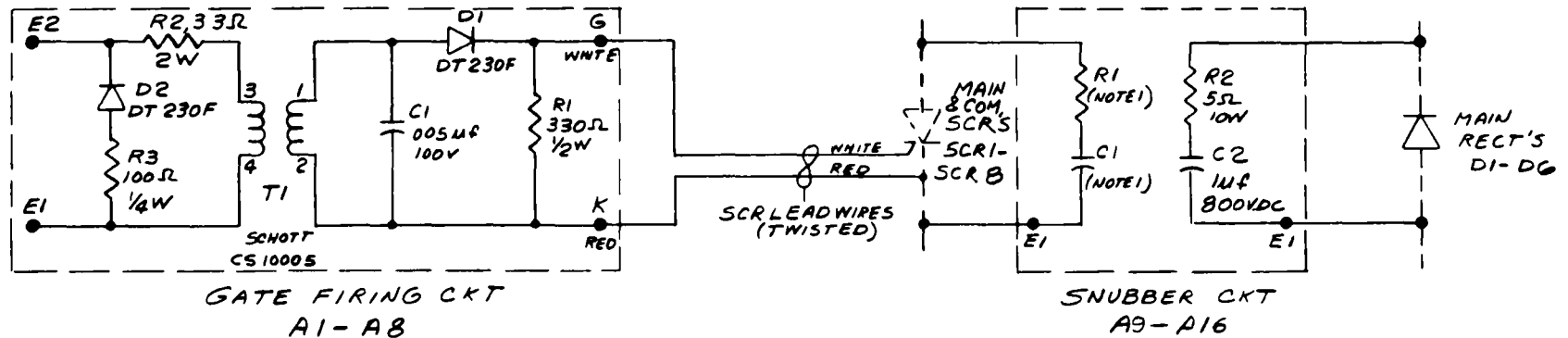
SK - 1102882 Microprocessor Board (A8)

REVISIONS			
NO.	DESCRIPTION	DATE	APPROVAL
1	COMPONENT CHANGES		
2	REVISED		



- NOTES
- 1) ALL RESISTORS  $\frac{1}{4}$  W UNLESS SPECIFIED
  - 2) U1 CD4013B
  - U4 CD4077B
  - U3 CD4011B
  - 1.1 AC = 1.1

TOLERANCES UNLESS OTHERWISE SPECIFIED	GROUP 1	DATE 10-10-70	FILE SCHEMATIC
FRACTION 1	ANALOG	DATE	
23 - 1			
SCALE			
DO NOT SCALE THIS DRAWING			
GOULD	GOULD LABORATORIES	ROLLING HEADQUARTERS	D 11 11 11



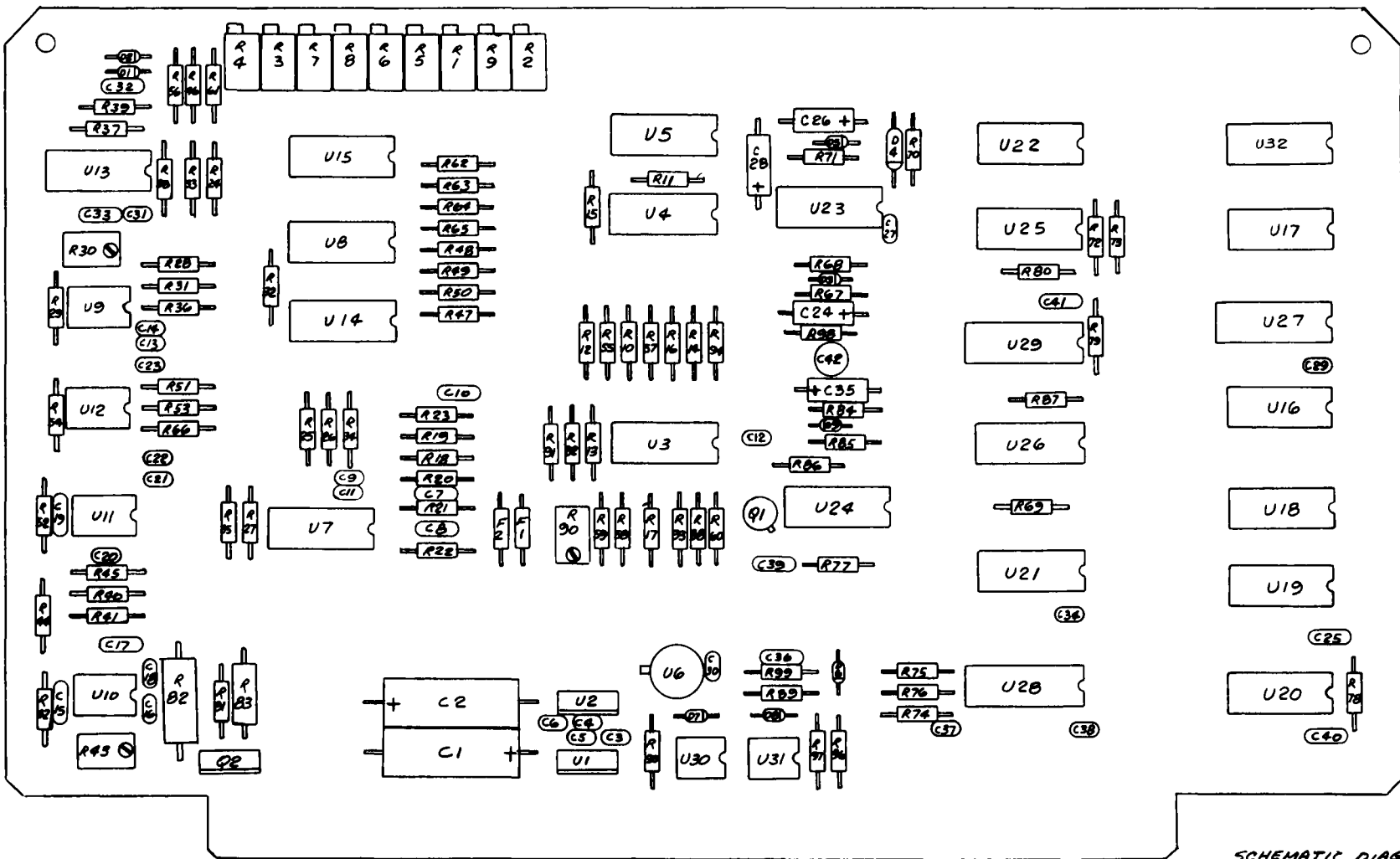
NOTES:

1 MAIN SCRS -  $R1 = 5\Omega, 10W$ ,  $C1 = 0.68\mu F, 800VDC$


COM SCRS -  $R1 = 10\Omega, 10W$ ,  $C1 = 1\mu F, 800VDC$

TOLERANCES UNLESS OTHERWISE SPECIFIED		DRAWN <i>KB</i>		DATE <i>7-1-82</i>		TITLE	
FRACTION = $\pm$		CHECKED		DATE		SCHEMATIC DIAGRAM	
JXX = $\pm$						GATE FIRING & SNUBBER CKTS	
JXXX = $\pm$						DRAWING NUMBER	
SCALE						ISSUE	
GOULD INC HAS PROPRIETARY RIGHTS IN THIS MATERIAL		GOULD		GOULD LABORATORIES		B	
DO NOT SCALE THIS DRAWING				ROLLING MEADOWS, ILL. 60068		SK-17182	

SK - 17182 Gate Drive and Snubber Circuits



SCHEMATIC DIAGRAM  
SK-110482

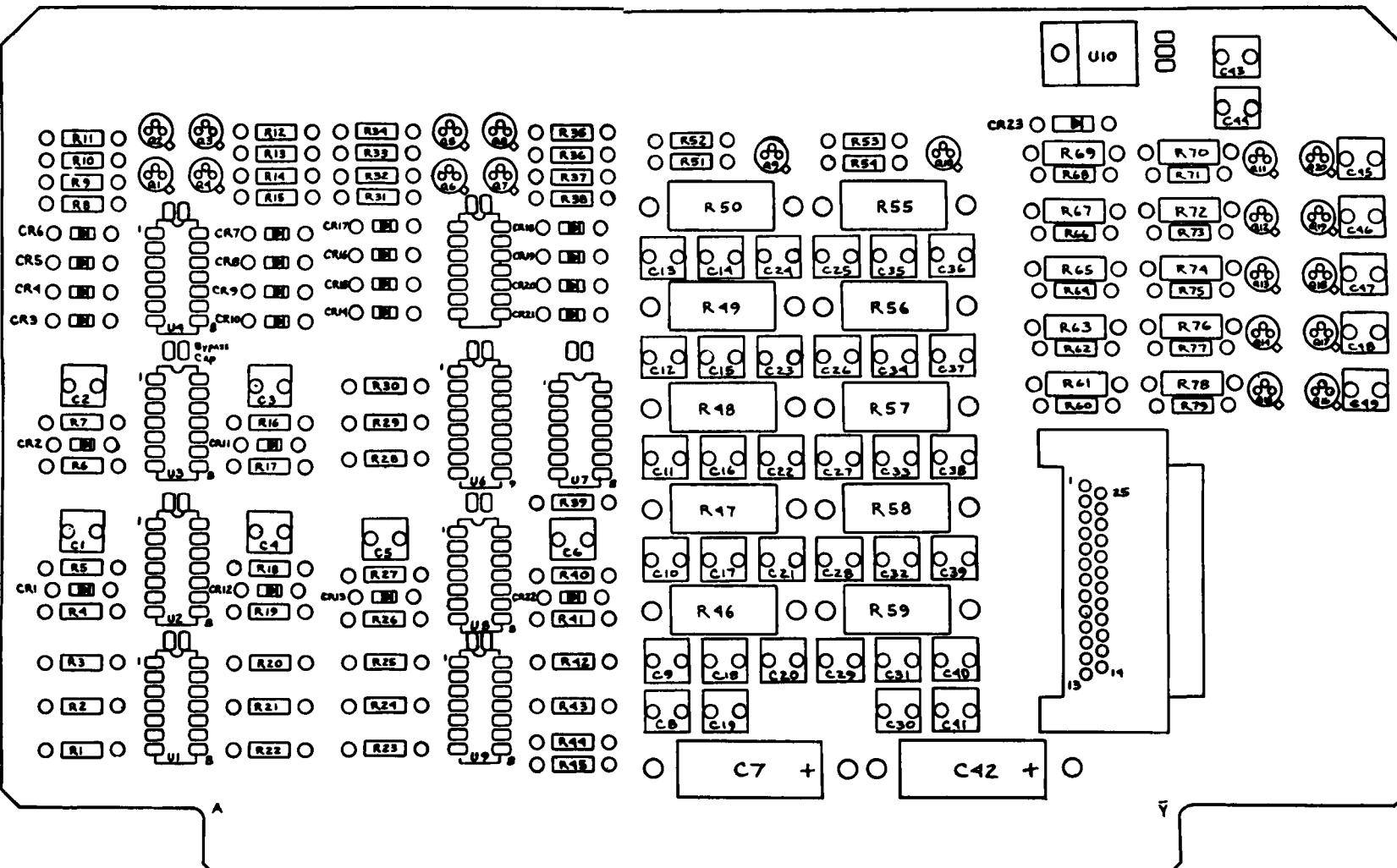
TOLERANCES UNLESS OTHERWISE SPECIFIED FRACTION = .01      ANGLES = .1 JOL = .1 JOL = .1 SCALE GOULD INC. HAS PROPRIETARY RIGHTS IN THIS MATERIAL. <b>DO NOT SCALE THIS DRAWING</b>	DRAWN	DATE	TITLE <b>COMPONENT LAYOUT CHARGER CONTROL</b>		
	CHECKED	DATE			
				DRAWING NUMBER	ISSUE
	 <b>GOULD</b>		GOULD LABORATORIES ROLLING MEADOWS, ILL. 60018		
			<b>C</b>	<b>SK-410482</b>	

SK - 410482 Charger PCB Layout (A0)



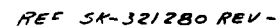
C - 15

COMPONENT SIDE VIEW

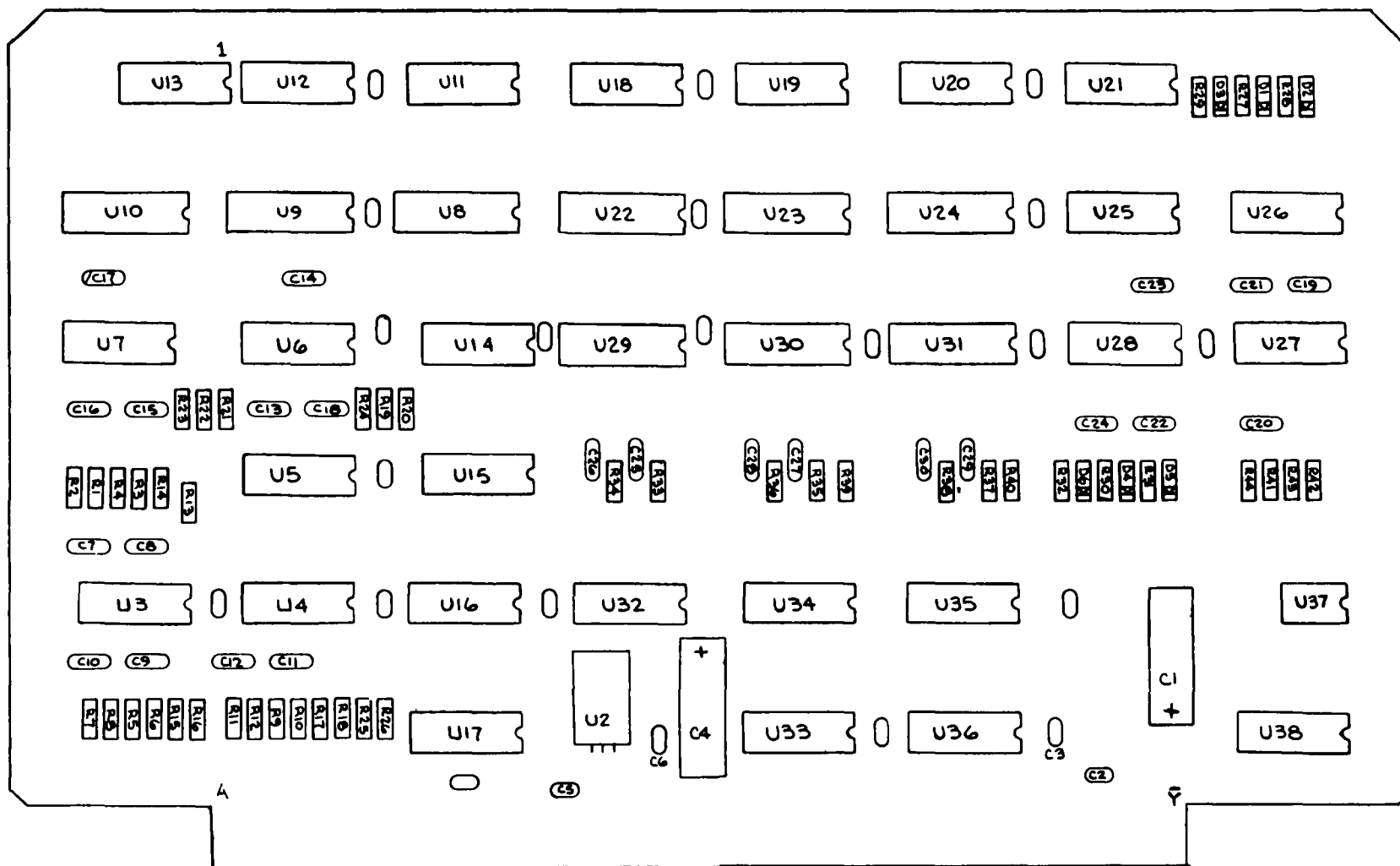


TOLERANCES: UNLESS OTHERWISE SPECIFIED		DATE		TITLE
FUNCTION =	ANALOG =	CHECKED	DATE	
JE =				GATE DRIVE AMP PCB. A1
JES =				
SCALE				DRAWING NUMBER
GOULD INC. HAS PROPRIETARY RIGHTS IN THIS MATERIAL		GOULD		ISSUE
DO NOT SCALE THIS DRAWING		GOULD LABORATORIES ROLLING MEADOWS, ILL. 60068		SK-4102182

SK - 4102182 Gate Drive PCB Layout (A1)

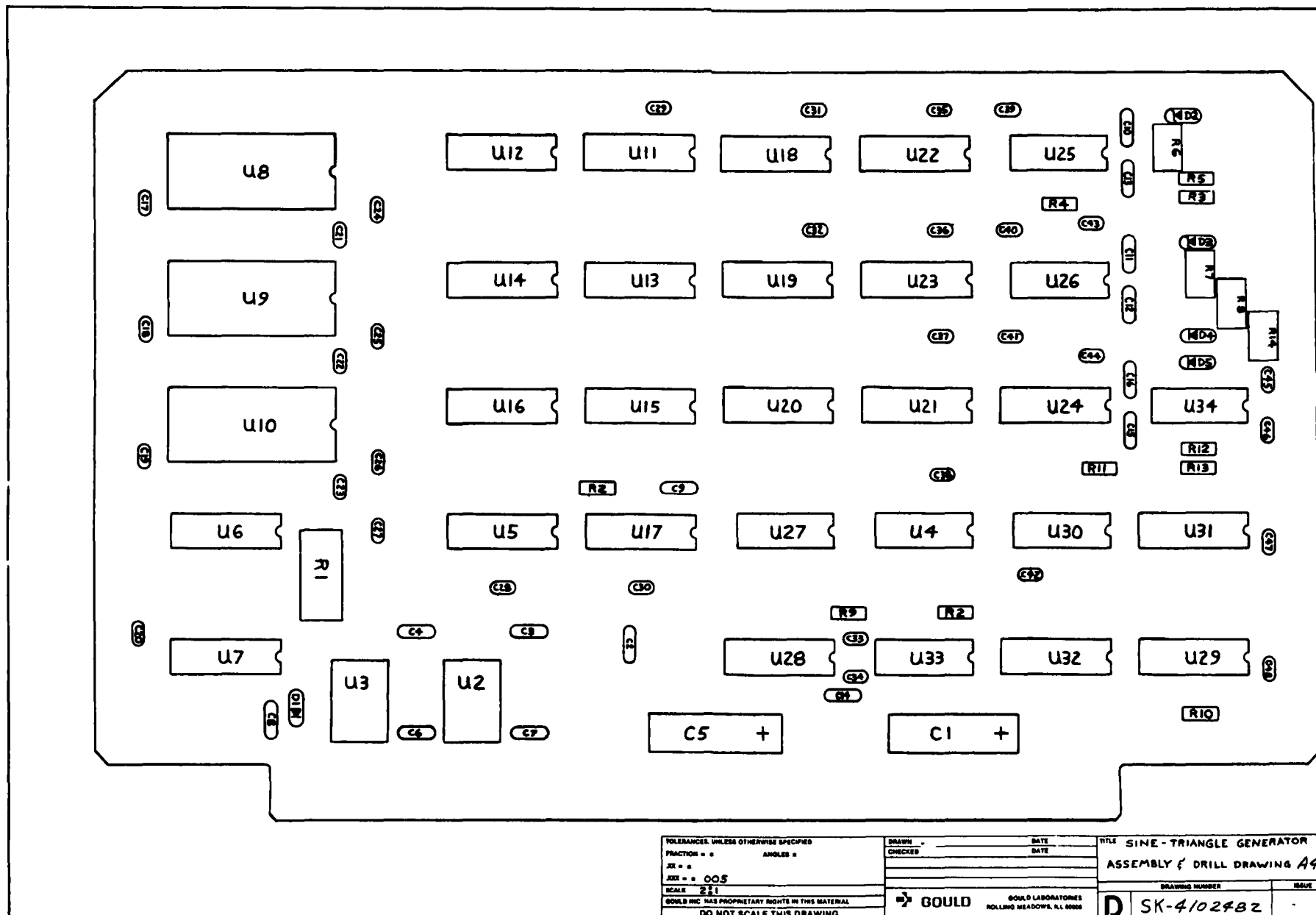


REF SK-321280 REV-

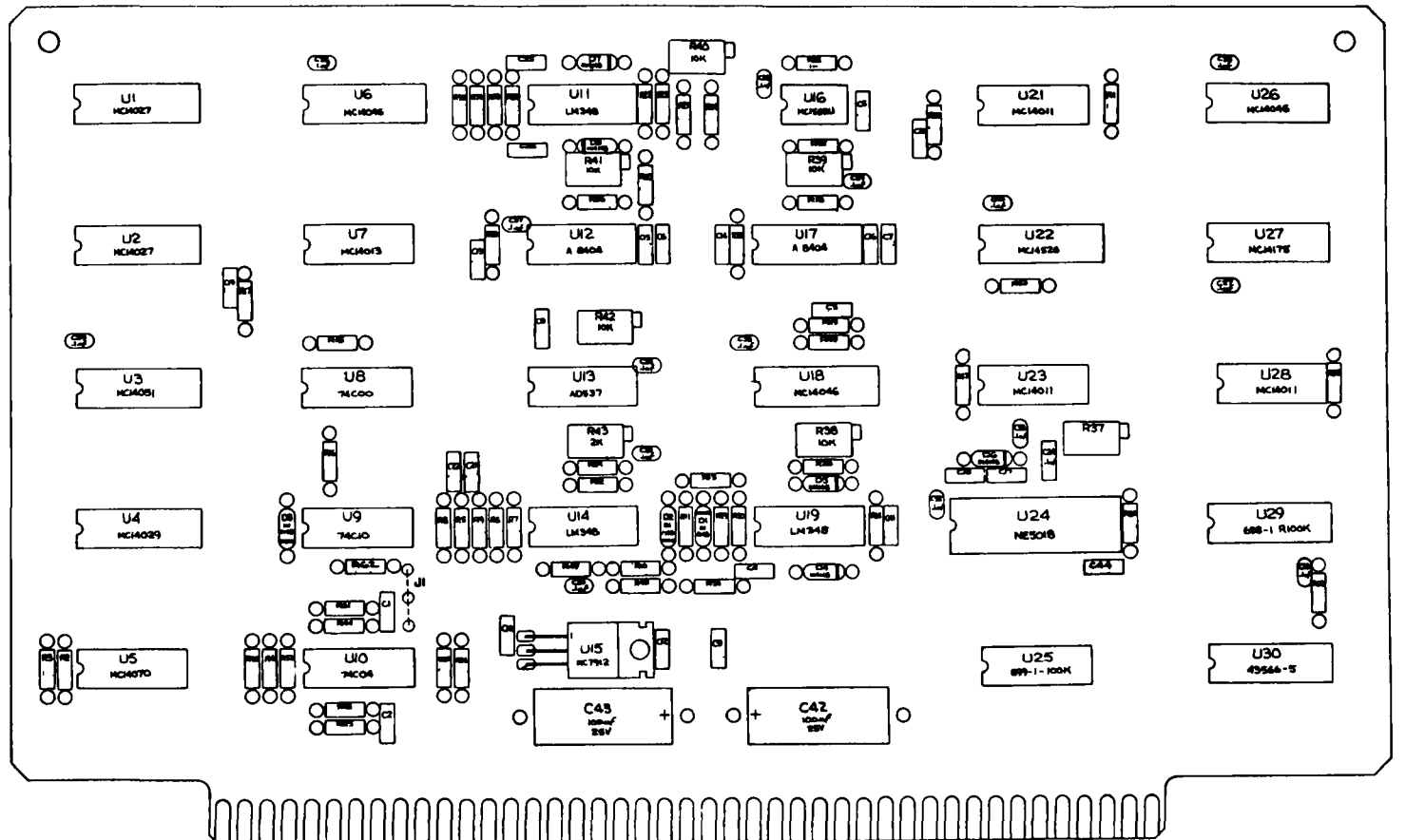


TOLERANCES UNLESS OTHERWISE SPECIFIED		DRAWN _____ DATE _____		TITLE P C BOARD ASSY A3	
FRACTION - "		CHECKED _____ DATE _____		MAIN THYRISTOR GATING Ckt	
JES - "					
JDS - "					
SCALE		GOULD		DRAWING NUMBER	
GOULD INC HAS PROPRIETARY RIGHTS IN THIS MATERIAL		GOULD LABORATORIES		NAME	
DO NOT SCALE THIS DRAWING		ROLLING MEADOWS, ILL 60068		D SK-4102382	

SK - 4102382 Main Thyristor PCB Layout (A3)



SK - 4102482 Sine - Triangle PCB Layout (A4)



REF SK-32480 REV-

TOLERANCES UNLESS OTHERWISE SPECIFIED		DRAWN		DATE		TITLE	
FRACTION - 8	ANGLES - 8	CHECKED		DATE		SLIP FREQUENCY CONTROL PCB BOARD, A5X A5	
JXX - 8							
XXX - 8							
SCALE		GOULD		GOULD LABORATORIES		DRAWING NUMBER	
GOULD INC HAS PROPRIETARY RIGHTS IN THIS MATERIAL				ROLLING HEADWORK S. 8000		D SK-41025B2	
DO NOT SCALE THIS DRAWING						REV	

SK - 4102582 Frequency Control PCB Layout (A5)

C-20

C-21

## 7. DEFINITIONS

A	- Amps
ac	- Alternating Current
C	- Commutation Circuit Total Capacitance
CB	- Circuit Breaker
$C_T$	- Charger Total Resonant Circuit Capacitance
$^{\circ}\text{C}$	- Degrees Centigrade
D	- Silicon Rectifier
dc	- Direct Current
$E_s$	- Commutation Circuit Stored Energy
gm	- Grams
hp	- Horsepower
Hz	- Hertz
$I_{pk}$	- Peak Motor Line Current
$I_m$	- Peak Resonant Circuit Current - Charger Operation
$I_T$	- T1A Winding Current When D7 Forward-Biased
in	- Inches
$K_c$	- Resonant Circuit Loss Factor
kg	- Kilograms
kW	- Kilowatts
km/h	- Kilometers/hour
L	- Commutation Circuit Inductance (T1A Winding)
$L_{STRAY}$	- Commutation Circuit Stray Inductance
lbs	- Pounds
m	- Meters
MPH	- Miles/hour
N-M	- Newton - Meters
NA	- Number of Turns (A Winding)
NB	- Number of Turns (B Winding)
$P_{LOSS}$	- Charger Power Loss
$P_{OUT}$	- Charger Output Power
PWM	- Pulse-Width-Modulation
Q	- Quality Factor
RMS	- Root-Mean-Square



Rad	- Radians
SCR	- Silicon-Controlled Rectifier
SAE	- Society of Automotive Engineers
T	- Commutation Transformer
trev	- Reverse-Bias Time Applied to Main Thyristor
VB	- Propulsion Battery Voltage
Voc	- Commutation Capacitor Initial Voltage
VC4	- Input Line Capacitor Voltage
$\theta_T$	- Angle at Which D7 Forward-Biased
$\eta$	- Charger Efficiency

## 8. REFERENCES

- 1) T.S. Latos, "Improved SCR AC Motor Inverter for Battery Powered Urban Electric Vehicles," Final Report Contract DOE/NASA/0060-82/1, December 1982.
- 2) S.C. Peak, "Improved Transistorized AC Motor Inverter for Battery Powered Urban Electric Passenger Vehicles," Final Report Contract DOE/NASA/0059-82/1, September 1982.
- 3) S. Geppert, "AC Propulsion system for an electric vehicle," Final Report Contract DOE/NASA/0125-1, August 1981.
- 4) A. Abbondanti and P. Wood, "A criterion for performance comparison between high power inverter circuits," IEEE Transactions on Industry Applications, pp. 154-160, March/April 1977.
- 5) S.B. Dewan and D.L. Duff, "Optimum design of an input commutation inverter for ac motor control," IEEE Transactions on Industry and General Applications, pp. 699-705, Nov/Dec 1969.
- 6) R.M. Davis, "Power Diode and Thyristor Circuits," IEEE Monograph Series 7, Copyright 1971, Peter Peregrinus LTD Publisher.
- 7) W.E. Rippel, "Optimizing Boost Chopper Charger Design, "Proceedings of Powercon 6, May 1979.
- 8) J.M.D. Murphy, "Thyristor Control of AC Motors," Pergamon Press, Copyright 1973.
- 9) D.A. Bradley, C.D. Clarke, R.M. Davis, D.A. Jones, "Adjustable frequency inverters and their application to variable speed driver," Proc. IEE, VOC III No. 11, November 1964.

1 Report No. NASA-CR-168177		2. Government Accession No. -		3. Recipient's Catalog No. -	
4 Title and Subtitle Integral AC Controller/Battery Charger for Use in Electric Vehicles				5 Report Date September 1983	
				6 Performing Organization Code 778-36-06	
7 Author(s) David M. Thimmesch				8 Performing Organization Report No. -	
9 Performing Organization Name and Address Gould Inc., Gould Research Center Electrical & Electronics Research 40 Gould Center Rolling Meadows, IL 60008				10 Work Unit No. -	
				11 Contract or Grant No. DEN 3-249	
12 Sponsoring Agency Name and Address U.S. Department of Energy Office of Vehicle and Engine R&D Washington, DC 20545				13 Type of Report and Period Covered Contractor Report	
				14 Sponsoring Agency Code DOE/NASA/0249-83/1	
15 Supplementary Notes Final Report. Prepared under Interagency Agreement DE-AI01-77CS51044. Project Manager, F. Gourash, Transportation Propulsion Division, NASA-Lewis Research Center, Cleveland, OH 44135.					
16 Abstract This report discusses the design and test results of a thyristor based inverter/charger. A battery charger is included integral to the inverter by using a subset of the inverter power circuit components. The resulting charger provides electrical isolation between the vehicle propulsion battery and ac line and is capable of charging a 25 kWh propulsion battery in 8 hours from a 220 volt ac line. The integral charger employs the inverter commutation components as a resonant ac/dc isolated converter rated at 3.6 kW. Charger efficiency and power factor at an output power of 3.6 kW are 86% and 95% respectively.  The inverter, when operated with a matching polyphase ac induction motor and nominal 132 volt propulsion battery, can provide a peak shaft power of 34 kW (45 hp) during motoring operation and 45 kW (60 hp) during regeneration. Thyristors are employed for the inverter power switching devices and are arranged in an input-commutated topology. This configuration requires only two thyristors to commute the six main inverter thyristors. Inverter efficiency during motoring operation at motor shaft speeds above 450 rad/sec (4300 rpm) is 92-94% for output power levels above 11 kW (15 hp). The combined ac inverter/charger package weighs 47 kg (103 lbs).					
17 Key Words (Suggested by Author(s)) Electric Vehicle, Inverter Battery Charger, Thyristor			18 Distribution Statement Unclassified - unlimited STAR Category 85 DOE Category UC-96		
19 Security Classif. (of this report) Unclassified		20 Security Classif (of this page) Unclassified		21 No of Pages 130	
				22 Price* A07	

\* For sale by the National Technical Information Service, Springfield Virginia 22161

**End of Document**